Aus der Klinik und Poliklinik für Nuklearmedizin
Klinik der Ludwig-Maximilians-Universität München
Direktor: Prof. Dr. med. Peter Bartenstein

In vivo Bildgebung von Neuroinflammation und Tau-Pathologie mittels Positronen-Emissions-Tomographie in Alzheimer-Mausmodellen

Dissertation
zum Erwerb des Doktorgrades der Medizin
an der Medizinischen Fakultät der
Ludwig-Maximilians-Universität zu München

vorgelegt von

Maximilian Valentin Deußing
aus
Reutlingen

2019

Mit Genehmigung der Medizinischen Fakultät
der Universität München

Berichterstatter:	Prof. Dr. Axel Rominger
Mitberichterstatter:	PD Dr. Johannes Levin
	Prof. Dr. Jochen Herms
	Prof. Dr. Oliver Pogarell
Mitbetreuung durch den promovierten Mitarbeiter:	Dr. Matthias Brendel
Dekan:	Prof. Dr. med. dent. Reinhard Hickel
Tag der mündlichen Prüfung:	11.07.2019

I. Eidesstattliche Versicherung

Deußing, Maximilian Valentin

Name, Vorname

Ich erkläre hiermit an Eides statt,
dass ich die vorliegende Dissertation mit dem Titel

In vivo Bildgebung der Neuroinflammation und Tau-Pathologie mittels Positronen-Emissions-Tomographie in Alzheimer-Mausmodellen

selbständig verfasst, mich außer der angegebenen keiner weiteren Hilfsmittel bedient und alle Erkenntnisse, die aus dem Schrifttum ganz oder annähernd übernommen sind, als solche kenntlich gemacht und nach ihrer Herkunft unter Bezeichnung der Fundstelle einzeln nachgewiesen habe.

Ich erkläre des Weiteren, dass die hier vorgelegte Dissertation nicht in gleicher oder in ähnlicher Form bei einer anderen Stelle zur Erlangung eines akademischen Grades eingereicht wurde.

München, 11.07.2019	Maximilian Deußing
Ort, Datum	Unterschrift Doktorandin bzw. Doktorand

Kumulative Dissertation gemäß § 4a der Promotionsordnung

II. Inhaltsverzeichnis

III. Abkürzungsverzeichnis

APP	Amyloid-Precursor-Protein
ß	Beta
BL	Baseline
^{11}C	Kohlenstoff-Isotop mit der Massenzahl 11
^{18}F	Fluor-Isotop mit der Massenzahl 18
FDG	Fluordesoxyglucose
FU	Follow-up
MAO-A	Monoaminoxidase A
MAO-B	Monoaminoxidase B
MAPT	Mikrotubuli assoziiertes Tau-Protein
MR	Magnet-Resonanz
PET	Positronen-Emissions-Tomographie
PRGN	Progranulin
PS	Presenilin
qPCR	quantitative Polymerase-Kettenreaktion
SUV	standardisierter Uptake-Wert
SUVR	Quotient des standardisierten Uptake-Werts
TREM2	Triggering receptor expressed on myeloid cells 2
TSPO	18 kDa Translokator-Protein
VOI	Volume of interest / Zielvolumen
ZNS	zentrales Nervensystem

IV. Publikationsliste

Die vorliegende kumulative Dissertation umfasst drei bereits publizierte Manuskripte:

Deussing, M., Blume, T., Vomacka, L., Mahler, C., Focke, C., Todica, A., Unterrainer, M., Albert, N.L., Lindner, S., von Ungern-Sternberg, B., Baumann, K., Zwergal, A., Bartenstein, P., Herms, J., Rominger, A., Brendel, M., 2017. **Coupling between physiological TSPO expression in brain and myocardium allows stabilization of late-phase cerebral [^{18}F]GE180 PET quantification**. Neuroimage. 2018 165:83-91.

Deussing, M., Blume, T., Vomacka, L., Mahler, C., Focke, C., Todica, A., Unterrainer, M., Albert, N.L., Lindner, S., von Ungern-Sternberg, B., Baumann, K., Zwergal, A., Bartenstein, P., Herms, J., Rominger, A., Brendel, M., 2017. **Data on specificity of [18F]GE180 uptake for TSPO expression in rodent brain and myocardium.** Data Brief. 2018 19:331-336.

Brendel, M., Yousefi, B.H., Blume, T., Herz, M., Focke, C., **Deussing, M.**, Peters, F., Lindner, S., von Ungern-Sternberg, B., Drzezga, A., Bartenstein, P., Haass, C., Okamura, N., Herms, J., Yakushev, I., Rominger, A., 2017. **Comparison of 18F-T807 and 18F-THK5117 PET in a Mouse Model of Tau Pathology**, Front Aging Neurosci. 2018 10:174.

1. Einführung

Die Demenz bei Alzheimer Krankheit ist eine fortschreitende, unheilbare Störung des Gehirns und die häufigste Form der senilen Demenzen (Scheichenberger & Scharb, 2018). Zu den Symptomen zählen unter anderem Gedächtnisverlust, Verwirrtheit, Desorientierung, Wesensänderungen, beeinträchtigtes Urteilsvermögen und Verlust der Sprachfähigkeit (Wirths et al., 2009). Die Häufigkeit von Demenzerkrankungen nimmt mit dem Lebensalter zu, so leiden derzeit schätzungsweise 1,3 Millionen Menschen in Deutschland (Sütterlin, Hoßmann, & Klingholz, 2001) und 40 - 50 Millionen Menschen weltweit (Brookmeyer, Johnson, Ziegler-Graham, & Arrighi, 2007) an der Alzheimer-Demenz. Da die ältere Bevölkerung aufgrund des demografischen Wandels in den nächsten Jahren weiter wachsen wird, ist davon auszugehen, dass die Zahl der Demenzkranken in Deutschland bis zum Jahr 2050 auf über 2,6 Millionen Menschen steigen wird, sofern kein Durchbruch in der Diagnostik und Therapie der Erkrankung gelingt (Bickel, 2000; Reitz & Mayeux, 2014). Daher ist es wichtig, neue diagnostische Früherkennungsverfahren zu entwickeln, um möglicherweise auch früh im Krankheitsverlauf eine Therapie einleiten zu können (Buch et al., 1998).

Neuropathologisch ist die Alzheimer-Demenz insbesondere durch die Atrophie des frontalen, parietalen und temporalen Cortex gekennzeichnet. Zudem kommt es zum Verlust von Nervenzellen sowie zur Degeneration von Axonen und Synapsen (Ballatore, Lee, & Trojanowski, 2007). Bislang ist eine definitive Diagnosestellung nur *post mortem* möglich, jedoch befinden sich die Diagnosekriterien durch die Entwicklung neuer Biomarker im Umbruch (Jack et al., 2018). In der molekularen Bildgebung wird angestrebt die neuropathologischen Korrelate der Erkrankung auch am lebenden Patienten detektieren zu können. Forschungsziele sind hierbei neben der frühen Diagnosestellung auch die Messung personalisierter Therapieerfolge (Souslova, Marple, Spiekerman, & Mohammad, 2013).

1.1 Amyloidakkumulation vs. Tau-Pathologie vs. Neuroinflammation

Die neurobiologischen Grundlagen der Alzheimer-Krankheit sind vielfältig. Hierbei fällt makroskopisch vor allem der fortschreitende Verlust von Nervenzellen auf, wodurch es zur Atrophie des Gehirns um bis zu 20% und zu einer damit

verbundenen Vertiefung der Sulci an der Gehirnoberfläche sowie einer Erweiterung der Liquorräume kommt. Der Verlust von Synapsen und Nervenzellen sowie die Hippocampusatrophie (Fox et al., 1996) bewirken eine Störung der Informationsverarbeitung des Gehirns und sind ursächlich am Gedächtnisverlust beteiligt (Selkoe, 2002; Terry et al., 1991). Als Grund für diesen neuronalen Untergang sowie wesentlichen Bestandteil der Neuropathophysiologie der Alzheimer-Erkrankung gelten ß-Amyloid-Ablagerungen (Hardy & Selkoe, 2002), hyperphosphorylierte Tau-Ablagerungen (LaFerla, 2010) und die Aktivierung von Mikroglia (Monson et al., 2014) sowie deren Interaktionen. Die typische extrazelluläre Ablagerung von Amyloid-Plaques tritt bereits Jahre vor Auftreten von klinischen Symptomen auf, sodass eine frühzeitige Diagnosestellung auch eine frühzeitige, vorbeugende Therapie ermöglichen könnte (Selkoe, 1999, 2002). Demgegenüber zeigen die Ablagerungen hyperphosphorylierter Tau-Fibrillen die beste Korrelation zur klinischen Symptomatik und der neuronalen Funktionalität (Ossenkoppele et al., 2016). Die Neuroinflammation (aktivierte Mikroglia) spielt in der Endstrecke der Neurodegeneration eine wesentliche Rolle und wird auch in frühen Stadien ebenfalls diskutiert, wobei die Datenlage zu den exakten Auswirkungen der inflammatorischen Prozesse im Rahmen der Alzheimer Erkrankung derzeit noch gering ist (Heneka et al., 2015; Zimmer, Leuzy, et al., 2014).

1.2 Bildgebung der Neuroinflammation und Tauopathien

Die molekulare Bildgebung mittels PET stellt im Bereich der Diagnostik und der Erforschung der Alzheimer Erkrankung einen schnell wachsenden Sektor dar (Adlard et al., 2014). ß-Amyloid und der Glukosemetabolismus können durch Fluorid-markierte Radiotracer ([^{18}F]-Florbetaben; [^{18}F]-FDG) im Gehirn nicht-invasiv detektiert werden, um sowohl die Progression der Amyloidogenese als auch die synaptische Dysfunktion zu verfolgen (Barthel et al., 2011; Cohen & Klunk, 2014; Rice & Bisdas, 2017).

Neue Therapieansätze zielen auf neuropathophysiologische Prozesse und Strukturen ab, im Sinne einer sogenannten „targeted therapy“. So werden auch im Bereich der Tau-Fibrillen sowie der Neuroinflammation aktuell Strategien entwickelt, mit dem Ziel, letztendlich die kognitive Leistungsfähigkeit zu verbessern. Zu bewältigende Schwierigkeiten an diesen neuartigen Therapieverfahren sind zum

einen die hohen Kosten und zum anderen muss die entsprechende Zielstruktur des Therapeutikums im spezifischen Patienten auch pathologisch verändert vorliegen, um diese Therapie erfolgversprechend durchführen zu können.

Die nicht-invasive Bildgebung der Amyloid-Ablagerungen, der Tau Fibrillen sowie der aktivierten Mikroglia mittels Positronen-Emissions-Tomographie (PET) könnte dabei einen entscheidenden Beitrag liefern (Latta, Brothers, & Wilcock, 2014). Zum einen können hierdurch *in vivo* die entsprechenden Zielstrukturen nachgewiesen werden und zum anderen kann diese Technik auch zur Bewertung eines Therapieansprechens dienen. Hierdurch können im Rahmen personalisierter Medizin Nebenwirkungen und Kosten gespart werden, indem eine Therapie nur dann eingesetzt wird, wenn sie durch den initialen Nachweis der Zielstruktur erfolgversprechend ist.

1.3 Radioliganden zur Bildgebung der Neuroinflammation und Tau-Pathologie

Bezüglich der Neuroinflammation und der Tau-Ablagerungen stehen hier vielversprechende [^{18}F]-markierte Radiotracer zur Verfügung, die sowohl im präklinischen Sektor als auch im Humanbereich Gegenstand aktueller Forschung sind (Dupont et al., 2017; Villemagne & Okamura, 2016).

Als Zielstruktur zur Detektion aktivierter Mikroglia dient das 18 kDa Translokator-Protein (TSPO), ein Membran-Protein der äußeren Mitochondrienwand, welches in enger Verbindung zur Neuroinflammation steht (Brown & Papadopoulos, 2001). Während sich peripher in multiplen Geweben eine hohe TSPO-Expression findet, zeigt sich diese im gesunden Gehirn nur geringfügig erhöht mit starker Hochregulation bei neuroinflammatorischen Prozessen (Chaney, Williams, & Boutin, 2018).

Bisherige Studien zur Bildgebung der Neuroinflammation verwendeten häufig den TSPO-Liganden [^{11}C]-PK11195, erbrachten aber aufgrund einer geringen ZNS-Verfügbarkeit durch geringen Übertritt durch die Bluthirnschranke, einen geringen Signal-zu-Hintergrund Kontrast und einen störenden peripheren Metabolismus bei diesem Tracer meist uneindeutige Ergebnisse (Hommet et al., 2014; Stefaniak & O'Brien, 2016).

Weiterentwickelte TSPO-Liganden der dritten Generation, wie beispielsweise [^{18}F]-GE180, überzeugen dagegen durch eine effizientere klinische Anwendung bei längerer Halbwertszeit sowie einen verbesserten Signal-zu-Hintergrund Kontrast bei der Detektion der Neuroinflammation (Dickens et al., 2014; Wickstrom et al., 2014).

Die Entwicklungen [^{18}F]-markierter Radioliganden mit Bindung an Tau-Aggregate bewirkte einen großen Fortschritt für die Tau-PET Bildgebung bei Alzheimer Demenz und nicht-Alzheimer Tauopathien (Villemagne & Okamura, 2016). Die verfügbaren Tau-Tracer der ersten Generation konnten klinisch bereits erfolgreich eingesetzt werden (Okamura et al., 2014; Smith et al., 2016), zeigten jedoch eine relevante Off-Target Bindung an die Monoaminoxidasen A und B (MAO-A, MAO-B) (Ng et al., 2017). Dadurch führte neben dem Vorliegen von Tau-Fibrillen auch ein erhöhtes Vorkommen von MAO-A/MAO-B, z.B. im Rahmen einer Astrozytose, zu einer erhöhten Bindung dieser Radioliganden. Um präzise wissenschaftliche Aussagen treffen zu können, ist es daher erstrebenswert, einen Tau-Tracer ohne relevante Off-Target Bindung zu finden. Die aktuell am meist verwendeten Radioliganden stammen hierbei aus den Strukturfamilien der Arylquinoline und Pyridoindole mit jedoch nur spärlich vergleichenden Daten über deren Leistungsvermögen *in vivo*.

1.4 Kleintier Modelle der Alzheimer Demenz

Experimentelle Kleintiermodelle der Alzheimer Demenz sind zur Erforschung ablaufender neurobiologischer Prozesse und präklinischer Erprobung neuer Therapeutika im lebenden Organismus unerlässlich (Drummond & Wisniewski, 2017). Dabei werden humane Gen-Mutationen, die in Assoziation mit der hereditären Form der Alzheimer Demenz stehen, durch Klonierung oder Insertion in Maus- oder Rattenstämme eingebracht. Diese bestehen primär aus Veränderungen in den Amyloid Precursor Protein-, Presenilin1/2- oder MAPT (Microtubule-associated protein tau) - Genen und resultieren in der frühzeitigen Bildung von Amyloid Plaques und neurofibrillären Bündeln (Teipel, Buchert, Thome, Hampel, & Pahnke, 2011).

Das PS2APP Mausmodell mit C57Bl/6 Hintergrund ist gekennzeichnet durch eine sogenannte schwedische Mutation im Amyloid Precursor Protein (APP) Gen und einer zusätzlichen Mutation im Presenilin 2 (PS2) Gen (Richards et al., 2003).

Vorteil dieses Modells ist neben der Nähe zur humanen Pathologie ein früh einsetzender Beginn der Plaquebildung im Cortex und Hippocampus ab dem Alter von 5-6 Monaten (Ozmen, Albientz, Czech, & Jacobsen, 2009).

Transgene P301S Mäuse mit C57BL/6 Hintergrund exprimieren die P301S Mutation im humanen Mikrotubuli assoziierten Tau Protein (MAPT-Gen) (Allen et al., 2002). Dieses Mausmodell ist gekennzeichnet durch eine überwiegend den Hirnstamm betreffende Hyperphosphorylierung und Bildung von Tau-Fibrillen, die den bei der Alzheimererkrankung beobachteten Fibrillen entsprechen. Die Pathologie manifestiert sich ab dem Alter von 2-3 Monaten durch progrediente Lerndefizite und dem Auftreten von motorischen Beeinträchtigungen ab 4 Monaten.

1.5 Kleintier PET

Speziell entwickelte PET Scanner zur Anwendung im Kleintierbereich ermöglichen trotz kleiner Untersuchungsvolumina eine hohe Sensitivität und hohe räumliche Auflösung (Visser et al., 2009). Im Gegensatz zu histologischen Untersuchungen, bei denen meist nur der Endpunkt einer Studie bestimmt werden kann, bietet die nicht invasive PET Untersuchung die Möglichkeit im Mausmodell neben der Analyse von Ausgangs- und Endwerten auch *in vivo* die individuelle Kinetik zu erfassen und dadurch die hohe Variabilität in Einzeltieren zu berücksichtigen (Rominger et al., 2013).

Neuartige Therapien der Alzheimer Demenz müssen zwangsläufig im präklinischen Langzeitverlauf getestet werden, um einen positiven oder negativen Einfluss auf die Erkrankung verlässlich messen zu können. Hier bietet nur eine longitudinale *in vivo* Diagnostik die Möglichkeit, Interventionen in Bezug auf die Interaktion der neuropathologischen Charakteristika im Verlauf zu beurteilen. Des Weiteren ermöglicht die Kleintier-PET Diagnostik unter Betrachtung des translationalen Aspektes eine schnelle Übertragbarkeit der Ergebnisse vom Tiermodell auf den Menschen, indem sie Teile der systemphysiologischen Mechanismen darstellen kann, die auch im Humanbereich mittlerweile erfolgreich detektiert werden (Zimmer, Parent, Cuello, Gauthier, & Rosa-Neto, 2014).

1.6 Kleintier PET Studien zur Detektion von Neuroinflammation und Tau-Pathologie

Bisherige präklinische Grundlagenstudien konnten im Bereich der Amyloidpathologie bereits überzeugende PET-Ergebnisse liefern (Brendel et al., 2015). Darauf aufbauend konnte in Studien zur Neuroinflammation zum einen der TSPO-Tracer [^{18}F]-GE180 etabliert und eine enge Beziehung zwischen Amyloidakkumulation und reaktiver Neuroinflammation gezeigt werden (Brendel, Probst, et al., 2016). Die vielfältigen Einsatzmöglichkeiten des TSPO-Tracers zur Detektion der Mikogliaaktivierung zeigte sich in weiteren präklinischen Arbeiten zu traumatischen Schädigungen des Gehirns (Israel et al., 2016), der Multiplen Sklerose (Airas, Rissanen, & Rinne, 2015), der amyotrophen Lateralsklerose (Gargiulo et al., 2016) sowie bei Glioblastomen (Buck et al., 2015).

Im Bereich der Tau-Bildgebung existierten bis zum Zeitpunkt unserer Arbeit allerdings nur wenige präklinische PET Studien in Wildtyp- oder transgenen Mausmodellen (Maruyama et al., 2013; Okamura et al., 2013). Eine PET-Studie zur Charakterisierung des Arylquinolins [^{18}F]-THK5117 zeigte zwar im Vergleich zur Wildtyp-Kontrollgruppe ein gesteigertes zerebrales PET-Signal sowie eine Korrelation mit autoradiographischen und immunhistochemischen Untersuchungen, doch zeigte sich insgesamt eine geringe Sensitivität und schwache Detektionsrate durch raschen Wash-out des Radiotracers aus dem Gehirn bei dennoch hoher einstrahlender Aktivität durch umliegende extrazerebrale Strukturen (Brendel, Jaworska, et al., 2016).

In Zusammenschau mit der Notwendigkeit, weitere Erkenntnisse der Tau-Pathologie aufzudecken, ist daher die weitere Erprobung neuer Radiotracer zur Etablierung der präklinischen Tau-Bildgebung im Mausmodell unerlässlich.

1.7 Referenzregion und Pseudo-Referenzregion

Der Goldstandard zur Normalisierung von PET Messungen erfordert die absolute Quantifizierung durch mehrfache Bestimmung der Konzentration des applizierten Radioliganden im arteriellen Blut (Tang, Nickels, Tantawy, Buck, & Manning, 2014). Dennoch impliziert diese aufwendige und invasive Technik einige Schwierigkeiten, da beispielsweise spezielles Equipment und Expertise benötigt wird, da andernfalls Messfehler bei der Blutabnahme die finale Auswertung maßgeblich beeinflussen.

Zur Steigerung der Effizienz, speziell in der klinischen Routine sowie präklinischen Studien mit hohen Tierzahlen, bedient man sich daher an einer relativen Quantifizierung durch eine Referenzregion/Pseudoreferenzregion. Bei dieser Methodik dient eine zerebrale Vergleichsregion ohne spezifische Tracer-Bindung bzw. frei von Pathologie als Divisor zur Berechnung des SUVR (=Standard-uptake-value-ratio). Vorteile dieser Methode sind eine geringe Variabilität durch fehlende Störgrößen wie der Blutabnahme sowie eine praktikablere Durchführung ohne zusätzlichen Mehraufwand.

Zur Bildgebung der Neuroinflammation konnte in diesem Sinne im humanen Sektor das Cerebellum (Lyoo et al., 2015) sowie im präklinischen Sektor eine Cerebellum/Hirnstamm Referenzregion (Brendel, Probst, et al., 2016) etabliert werden. Bei der Bildgebung der Tau-Pathologie dient präklinisch ebenfalls das Cerebellum (Brendel, Jaworska, et al., 2016) sowie in humanen Studien das Cerebellum beziehungswiese dessen graue Substanz (Jonasson et al., 2019) als Referenzgewebe.

2. Inhalte der Promotionsarbeit

2.1 Quantifizierung der PET-Daten mittels extrazerebraler Pseudo-Referenzregion

Während in den bisherigen präklinischen TSPO-PET Beobachtungsstudien eine intrazerebrale Pseudo-Referenzregion zur Normalisierung des PET-Signals Anwendung fand, ergab diese Methodik unschlüssige PET-Ergebnisse bei der Evaluation erster Pilot-Messwerte einer Interventionsstudie zur Modulation der Mikrogliaaktivität. Hier stellte sich die Problematik dar, dass eine klassische intrazerebrale Referenzmethode bei therapeutischen Interventionen nur deutlich eingeschränkt verwendet werden kann, da die Änderung durch die Modulation der Neuroinflammation meist das gesamte Gehirn betrifft. Somit erfasst jede Referenzregion zumindest partiell auch den Therapieeffekt. Auch bei Erkrankungen wie der Multiplen Sklerose (Airas et al., 2015), Epilepsie (Brackhan et al., 2018) und malignen Hirntumoren wie dem Glioblastom (Buck et al., 2015) ergab sich durch die ubiquitär vorliegende Neuroinflammation eine eingeschränkte Anwendbarkeit einer intrazerebralen Referenzregion.

Auf der Suche nach einer extrazerebralen Referenzregion greifen andere Autoren auf Methoden, wie der Normalisierung über die Tracer-Aufnahme im Skelett- (James et al., 2015) oder Herzmuskel (Mirzaei et al., 2016) zurück. Alternativ kann die Normalisierung über die injizierte Tracer-Dosis (Pihlaja et al., 2015; Zheng, Winkeler, Peyronneau, Dolle, & Boisgard, 2016) oder dem standardisierten Uptake-Wert (SUV) (Biesmans et al., 2015) erfolgen. Diese Methoden weisen jedoch präklinisch eine hohe Variabilität auf (Brendel, Probst, et al., 2016).

In meiner Erstautorenschaft „*Coupling between physiological TSPO expression in brain and myocardium allows stabilization of late-phase cerebral [18F]GE180 PET quantification*" befasste ich mich mit einem systematischen Vergleich unterschiedlicher Normalisierungs-Methoden und entwickelte eine valide Methodik zur Quantifizierung von TSPO-PET Messungen mittels extrazerebraler Myokard-Korrektur, welche in mehreren Folgestudien ihre Anwendung fand.
Zunächst erhielten zehn C57Bl/6 Wildtyp Mäuse im Alter von 16,0 ± 3,7 Monaten, eine [^{18}F]-GE180 PET-Messung mit anschließender Extraktion des Gehirns zur *ex vivo* Bestimmung des Hirngewichts und Aktivitätsmessung im Gamma-Counter. Diese diente als Goldstandard.

Eine Regressionsanalyse mit den Prädiktoren injizierte Dosis, Körpergewicht, sowie der Tracer-Aufnahme in Skelett- und Herzmuskel, berechnet aus der PET Messung, diente zur Identifikation signifikanter Einflussgrößen auf die zerebrale Tracer-Aufnahme als abhängige Variable.

Die Bestimmung der Tracer-Aufnahme in den Herzmuskel erfolgte dabei in Anlehnung an eine Studie zur myokardialen Hypertrophie (Gross et al., 2016) durch Platzieren eines ellipsoiden Zielvolumens (VOI) über der Vorderwand der linken Herzkammer und durch die Berechnung des Mittelwerts der 30% heißesten Voxel. Eine visuelle Kontrolle in axialer, sagittaler und coronaler Projektion gewährleistete eine korrekte Position der VOI ohne Überstrahlung durch angrenzende Gewebe (z.B. Lunge). Die resultierende VOI mit 34,8 ± 6,5 mm^3 beinhaltete 73 ± 14 Voxel.
Die mittlere Tracer-Aufnahme im Skelettmuskel wurde über manuelle Eingrenzung von je zwei Zielvolumina in jedem Vorderglied der Maus bestimmt, zeigte in Test-Retest Versuchen aber im Vergleich zur Myokardaktivität eine deutlich höhere Schwankung (Variabilität: 17,3 ± 11,7% vs. 1,6 ± 2,5%) und schied damit aus weiteren Untersuchungen aus.

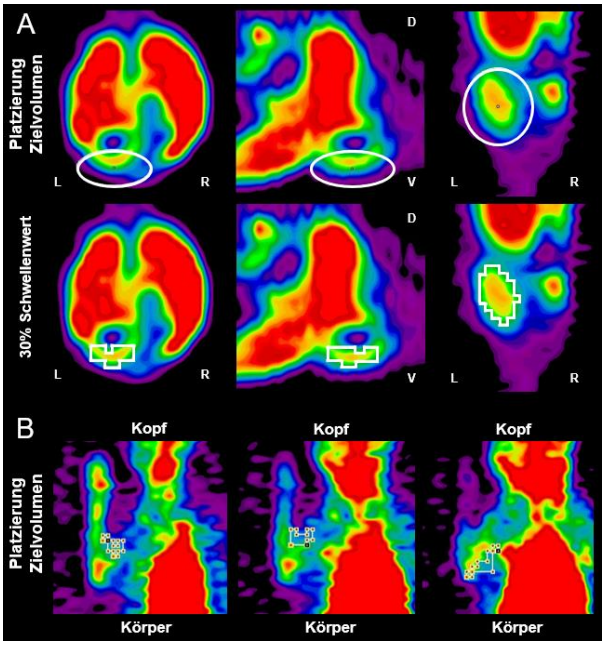

Abbildung 1: Definition des Herz- und Skelettmuskel-Zielvolumens (VOI). **(A)** Die obere Reihe zeigt das Platzieren des Zielvolumens in die ventrale Herzwand. Die untere Reihe zeigt den berechneten 30% Schwellenwert der heißesten Voxel. Von links nach rechts: axiale, sagittale und coronale Projektion; L = links, R = rechts, V = ventral, D = dorsal **(B)** Darstellung des Skelettmuskel-Zielvolumens in coronaler Schnittführung.

Sowohl die injizierte Dosis (β = 0,40; p = 0,006), das Körpergewicht (β = 0,30; p = 0,002) als auch die durch PET bestimmte [^{18}F]-GE180 Aktivität im ventralen Myokard (β = 0,64; p = 0,0003) trugen signifikant zur *ex vivo* gemessenen zerebralen Aktivität bei ($F_{(3, 6)}$ = 226,0; p < 0,001; R^2 = 0,991; R^2 adjustiert = 0,987).

Anhand eines großen Datensatzes bestehend aus N=79 Wildtyp TSPO-PET-Messungen im Alter von 7,4 ± 1,6 Monaten wurde anschließend die Wertigkeit der ermittelten Einflussgrößen (injizierte Dosis, standardisierter Uptake-Wert [SUV] und Aktivität im Herzmuskel) und deren Auswirkung auf die Varianz in Bezug zur Gehirnaktivität analysiert.

Die Regressionsanalyse ergab die höchste Varianz bei Skalierung durch injizierte Dosis ($F_{(1, 77)}$ = 57,4; p < 0,001; R^2 = 0,427; R^2 adjustiert = 0,420; Abb. 2A), gefolgt von der Berechnung des SUV ($F_{(2, 76)}$ = 36,9; p < 0,001; R^2 = 0,493; R^2 adjustiert = 0,480; Abb. 2B).

Die mit Abstand besten Ergebnisse lieferte eine Kombination aus myokardialer Aktivität mit injizierter Dosis und Körpergewicht ($F_{(3, 75)}$ = 406,7; p < 0,001; R^2 = 0,942; R^2 adjustiert = 0,940; Abb. 2C), nachfolgend Myokardkorrekturmethode genannt.

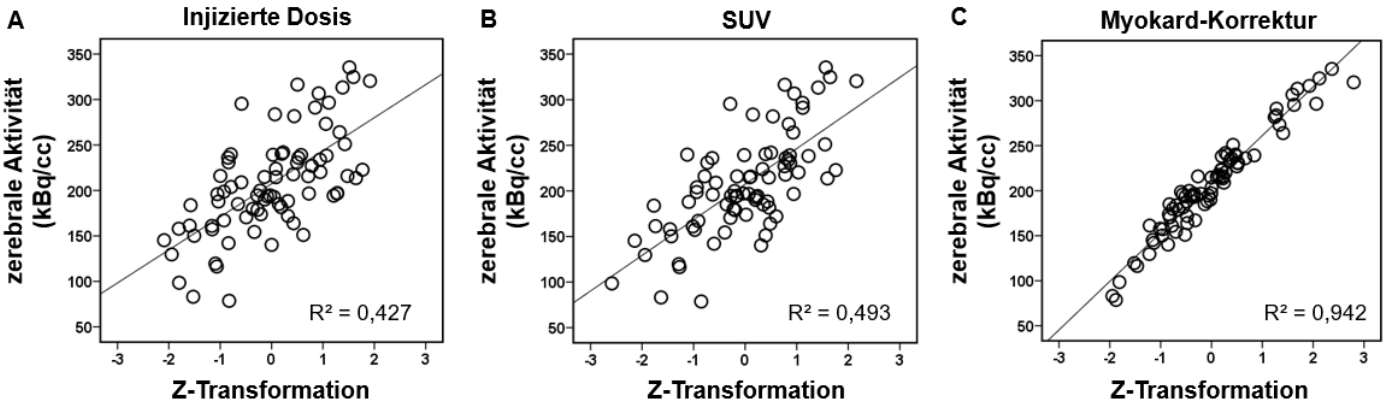

Abbildung 2: Regressionsanalyse des Vergleichs unterschiedlicher Normalisierungsmethoden anhand eines großen Datensatzes von PET-Messungen (N=79 C57Bl/6 Wildtyp-Mäuse). Die Prädiktoren (injizierte Dosis, SUV und Myokard-Korrektur sind dargestellt nach Z-Transformation. Die Schaubilder visualisieren die geringe Erklärung der Varianz der Gehirnaktivität bei Berechnung der injizierten Dosis (**A**) oder SUV (**B**). Eine deutliche Verbesserung zeigt sich unter Einbeziehung der Herzaktivität zu injizierter Dosis und SUV (**C**).

Für die Myokardkorrekturmethode wurden nach Standardisierung der individuellen Werte durch Z-Transformation die Regressionskoeffizienten berechnet (Tabelle 1). Den größten Anteil nahm die Herzaktivität ein (β = 0,846), gefolgt von injizierter Dosis (β = 0,191) und Körpergewicht (β = - 0,031).

Tabelle 1

Normalisierung	Mittelwert	SD	β	RC	p-Wert
Injizierte Dosis (MBq)	14,3	1,6	0,191	9,794	p < 0,001
Körpergewicht (g)	25,4	3,7	-0,031	-2,420	p = 0,294
Myokardiale Aktivität (kBq/cc)	844,2	273,6	0,846	44,578	p < 0,001

Tabelle 1: Regressionsanalyse zur Bestimmung der Wichtung der Einflussfaktoren auf die zerebrale [^{18}F]-GE180 Aufnahme. β = beta, SD = Standardabweichung, RC = Regressionskoeffizient.

[^{18}F]-GE180 PET Daten aus dem oben genannten PS2APP Mausmodell (N = 24; 5-16 Monate alt) dienten zur Bestimmung der Test-Retest Variabilität (N = 10) und der Übereinstimmung der normalisierten PET Ergebnisse mit histologischen Untersuchungen (N = 24). Die Korrelation der zerebralen [^{18}F]-GE180 Aufnahme mit der immunhistochemischen Bestimmung der Mikrogliaaktivität durch Markierung mittels monoklonalen IBA-1 Antikörper (Brendel, Probst, et al., 2016), erbrachte ebenfalls die beste Übereinstimmung durch Myokardkorrektur (R = 0,51; p < 0,01). Geringere Korrelationen zeigten sich bei Korrektur durch die injizierte Dosis (R = 0,44; p < 0,05) und SUV (R = 0,42; p < 0,05).

Die abschließende Validierung erfolgte durch praktische Anwendung der Normalisierungsmethodik auf longitudinale [^{18}F]-GE180 PET Daten von transgenen PS2APP Mäusen (N = 10; weiblich; unbehandelt) zu je vier Alterszeitpunkten von 9 bis 14 Monaten.

Die visuelle Interpretation der individuellen longitudinalen TSPO-Kinetik über 20 Wochen sowie die Berechnung der mittleren quadratischen Abweichung zeigte eine weitaus höhere Stabilität und verminderte Anzahl an Ausreißern bei Verwendung der Myokardkorrekturmethode (7,7%) im Vergleich zu injizierter Dosis (13,5%; p < 0,005) oder SUV (13,5%; p < 0,005); die Anwendung der etablierten intrazerebralen Referenzregion erzielte die geringsten Abweichungen (2,8%).

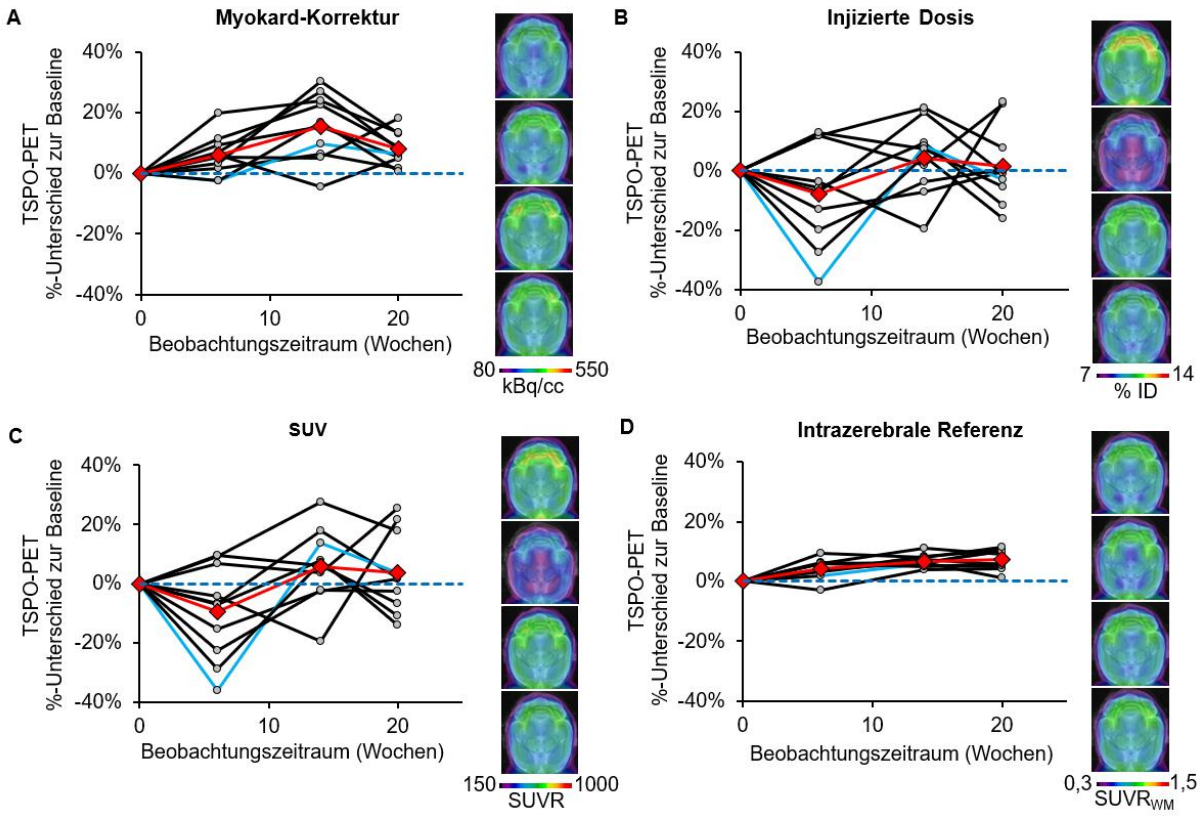

Abbildung 3: Longitudinale [^{18}F]-GE180 PET Messungen über 20 Wochen zeigen eine höhere Stabilität und eine geringe Varianz bei Verwendung der Myokardkorrekturmethode (**A**) verglichen mit injizierter Dosis (**B**) oder SUV (**C**); die intrazerebrale Referenzregion erzielte die geringsten Abweichungen (**D**). Die schwarzen Linien stellen den individuellen Verlauf, die roten Linien die Mittelwerte dar. Exemplarische Darstellung einer repräsentativen Einzelmaus (blaue Linie) und deren axialen PET/MR Bilder.

Zusammenfassend konnte gezeigt werden, dass neben der Normalisierung durch intra-zerebrale Referenzregionen die Myokardkorrekturmethode eine valide und robuste Technik zur Stabilisierung zerebraler TSPO Kleintier PET Messungen mit [^{18}F]-GE180 darstellt.

Die Methodik wurde darüber hinaus in weiteren Tiermodellen der Mikrogliamodulation mittels TREM2-Mutation (Parhizkar et al., 2019) sowie PRGN-Mutation (Götzl et al.; 2019 submitted), der Multiplen Sklerose (Nack et al., 2019), einer longitudinalen PET Studie mit anschließender Verhaltenstestung (Focke et al., 2018) und weiteren zum Zeitpunkt des Einreichens der Arbeit noch nicht publizierten Studien erfolgreich angewendet.

2.2 Spezifität der [^{18}F]-GE180 Bindung zur Darstellung der TSPO-Expression im Gehirn und Herz der Maus

Die enge Verknüpfung zwischen zerebraler und kardialer TSPO Expression, die unter physiologischen Bedingungen die Quantifizierung der Tracer-Aufnahme im Gehirn der Maus stabilisiert, ermutigte uns zu weiteren Untersuchungen.

Zur Bestimmung der Spezifität der [^{18}F]-GE180 Bindung im Gehirn und dem Herz der Maus führten wir Blocking-Experimenten mit zwölf C57/Bl6 Wildtyp-Mäusen im Alter von 7 Monaten durch. Hierzu erhielt eine Gruppe von N=7 Mäusen vor der eigentlichen Injektion des Radioliganden einen hochdosierten, nicht-radioaktiven, sogenannten kalten Tracer (Verhältnis kaltes GE180 zu [^{18}F]-GE180: 1000 : 1). Durch Gabe des kalten Tracers werden vorab die TSPO-Bindungsstellen gesättigt und können bei der nachfolgenden Applikation den radioaktiv-markierten Tracers nicht mehr binden.

Anschließende *ex vivo* Gamma-Counter Messungen erbrachten eine spezifische [^{18}F]-GE180 Bindung von 36% im Gehirn und 80% in der Herzmuskulatur. Die absolute spezifische Bindung im Herz war damit im Vergleich zum Gehirn 17-fach erhöht.

Die Korrelation der individuellen Messwerte aus den beiden Geweben bestätigte unsere bisherigen Beobachtungen über den engen Zusammenhang zwischen der zerebralen und kardialen TSPO-Expression und zeigte eine exzellente Korrelation der spezifischen Tracer-Bindung (R^2=0,9), während die nicht spezifische Bindung nicht korrelierte (R^2=0,2).

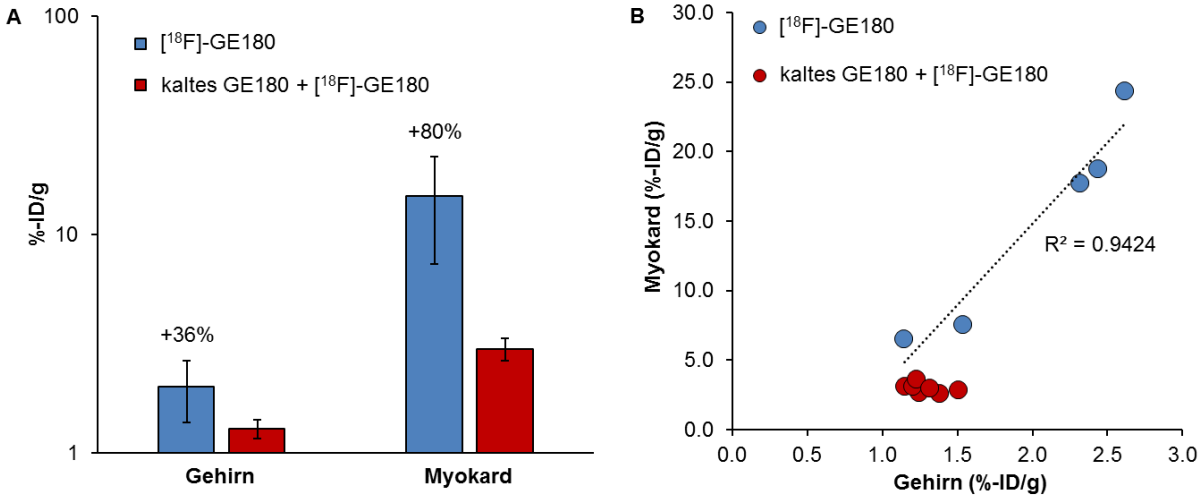

Abbildung 4: Ex-vivo Gamma-Counter Messungen der Tracer Aufnahme in Gehirn und Myokard, jeweils mit (rot) oder ohne (blau) vorheriger Sättigung durch kalten GE180-Tracer.

(**A**) Säulendiagramme (logarithmisch skaliert) zeigen die injizierte Dosis pro Gramm (ID/g) 107 Minuten nach Injektion von [^{18}F]-GE180, Fehlerbalken stellen die Standardabweichung dar. (**B**) Korrelation der individuellen Messwerte des Gehirns und des Herzmuskels.

Eine Untergruppe aus blockierten (N=5) und unblockierten (N=3) Mäusen erhielt zusätzliche dynamische [^{18}F]-GE180 PET Messungen (0 - 90 Minuten) zur Erfassung regionaler zerebraler Unterschiede. Voxel-weise Analysen erbrachten die höchste spezifische Bindung in Hirnregionen, die eine hohe Dichte an ependymalen Gliazellen aufweisen, wohingegen die spezifische Bindung im Cortex nur gering ausfiel.

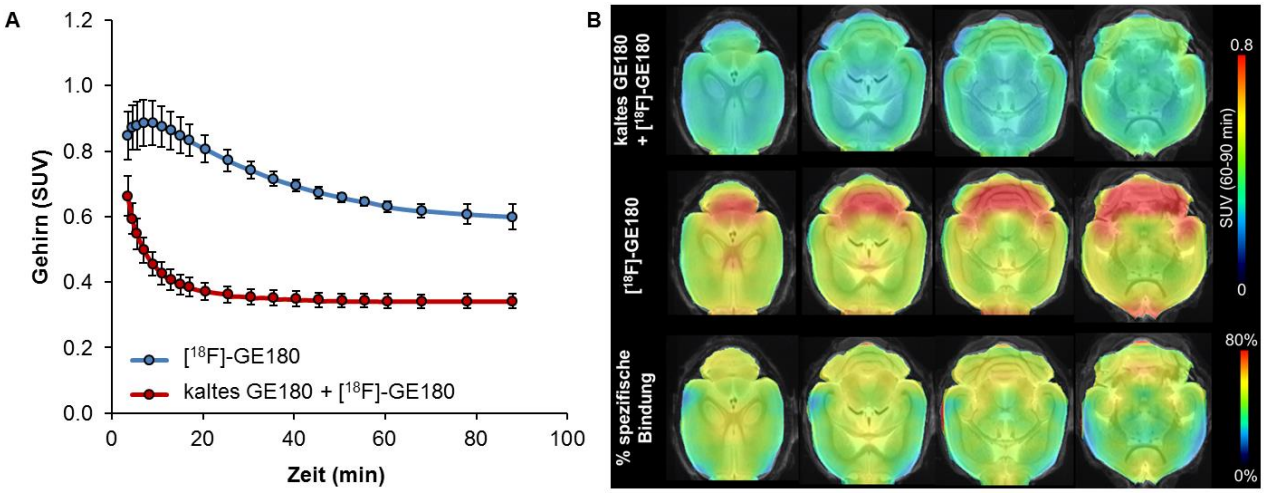

Abbildung 5: (**A**) Zeit-Aktivitäts-Kurven der dynamischen [^{18}F]-GE180 PET Messungen (0-90 Minuten) zeigen die Durchschnittswerte des gemessenen standardisierten Aufnahmewertes (SUV) des Gehirns von geblockten (rot) und ungeblockten (blau) Mäusen. Fehlerbalken repräsentieren die Standardabweichung. (**B**) Axiale Schnittbilder eines statischen 60 – 90 Minuten [^{18}F]-GE180 PET fusioniert auf ein MRT-Mausatlas. Obere Reihe: geblockte Maus, mittlere Reihe: ungeblockte Maus, untere Reihe: % spezifische zerebrale [^{18}F]-GE180-Bindung.

Ergänzende Tracer-unabhängige Untersuchungen zur TSPO-Genexpression in sechs Wildtypmäusen mittels quantitativer Polymerase-Kettenreaktion (qPCR) untermauerten unsere Ergebnisse und ergaben eine 11-fach höhere TSPO-Genexpression im Myokard verglichen zum Herzen der Maus.

Somit konnten wir abschließend zeigen, dass physiologisch ein enger Zusammenhang zwischen TSPO-Expression und spezifischer [^{18}F]-GE180-Bindung im Myokard und Gehirn bei Mäusen besteht, welcher in meiner zweiten Erstautorenschaft **"***Data on specificity of [^{18}F]GE180 uptake for TSPO expression in rodent brain and myocardium*" im Mai 2018 in Data in Brief publiziert wurde.

2.3 Vergleich der Radioliganden [^{18}F]-T807 vs. [^{18}F]-THK5117 in einem Tau-Mausmodell

Ziel meiner Koautorenschaft war der Vergleich zweier Tau-Radioliganden im Hinblick auf die Fähigkeit, longitudinal die Expression der Tau-Pathologie zu überwachen. Dazu erhielten oben beschriebene P301S und Wildtyp-Mäuse (jeweils N = 5 - 7) ab einem Alter von 6 Monaten eine direkte Vergleichsmessung der aktuell am häufigsten verwendeten Gruppen von Tau-Radioliganden ([^{18}F]-T807 versus [^{18}F]-THK5117).

Mein Anteil an dieser Arbeit bestand dabei vor allem in der Charakterisierung des dynamischen Verlaufs von PET Zeitaktivitätskurven der jeweiligen Radioliganden zur Bestimmung des optimalen Akquisitionsfensters und in der Anwendung der gewonnenen Daten auf ein longitudinales Studienkonzept mit anschließender immunhistochemischer Validierung *ex vivo*.

Hierfür wurden dynamische Scans (5 - 65 Minuten nach Injektion) für beide Tracer akquiriert, nach individueller Bewegungskorrektur durch manuelle Co-Registrierung auf ein standardisiertes anatomisches Magnetresonanztomographie-Template des Mäusegehirnes (Dorr, Sled, & Kabani, 2007) fusioniert und anatomische Zielregionen festgelegt (Abb. 6). Aufgrund ausgeprägter extrazerebraler Aktivität durch Tracerbindung im Schädelknochen, diente ein modifiziertes striatales und cerebelläres Zielvolumen als Referenzregion zur Berechnung des jeweiligen standardisierten Uptake-Wertes (SUVR).

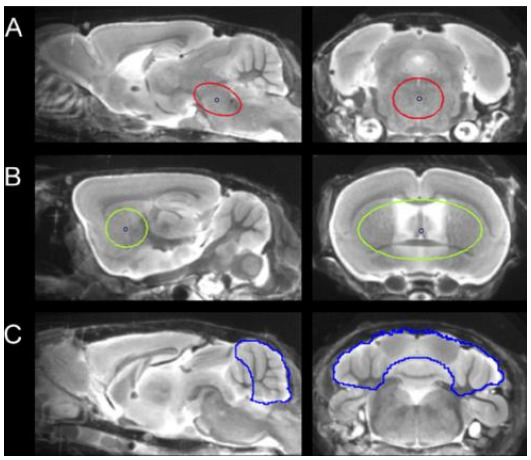

Abbildung 6: Festlegung der anatomischen Zielregionen im MRT-Mausatlas des Mäusegehirnes in sagittalen and coronalen Schnittebenen: Hirnstamm-Zielregion mit Teilen des Pons und des Mittelhirns (rot) (**A**), striatale Zielregion (grün) (**B**) und cerebelläre Zielregion (blau) (**C**).

Wir konnten zeigen, dass sich ab 30 Minuten nach Injektion das PET-Signal stabilisiert und bei [^{18}F]-T807 ein Zeitfenster von 40 - 60 Minuten nach Injektion, für [^{18}F]-THK5117 ein Zeitfenster von 30 - 60 Minuten nach Injektion am besten eignet, um zwischen P301S - und Wildtyp-Mäusen zu differenzieren.

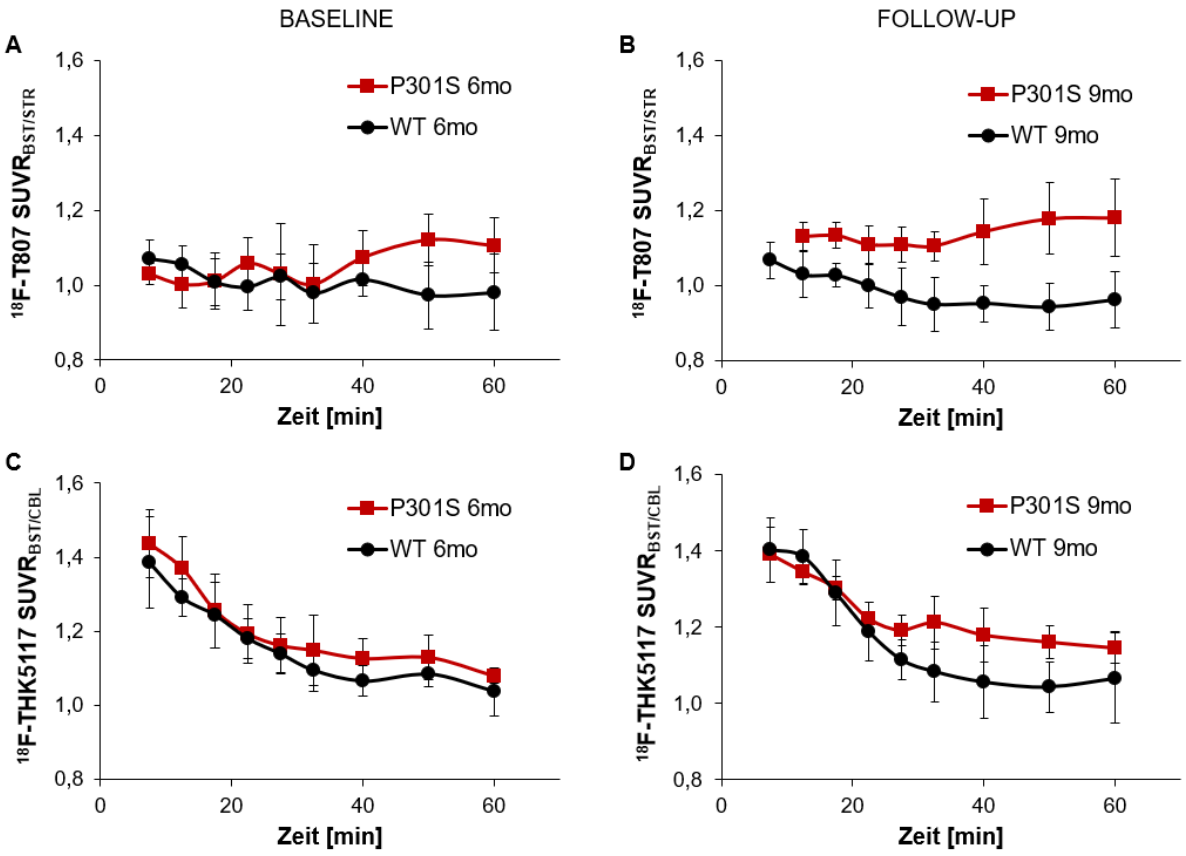

Abbildung 7: Zeit-Aktivitäts-Kurven von [^{18}F]-T807 (**A, B**) und [^{18}F]-THK5117 (**C, D**). Die Messwerte zeigen die Durchschnittswerte des gemessenen standardisierten Hirnstamm-Aufnahmewertes von (rot) transgenen P301S und (schwarz) Wildtyp-Mäusen als Funktion der Messdauer; Fehlerbalken repräsentieren die Standardabweichung.

Durch Anwendung des passenden Zeitfensters und durch die Normalisierung mittels tracer-spezifischer Referenzregion konnten wir eine deutliche Anreicherung von [^{18}F]-T807 im Hirnstamm im Vergleich zur Wildtyp-Kontrollgruppe (+14%, $p < 0,01$) sowie eine starke longitudinale Progression zum Zeitpunkt der Nachverfolgung (Follow-up) (+23%, $p < 0,001$) beobachten. Die Aufnahme von [^{18}F]-THK5117 im Hirnstamm war zu Beginn der Studie ebenfalls gering erhöht (+5%, $p < 0,05$) und stieg bis zum Zeitpunkt der Nachverfolgung weiter an (+10%, $p < 0,05$), die Effektgröße und Sensitivität war bei [^{18}F]-T807 jedoch deutlich höher.

Statistische parametrische voxel-basierte Analysen mittels SPM8 (Statistical Parametric Mapping; Wellcome Departement of Cognitive Neurology) (Rominger et al., 2013) dienten zur Detektion relevanter Unterschiede zwischen transgener und Wildtyp-Gruppe. Insgesamt zeigte sich eine regionale Übereinstimmung der beiden Radioliganden von 71% zum 9-Monats Zeitpunkt.

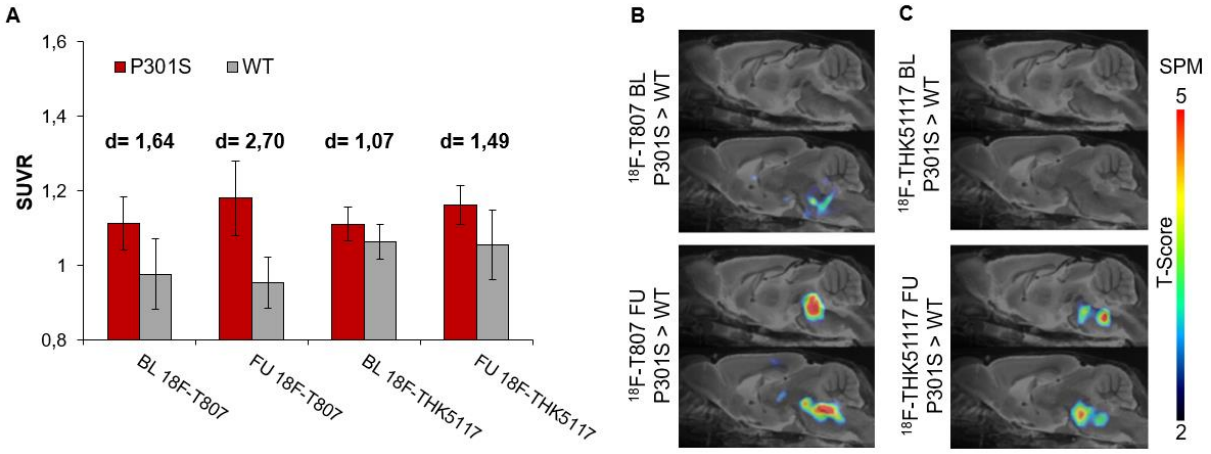

Abbildung 8: (**A**) Hirnstamm PET-Mittelwerte der P301S (rot) und Wildtyp (grau) Mäuse von [^{18}F]-T807 und [^{18}F]-THK5117 zu Beginn (BL) und Follow-up (FU). Fehlerbalken zeigen die Standardabweichung; Effektgrößen sind repräsentiert durch Cohen's d. Voxel-basierte Analysen, fusioniert auf sagittale MRT-Schnittbilder, zeigen den Gruppenvergleich von P301S mit Wildtyp-Mäusen zu Beginn und Follow-up für [^{18}F]-T807 (**B**) und [^{18}F]-THK5117 (**C**). Der T-Score kennzeichnet die Abweichung vom Wildtyp-Kollektiv, ein T-Score >2 entspricht dabei einem Signifikanzniveau $p<0,01$.

Durch Anwendung der bisherigen Ergebnisse auf ein longitudinales Studienkonzept mit Betrachtung der individuellen Kinetik erbrachte für P301S Mäuse eine Zunahme von 5,9 ± 4,5 % mit [^{18}F]-T807 ($p < 0,05$) sowie 4,7 ± 4,4 % bei Verwendung von [^{18}F]-THK5117 (p = nicht signifikant), während Wildtyp-Mäuse im Beobachtungszeitraum bei beiden Tracern stabile Messwerte ohne relevante Veränderungen zeigten. Die im Anschluss an die finalen PET-Messungen durchgeführten immunhistochemischen Untersuchungen ergaben eine positive Korrelation ([^{18}F]-T807: R = 0,68; [^{18}F]-THK5117: R = 0,42) der Traceraufnahme mit der Menge an durch Antikörper gefärbten Mikrotubuli assoziiertem Tau-Protein (MAPT). Darüber hinaus bestätigte sich die Tau-Deposition überwiegend im Hirnstamm bis in die Kleinhirnschenkel reichend, sowie das Fehlen von Tau-Protein in den cerebellären Hemisphären und im Striatum.

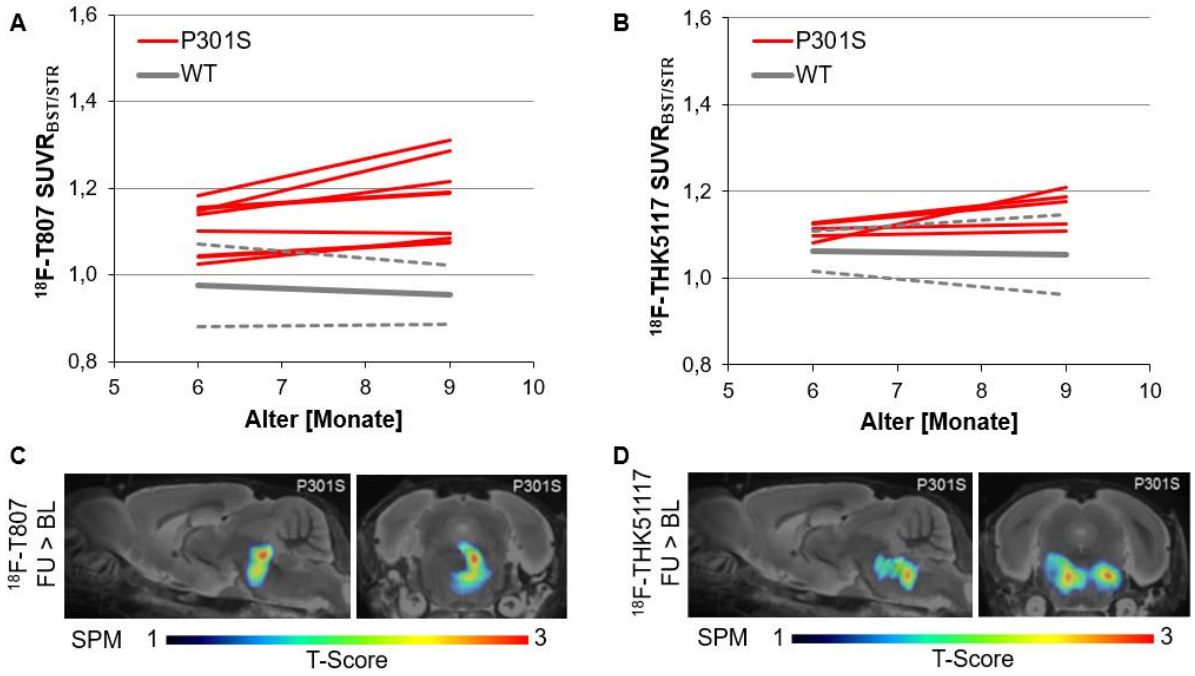

Abbildung 9: Longitudinale Untersuchung für (**A**) [^{18}F]-T807 und (**B**) [^{18}F]-THK5117 in individuellen transgenen und Wildtyp-Mäusen. Dabei repräsentieren die roten Linien die individuelle Kinetik des standardisierten Aufnahmewerts (SUVR) der P301S Mäuse, Wildtyp-Mäuse sind dargestellt durch den Gruppen-Mittelwert mit Standardabweichung (grau). (**C**) Sagittale und coronale Schnitte zeigen voxel-weise Ergebnisse der signifikant zunehmenden Tau-Liganden Bindung in transgenen P301S Mäusen fusioniert auf ein MRT-Template für [^{18}F]-T807 bzw. [^{18}F]-THK5117 (**D**); ein T-Score > 1 entspricht dabei einem Signifikanzniveau von $p < 0,05$.

Insgesamt konnten wir zeigen, dass sich beide Radioliganden zur Durchführung longitudinaler präklinischer Tau-Bildgebung eignen. Im Vergleich zu [^{18}F]-THK5117 zeigte sich für [^{18}F]-T807 eine geringfügig höhere Sensitivität bei der Detektion der Tau-Akkumulation im Hirnstamm, bei jedoch überwiegend hoher regionaler Übereinstimmung beider Liganden.

Diese Ergebnisse wurden im Rahmen meiner Koautorenschaft "*Comparison of 18F-T807 and 18F-THK5117 PET in a Mouse Model of Tau Pathology*“ im Juni 2018 in Frontiers in Aging Neuroscience veröffentlicht.

3. Zusammenfassung

Im Rahmen meiner Promotionsarbeit widmete ich mich zweier Probleme bzw. Fragestellungen bei der präklinischen Bildgebung neurodegenerativer Erkrankungen: 1.) Die bisher etablierte Quantifizierung des TSPO-PET Signals erbrachte unschlüssige Ergebnisse bei Anwendung auf eine Interventionsstudie zur Modulation der Neuroinflammation. Hier galt es eine alternative Methodik zu entwickeln und diese auf Stabilität und Validität zu prüfen. 2.) Es existierten keine direkt vergleichenden PET-Daten der Tau-Tracer der ersten Generation. Hier galt es herauszufinden, welcher Tracer die besten Eigenschaften zur Bildgebung der Tau-Pathologie aufweist.

In meinen beiden Erstautorenschaften befasste ich mich mit einem systematischen Vergleich unterschiedlicher Normalisierungs-Methoden und entwickelte daraus eine alternative Methodik zur Quantifizierung von TSPO-PET Messungen mittels extrazerebraler Myokard-Korrektur.

Hierfür erhielt zunächst eine Gruppe von zehn C57Bl/6 Wildtyp-Mäusen eine dynamische PET-Messung mit [^{18}F]-GE180 und anschließenden *ex vivo* Messungen im Gamma-Counter (Goldstandard). Die ermittelten Einflussgrößen wurden daraufhin anhand eines großen Datensatzes (N = 79) in Wildtyp-Tieren auf deren Wertigkeit und Varianz in Bezug zur Gehirnaktivität analysiert und mittels Regressionsanalyse die Koeffizienten zur Berechnung der Myokardkorrektur ermittelt. Zur Bestimmung der Test-Retest Variabilität, zur Übereinstimmung der normalisierten PET-Ergebnisse mit immunhistochemischen Analysen sowie zur Validierung in ein longitudinales Studienkonzept diente die Anwendung in transgenen PS2APP Mäusen.

Beim Vergleich der untersuchten Normalisierungsmethoden erbrachte eine Kombination aus myokardialer Aktivität zusammen mit injizierter Dosis und Körpergewicht die mit Abstand besten Ergebnisse. So lieferte diese Methodik sowohl die geringste Varianz bei Anwendung auf das große Kollektiv an Wildtyp-Messungen, als auch die beste Übereinstimmung mit der immunhistochemischen Bestimmung der Mikrogliaaktivität in PS2APP Mäusen (Myokard-Korrektur: $R = 0{,}51$; $p < 0{,}01$ vs. Injizierte Dosis: $R = 0{,}44$; $p < 0{,}05$ vs. standardisierter Uptake-Wert (SUV): $R = 0{,}42$; $p < 0{,}05$).

Im longitudinalen Versuchsaufbau über 20 Wochen zeigte sich darüber hinaus eine weitaus höhere Stabilität und eine verminderte Anzahl an Ausreißern bei Verwendung der neu entwickelten Myokardkorrekturmethode (7,7%) im Vergleich zu injizierter Dosis (13,5%; $p < 0,005$) oder SUV (13,5%; $p < 0,005$).

Zur näheren Präzisierung der Verknüpfung zwischen zerebraler und kardialer TSPO-Expression widmete ich mich insbesondere in meiner zweiten Erstautorenschaft der Bestimmung der spezifischen [^{18}F]-GE180-Bindung im Gehirn und Herzen von Wildtyp-Mäusen.
Durch Blocking-Experimente mit kaltem Tracer wurden vorab die TSPO-Bindungsstellen gesättigt und konnten bei der nachfolgenden Applikation des radioaktiv-markierten Tracers nicht mehr binden. Anschließende *ex vivo* Gamma-Counter Messungen erbrachten eine spezifische [^{18}F]-GE180 Bindung von 36% im Gehirn und 80% in der Herzmuskulatur sowie eine exzellente Korrelation der spezifischen Tracer-Bindung in beiden Geweben ($R^2 = 0,9$). PET-Messungen zur Untersuchung der regionalen zerebralen Unterschiede erbrachten die höchste spezifische Bindung in Hirnregionen, die eine hohe Dichte an ependymalen Gliazellen aufweisen sowie verminderte spezifische Bindung im Cortex.
Zusammenfassend ließ sich zeigen, dass physiologisch eine enge Verknüpfung der zerebralen und kardialen TSPO-Expression besteht und sich dadurch die Myokard-Korrektur neben der Normalisierung durch intra-zerebrale Referenzregionen als valide und robuste Methodik zur Stabilisierung zerebraler TSPO Kleintier-PET Messungen mit [^{18}F]-GE180 eignet, welche bereits in Folgestudien erfolgreich ihre Anwendung fand.

Meine Koautorenschaft beschäftigte sich mit dem direkten Vergleich der zwei am häufigsten verwendeten Gruppen von Tau-Radioliganden im Hinblick auf deren Fähigkeit, die Tau-Pathologie longitudinal zu quantifizieren.

Zur Charakterisierung der Tau-Radioliganden [^{18}F]-T807 und [^{18}F]-THK5117 wurden dynamische PET-Scans für beide Tracer in 6 - 9 Monate alten P301S und Wildtyp-Mäusen akquiriert. Nach individueller Bewegungskorrektur und manueller Co-Registrierung wurde aus anatomischen Zielregionen der standardisierte Uptake-Wert (SUVR) berechnet. Nach Bestimmung des optimalen Akquisitionsfensters erfolgte die

Anwendung auf longitudinale Messungen mit anschließender *ex vivo* Validierung mittels immunhistochemischen Färbungen.

Die dynamischen Tau-PET Messungen konnten darstellen, dass sich ab 30 Minuten nach Injektion das PET-Signal stabilisiert und sich für [^{18}F]-T807 ein Zeitfenster von 40 - 60 Minuten, für [^{18}F]-THK5117 ein 30 - 60 Minuten Zeitfenster am besten eignet, um zwischen P301S- und Wildtyp-Mäusen zu differenzieren. Gegenüber der Wildtyp-Kontrollgruppe wiesen P301S-Mäuse für [^{18}F]-T807 einen Anstieg des Hirnstamm-PET Signales bereits im Alter von 6 Monaten auf (+14%, $p < 0,01$) und das PET-Signal stieg bis zum Alter von 9 Monaten weiter an (+23%, $p < 0,001$). [^{18}F]-THK511 zeigte eine geringere Erhöhung gegenüber der Wildtyp-Kontrollgruppe zu den Zeitpunkten von 6 (+5%, $p < 0,05$) und 9 Monaten (+10%, $p < 0,05$). Die Betrachtung der individuellen Kinetik erbrachte für P301S Mäuse eine Zunahme von 5,9 ± 4,5 % des mittels [^{18}F]-T807 ($p < 0,05$) erfassten PET-Signales, sowie von 4,7 ± 4,4 % bei Verwendung von [^{18}F]-THK5117 (p = nicht signifikant), während Wildtyp-Mäuse im Beobachtungszeitraum bei beiden Tracern keine relevanten longitudinalen Veränderungen zeigten.

Insgesamt konnten wir zeigen, dass beide Radioliganden eine hohe regionale Übereinstimmung aufweisen und zur Durchführung longitudinaler präklinischer Tau-Bildgebung eignen, [^{18}F]-T807 jedoch eine geringfügig höhere Sensitivität bei der Detektion der Tau-Akkumulation im Hirnstamm besitzt.

4. Summary

Within my doctoral thesis I focused on two recently upcoming problems in preclinical imaging of neurodegenerative diseases: 1.) Our established TSPO-PET normalization yielded inconclusive measuring data while evaluating the results of an interventional study to modulate neuroinflammation, so it was necessary to develop an alternative quantification method and verify the stability and validity. 2.) Present publications only scantly reported about comparative PET-performances of current first-generation tau-tracers. It therefore had to be established, which tracer shows best characteristics for PET-imaging of tau pathology.

Therefore, the aim of my two lead authorships was to compare different image normalization methods to generate an alternative method to quantify TSPO-PET measurements by extra-cerebral myocardium correction.

To establish a new normalization method a group of ten healthy female C57Bl/6 mice received dynamic PET imaging with [^{18}F]-GE180 followed by *ex vivo* gamma-counter experiments (gold standard). PET data from a large cohort of C57Bl/6 mice (N=79) served for detailed examination of the weighted influence and fitness of the different normalization methods to account for the variance of cerebral tracer uptake to calculate the coefficients for myocardium correction. Test-retest variability, agreement of PET results with immunohistology and application to a longitudinal cohort was tested in transgenic PS2APP mice to challenge and validate the different normalization methods in a practical application.

While testing the performance of the different normalization methods, best results were obtained when myocardial activity was considered in addition to injected dose and body weight. Application of myocardium correction on the large wildtype dataset and longitudinal study design in transgene PS2APP mice generated best stability with lowest variance (7.7%) compared to injected dose (13.5%; $p < 0.005$) or standard-uptake-value (SUV) (13.5%; $p < 0.005$) as well as highest agreement with immunohistochemical staining of microglia (myocardium-correction: $R = 0.51$; $p < 0.01$ vs. injected dose: $R = 0.44$; $p < 0.05$ vs. SUV: $R = 0.42$; $p < 0.05$).

For further specification of the relationship between cerebral and cardiac TSPO-expression my second lead authorship especially focused on characterization of the [^{18}F]-GE180 binding specificity in rodent wildtype brain and myocardium.

Blocking experiments by pretreatment with non-radioactive GE180 followed by gamma-counter measurements revealed a specific [^{18}F]-GE180 binding of 36% in brain and 80% in myocardium as well as excellent correlation between specific TSPO tracer binding in the two tissues (R^2=0.9). Regional *in vivo* positron-emission-tomography (PET) measurements of the brain showed highest specific binding in regions with high abundance of ependymal glia cells, whereas specific binding in the cortex was low.

In conclusion our data provided information about the physiological close relationship between cerebral and cardiac TSPO-Expression. In cases when intracerebral pseudo-reference regions are not suitable, myocardium correction presents a valid and robust approach for stabilization of late phase cerebral TSPO imaging by [^{18}F]-GE180 in rodent brain, which successful found application in further preclinical investigations.

The aim of my co-authorship was to directly compare the two major classes of tau radioligands with regard to their ability to quantify longitudinal expression of tau pathology.

For characterization of dynamic tau-PET performance dynamic PET-scans for each tracer ([^{18}F]-T807 and [^{18}F]-THK5117) were acquired in 6 to 9 months old P301S and wildtype mice. Following frame-wise motion correction and co-registration anatomical volume of interests were employed for calculation of the mean standard uptake value. After validation of the optimal time window by stability analysis of time activity curve ratios and application to longitudinal PET data immunohistochemistry staining of neurofibrillary tangles was performed for validation *ex vivo*.

The dynamic tau-PET signal stabilized after 30 minutes post injection with a 40 - 60 minutes interval giving the best discrimination between P301S and wildtype mice for [^{18}F]-T807. The 30 - 60 min interval gave best results for [^{18}F]-THK5117. Significantly elevated [^{18}F]-T807 binding in the brainstem of P301S mice in comparison to wildtype mice was already evident at 6 months (+14%, $p < 0.01$) and increased further at 9 months (+23%, $p < 0.001$). [^{18}F]-THK5117 indicated weaker increases at 6 months (+5%, $p < 0.05$) and 9 months (+10%, $p < 0.001$) in the same contrast. Individual longitudinal Tau-PET-kinetics in P301S mice were +5.9 ± 4.5% for [^{18}F]-T807 ($p <$

0.05) and +4.7 ± 4.4% for [^{18}F]-THK5117 (p = not significant), while wildtype mice did not show any longitudinal changes for both tracers.

To sum up, both tracers showed high regional binding similarities with the ability of longitudinal micro PET imaging of tau pathology, while analysis of brainstem uptake revealed moderate superiority of [^{18}F]-T807 regarding sensitivity.

NeuroImage 165 (2018) 83–91

Contents lists available at ScienceDirect

NeuroImage

journal homepage: www.elsevier.com/locate/neuroimage

Coupling between physiological TSPO expression in brain and myocardium allows stabilization of late-phase cerebral [^{18}F]GE180 PET quantification

Maximilian Deussing [a], Tanja Blume [a,b], Lena Vomacka [a], Christoph Mahler [c,d], Carola Focke [a], Andrei Todica [a], Marcus Unterrainer [a], Nathalie L. Albert [a], Simon Lindner [a], Barbara von Ungern-Sternberg [a], Karlheinz Baumann [e], Andreas Zwergal [f], Peter Bartenstein [a,g], Jochen Herms [b,g,h], Axel Rominger [a,g,1], Matthias Brendel [a,*,1]

[a] Dept. of Nuclear Medicine, Ludwig-Maximilians-Universität München, Munich, Germany
[b] Center for Neuropathology and Prion Research, Ludwig-Maximilians-Universität München, Munich, Germany
[c] Inst. of Clinical Neuroimmunology, Ludwig-Maximilians-Universität München, Munich, Germany
[d] Biomedical Center (BMC), Ludwig-Maximilians-Universität München, Munich, Germany
[e] Roche Pharma Research and Early Development, Neuroscience Discovery, Roche Innovation Center Basel, F. Hoffmann-La Roche Ltd, Basel, Switzerland
[f] Dept. of Neurology, Ludwig-Maximilians-Universität München, Munich, Germany
[g] Munich Cluster for Systems Neurology (SyNergy), Munich, Germany
[h] Department of Translational Brain Research, DZNE - German Center for Neurodegenerative Diseases, Munich, Germany

ARTICLE INFO

Keywords:
TSPO
[^{18}F]GE180
Small animal PET
Brain uptake normalization
Myocardium

ABSTRACT

Objectives: PET imaging of the 18 kDa translocator protein (TSPO), a biomarker of microglial activity, receives growing interest in clinical and preclinical applications of neuroinflammatory and neurodegenerative brain diseases. In globally affected brains, intra-cerebral pseudo reference regions are not feasible. Consequently, many brain-independent approaches have been attempted, including SUV analysis and normalization to muscle- or heart uptake, aiming to stabilize quantitative analysis. In this study, we systematically compared different image normalization methods for static late phase TSPO-PET imaging of rodent brain.

Methods: We first obtained gamma counter measurements for gold standard quantitation of [^{18}F]GE180 uptake in brain of C57Bl/6 mice (N = 10) after PET, aiming to identify factors contributing significantly to the quantitative results. Subsequently, data from a large cohort of C57Bl/6 mice (N = 79) were compiled to precisely determine the weighted influence and variance attributable these factors by regression analysis. Scan-rescan variability and agreement with histology were used to validate the tested normalization methods in an Alzheimer's disease (AD) mouse model with pathologically increased TSPO expression (PS2APP; N = 24). Longitudinal data from AD model mice (N = 10) scanned at four different ages were used to challenge and validate the different normalization methods in a practical application.

Results: Gamma counter results revealed that injected dose, body weight and PET-measured radioactivity concentration in the ventral myocardium all significantly accounted for [^{18}F]GE180 activity in the brain. Skeletal muscle activity had high test-retest variance in this PET only application and was therefore pursued no further. Regression analysis of the large scale evaluation showed that scaling to injected dose or SUV analysis accounted for little variance in brain activity ($R^2 < 0.5$), but inclusion of myocardial activity together with injected dose and body weight in the regression model accounted for most of the variance in brain uptake ($R^2 = 0.94$). Scan-rescan stability, correlation with histology and applicability for longitudinal examination in the disease model were also significantly improved by inclusion of myocadial uptake in the quantitative model.

Conclusion: Cerebral and myocardial TSPO expression are highly coupled under physiological conditions. Myocardial uptake has great potential for stabilization of static late phase [^{18}F]GE180 quantification in brain in the absence of a valid intra-cerebral pseudo-reference region.

* Corresponding author. Department of Nuclear Medicine, University of Munich, Germany.
E-mail address: matthias.brendel@med.uni-muenchen.de (M. Brendel).
[1] Contributed equally.

https://doi.org/10.1016/j.neuroimage.2017.10.006
Received 6 June 2017; Accepted 3 October 2017
Available online 5 October 2017
1053-8119/

Introduction

The 18 kDa translocator protein (TSPO) is a marker of microgliosis, which presents a molecular imaging target for diverse clinical and preclinical investigations of neuroinflammatory and neurodegenerative brain diseases (Chen and Guilarte, 2008; Turkheimer et al., 2015; Vivash and O'Brien, 2016). Indeed, positron emission tomography (PET) imaging of TSPO is of proven heuristic value in studies of microglia activation in traumatic head injury (Israel et al., 2016) multiple sclerosis (Airas et al., 2015), amyotrophic lateral sclerosis (Gargiulo et al., 2016), glioma (Buck et al., 2015), and neurodegenerative disorders such as Parkinson's disease (Gerhard, 2016), and Alzheimer's disease (AD) (Brendel et al., 2016; Liu et al., 2015; Mirzaei et al., 2016). So far, the quantitation of TSPO brain imaging presents several technical difficulties, which have yet to be resolved. In general, robust quantification based on brief static PET recordings is indispensable to reduce cost and drop-outs in preclinical studies, and to increase compliance and validity in clinical investigations. Quantitation relative to an arterial blood input (Tang et al., 2014) in conjunction with kinetic compartmental analysis of dynamic recordings remains the gold standard for TSPO-PET quantitation (Fan et al., 2016). Nonetheless, dynamic imaging with arterial sampling over 90 min is hardly feasible in clinical routine or in large scale preclinical applications. At least in preclinical imaging it is now widely accepted that late acquisition time frames give stable results for static imaging of TSPO (Brendel et al., 2016; Liu et al., 2015; Mirzaei et al., 2016), but the optimal normalization procedure for static images remains to be settled.

In our preclinical investigation using the third generation TSPO ligand [^{18}F]GE180 in an AD mouse model, we established the fitness of this tracer for quantifying microglial activity by PET (Brendel et al., 2016). In that study, we successfully validated a cerebellar/brainstem white matter pseudo-reference region, based on the very minor AD-like pathology in these brain areas. Furthermore, the stable quantification of microglia activation relative to this intracerebral pseudo-reference region was superior to standardized-uptake-value (SUV) approaches. Human AD studies have also utilized pseudo-reference regions for TSPO quantification (Lyoo et al., 2015). Nonetheless, such approaches may not be valid in disease conditions such as multiple sclerosis, epilepsy or glioblastoma, where widespread microgliosis can preclude the selection of a pseudo-reference tissue devoid of pathology. Others have used normalization to skeletal muscle uptake (James et al., 2015), myocardial uptake (Mirzaei et al., 2016), and %ID (Pihlaja et al., 2015; Zheng et al., 2016) for stabilization of quantitative results, or have simply calculated the SUV by normalization of brain uptake to the injected dose and the body weight (Biesmans et al., 2015). However, a systematic comparison of the different simplified normalization methods has not yet been conducted.

Therefore, the aim of this study was to compare different image normalization methods using preclinical PET recordings with the TSPO ligand [^{18}F]GE180 in wild-type (WT) mice. Gamma counting of tissue samples was used as the gold standard for assessment of PET measurements of brain concentrations, and to identify factors with significant contribution to the quantitative results. Subsequently, we used compiled data from a large cohort of WT mice to precisely determine by regression analysis the weighted influence of several normalization factors on the PET measurements. We also used scan-rescan variability and agreement with histology as indices for validation of the tested normalization methods. Finally, we applied the optimized methods to longitudinal brain PET recordings from a well characterized transgenic AD mouse model.

Material and methods

Study design

All experiments were performed in compliance with the National Guidelines for Animal Protection, Germany, with approval of the local animal care committee of the Government of Oberbayern (Regierung Oberbayern), and overseen by a veterinarian. The protocol was approved by the Government of Oberbayern. The study design consisted of four modularly structured blocks:

1.) Ten healthy female C57Bl/6 mice (aged 16.0 ± 3.7 months), assumed to have a uniform TSPO expression in brain, were used for gold standard gamma counter experiments. All mice underwent an [^{18}F]GE180 PET scan, whereupon they were immediately killed by decapitation; the entire brain was removed, weighed, and its radioactivity content measured by gamma counting. We recorded the injected dose, body weight, and the uptake of [^{18}F]GE180 to myocardium and skeletal muscle to PET (60–90 min), for regression analysis of factors influencing cerebral tracer uptake.
2.) [^{18}F]GE180 PET data from a total of 79 female C57Bl/6 mice (aged 7.4 ± 1.6 months), likewise assumed to have constitutively low and uniform TSPO expression in brain, were compiled from different ongoing investigations, and used for a detailed examination of the weighted influence of the factors established in 1), above. Furthermore, we compared the fitness of the different normalization methods to account for the variance of cerebral [^{18}F]GE180 uptake in the large cohort.
3.) [^{18}F]GE180 PET data from a well-characterized AD mouse model (PS2APP; N = 24; female; 5–16 months of age) were used to study scan-rescan variability (N = 10) and agreement of PET results for different normalization methods with histology (N = 24).
4.) Longitudinal [^{18}F]GE180 PET data from PS2APP mice (N = 10; female; untreated) at four ages extending from 9 to 14 months of age were used to challenge and validate the different normalization methods in a practical application.

Animal models

Female wild-type C57Bl/6 mice and data derived from female PS2APP transgenic mice were used in this investigation. C57Bl/6 mice were purchased from Charles River (Sulzberg, Germany). The double transgenic B6.PS2APP (line B6.152H) is homozygous for the human presenilin (PS) 2, N141I mutation and for the human amyloid precursor protein (APP) K670N, M671 L mutation. The APP and PS2 transgenes are driven by mouse Thy-1 and mouse prion promoters, respectively. This line had been created by co-injection of both transgenes into C57BL/6 zygotes (Richards et al., 2003). Homozygous B6.PS2APP (PS2APP) mice show first appearance of plaques in the cortex and hippocampus at 5–6 months of age (Ozmen et al., 2009).

Radiochemistry

Radiosynthesis of [^{18}F]GE180 was performed as previously described (Wickstrom et al., 2014), with slight modifications (Brendel et al., 2016), a procedure yielding radiochemical purity exceeding 98%, and specific activity of 1 400 ± 500 GBq/μmol at end of synthesis.

TSPO PET acquisition and reconstruction

Mice were anesthetized with isoflurane (1.5%, delivered via a mask at 3.5 L/min in oxygen) and received a bolus injection of 12.8 ± 2.4 MBq [^{18}F]GE180 in 150 μL of saline to a tail vein. Following placement in the tomograph (Siemens Inveon DPET), at 45 min post-injection, a 15 min transmission scan was obtained using a rotating [^{57}Co] point source, which was followed by a single frame emission recording for the interval 60–90 min post-injection. A subset of 24 PS2APP mice was imaged in a dynamic 0–90 min setting (21 frames: 3 × 60 s, 6 × 120 s, 9 × 300 s, 3 × 600 s) with emission starting directly after tracer injection which was followed by a 15 min transmission scan. In terminal experiments, the mice were killed at the end of the recording by cervical dislocation whilst

in a state of deep narcosis. The image reconstruction procedure consisted of three-dimensional ordered subset expectation maximization (OSEM) with four iterations and twelve subsets followed by a maximum *a posteriori* (MAP) algorithm with 32 iterations. Scatter and attenuation correction were performed and a decay correction for [^{18}F] was applied. With a zoom factor of 1.0 and a 128 × 128 x 159 matrix, a final voxel dimension of 0.78 × 0.78 × 0.80 mm was obtained.

Image analysis

Spatial brain co-registration

Static emission datasets (60–90 min) were manually co-registered to a MRI mouse atlas (Dorr et al., 2007) by a manual rigid-body transformation (TX_{rigid}) using the PMOD fusion tool (V3.5, PMOD Technologies Ltd.), after blinding the reader to the mouse identity. In the second step, a reader-independent automatic re-registration to tracer-specific templates was performed as reported previously (Overhoff et al., 2016). The templates had been generated by averaging all PET scans for a given age. Initial manual μPET-to-MRI atlas fusion images were normalized by non-linear brain normalization (TX_{BN}) to the template using the PMOD brain normalization tool (equal modality; smoothing by 0.6 mm; nonlinear warping; 16 iterations; frequency cutoff 3; regularization 1.0; no thresholding). The concatenation of TX_{rigid} and TX_{BN} was then applied to μPET frames in the native space to obtain optimal resampling with a minimum of interpolation. This procedure was as well applied to dynamic scans and the concatenation of transformations (deriving from 60 to 90 min) was finally applied to the 0–90 min multi-frame file.

Assessment of glial activity in brain

The whole brain [^{18}F]GE180 concentration (kBq/cc, 60–90 min) was measured in a volume-of-interest (VOI) defined by the MRI template. The VOI, comprising 525 mm^3, included the entire cerebrum, cerebellum, brainstem and olfactory bulb. For correlation analysis with histology, a spatially matched VOI placed on the frontal cortex (15 mm^3) was used to measure the local TSPO PET signal. Furthermore, white matter activity in cerebellum and brainstem was obtained by the previous established intracerebral reference region (Brendel et al., 2016). Full dynamic data of cohort 3) was used to calculate distribution volume ratios (DVR) for the frontal cortex by use of the white matter reference region, as described previously (Brendel et al., 2016).

Assessment of myocardial and muscle tracer uptake

Myocardial uptake was measured at circulation time 60–90 min by placing a standard cubic VOI (70 mm) around the anterior ventricle, with a threshold intensity set to 30% of the hottest voxels (Fig. 1A). Accurate VOI positioning was confirmed by inspection in axial, sagittal and coronal projections, to minimize spill-over effects from adjacent pulmonary tissue. The resulting VOI consisted of 34.8 ± 6.5 mm^3 and contained 73 ± 14 voxels after thresholding to 30% peak. Our threshold method is an adaption of an earlier PET study of myocardial hypertrophy (Gross et al., 2016). For calculating muscle tracer uptake, two skeletal muscle VOIs per forelimb, resulting in four VOIs per mouse, were drawn manually, and the mean muscle uptake was calculated (Fig. 1B) (James et al., 2015).

All data of myocardium and muscle VOI assessments were acquired twice in data examination sessions two weeks apart to assess methodological test-retest performance for these two muscle normalization methods.

Gamma counter measurements

10 C57BL/6 WT female mice (28.9 ± 4.5 g; 16.0 ± 3.7 months of age) were anesthetized with 1.5% isoflurane and [^{18}F]GE180 (13.3 ± 2.6 MBq) was injected through a tail vein. As above, emission recordings consisting of a single frame (60–90 min p.i.) were preceded by a 15 min transmission scan, and reconstruction algorithms were likewise as described above. Immediately upon conclusion of the PET sessions, mice were decapitated, and the brains removed. Whole brain was weighed, and radioactivity concentration measured in a gamma counter (Cobra Quantum 5002, Packard) cross-calibrated to the tomograph, with decay-correction to time of tracer injection for the final SUV calculations.

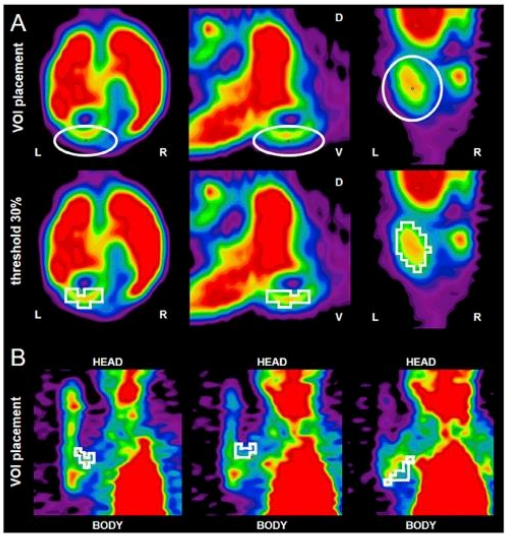

Fig. 1. VOI definition of myocardium and muscle. (**A**) Upper row shows placement of an oval-shaped myocardial VOI onto the anterior heart wall. Lower row depicts the automatic selection of 30% of the hottest voxels in the VOI by thresholding; from left to right: axial, sagittal, and coronal projection. L = left; R = right; V = ventral; D = dorsal. (**B**) Illustration of muscle VOI placement in coronal slices.

Immunohistochemistry

Immunohistochemical data assessed by IBA-1 staining for activated microglia were used from a previous study (Brendel et al., 2016). In brief, the summed area of stained microglia in the cerebral cortex was calculated as %-area. 24 PS2APP mice were available for this analysis.

Blocking experiments and TSPO expression analyses

Specificity of [^{18}F]GE180 uptake in brain and myocardium was characterized by blocking with cold radiotracer followed by [^{18}F]GE180 PET and gamma counter assessment *ex vivo* (Deussing et al., 2017). Expression levels of TSPO were quantified by polymerase chain reaction (qPCR) and compared with PET results (Deussing et al., 2017).

Statistics

IBM SPSS Statistics (version 23.0; SPSS, Chicago, IL) was used for all statistical tests. Multiple regression analysis was performed to investigate the association of injected dose, body weight, myocardial uptake, and skeletal muscle activity with measurements of cerebral tracer uptake *ex vivo* as the dependent variable. The standardized regression coefficients (β) are reported, and the significance of each factor was assessed. Test-retest variability (%) was calculated for assessments of myocardial and muscle uptake as well as for validation by a scan-rescan dataset.

Mean ± SD for injected dose, body weight and myocardial uptake were obtained for the large dataset of 79 C57Bl/6 mice. Z-transformation

was applied to express all covariates in terms of SD relative to the group mean. Step-wise multiple regression analysis was performed with z-transformed variates to investigate the precise contribution of each variate to the overall variance in cerebral [^{18}F]GE180 uptake.

Correlation between cortical TSPO signal to PET and %-area by immunohistochemistry was calculated as the Pearson's coefficient of correlation (R). DVR data deriving from dynamic imaging of 24 PS2APP mice were correlated with endpoints of all brain-independent methods.

In the longitudinal PET dataset, we applied a standardized measure of dispersion as the 'coefficient of variation' (CV), which was defined as the ratio of the standard deviation to the mean (expressed as %-SD). The intra-individual homoscedasticity was assessed using a Levine's test; Tamhane-T2 *post hoc* test for multiple comparisons was applied for inter-method contrasts. Root-mean-square-deviations (RMSD) in individual mice from the mean slope were obtained for the follow-up time points relative to the baseline. We considered a threshold of $p < 0.05$ to be significant for rejection of the null hypothesis in all statistical tests.

Results

Test retest of myocardium and muscle measures and gamma counter assessment

Test retest results deriving from PET data proved excellent stability for the threshold-based radioactivity extraction from the ventral myocardium (test-retest variability: 1.6 ± 2.5%). Mean myocardial uptake was 788 ± 258 kBq/cc. PET assessment of skeletal muscle activity had a considerably higher variance (test-retest variability: 17.3 ± 11.7%), such that we did not further pursue that normalization approach.

Injected dose ($\beta = 0.40$; $p = 0.006$), body weight ($\beta = -0.30$; $p = 0.002$) and [^{18}F]GE180 activity concentration in the myocardium obtained by PET ($\beta = 0.64$; $p = 0.0003$) significantly accounted for cerebral [^{18}F]GE180 radioactivity measured *ex vivo* ($F_{(3,\ 6)} = 226.0$; $p < 0.001$; $R^2 = 0.991$; $R^2_{adjusted} = 0.987$).

Large scale evaluation

We tested the performance of the different normalization methods in the large dataset of WT mice of comparable age (7.4 ± 1.6 months). Regression analysis revealed the lowest explanation of variance in brain activity through simple scaling to the injected dose ($F_{(1,\ 77)} = 57.4$; $p < 0.001$; $R^2 = 0.427$; $R^2_{adjusted} = 0.420$; Fig. 2A). Little improvement was observed with additional use of the body weight for calculation of SUV ($F_{(2,\ 76)} = 36.9$; $p < 0.001$; $R^2 = 0.493$; $R^2_{adjusted} = 0.480$; Fig. 2B). By far the highest explanation of variance was obtained when the myocardial activity was considered in addition to injected dose and body weight ($F_{(3,\ 75)} = 406.7$; $p < 0.001$; $R^2 = 0.942$; $R^2_{adjusted} = 0.940$; Fig. 2C).

Regression coefficients were obtained for the latter method to assess the weighted influence of the three contributory factors, after standadization of individual values by z-transformation (Table 1). The highest single contribution was observed for the myocardial uptake ($\beta = 0.846$) followed by the injected dose ($\beta = 0.191$) and the body weight ($\beta = -0.031$).

Validation by scan-rescan data, dynamic imaging and histology in a disease model

Application of different normalization methods to a dataset for PS2APP mice with two TSPO PET scans within a single week gave distinctly lower scan-rescan variability by the myocardium correction method (2.6 ± 2.4%) when compared to ID or SUV (both 12.4 ± 9.7%; $p < 0.05$), which was in the range of scan-rescan variability obtained for this tracer previously by white matter reference region normalization (1.9%) (Brendel et al., 2016).

Correlation of results of the scaling methods for TSPO quantification to the DVR in PS2APP mice indicated the highest correlation for the myocardium correction method (Fig. 3).

Correlation of cerebral [^{18}F]GE180 uptake with %-area values by IBA-1 staining in the frontal cortex, as the brain area of highest TSPO expression and amyloid deposition of PSPAPP mice, also indicated the highest agreement when the myocardium correction was applied ($R = 0.51$; $p < 0.01$), with lesser correlations seen for ID ($R = 0.44$; $p < 0.05$) and SUV ($R = 0.42$; $p < 0.05$) (Fig. 4). Performance of our previously reported scaling to an intracerebral reference region ($R = 0.61$) (Brendel et al., 2016) was superior to the present methods.

Application to longitudinal data in a disease model

Different normalization methods were applied to a longitudinal dataset of transgenic mice to investigate their fitness in a realistic study setting (in vivo monitoring of elevated TSPO expression in PS2APP mice). Levine's test for homoscedasticity between different normalization

Table 1
Regression analysis for assessment of the optimal weighting of contributing factors to cerebral [^{18}F]GE180 uptake. β = beta, RC = regression coefficient.

Normalization Method	Mean	SD	β	RC	p-value
Injected Dose (MBq)	14.3	1.6	0.191	9.794	$p < 0.001$
Body weight (g)	25.4	3.7	−0.031	−2.420	$p = 0.294$
Myocardial activity (kBq/cc)	844.2	273.6	0.846	44.578	$p < 0.001$

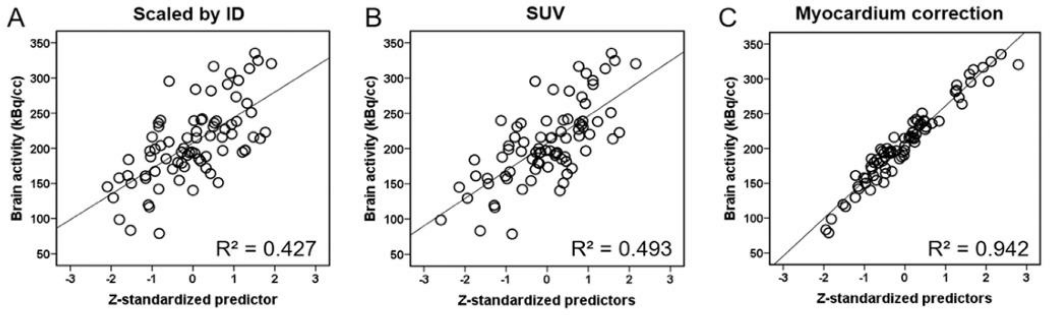

Fig. 2. Regression analysis for comparison of different normalization methods in a large dataset of WT mice. Plots depict the low explanation of variance in brain activity when scaling to the injected dose (**A**) or calculated SUV (**B**). A considerably higher explanation of variance was achieved when the myocardial activity was considered in addition to injected dose and body weight (**C**). Predictors (injected dose, body weight, myocardial uptake) are expressed after z-transformation.

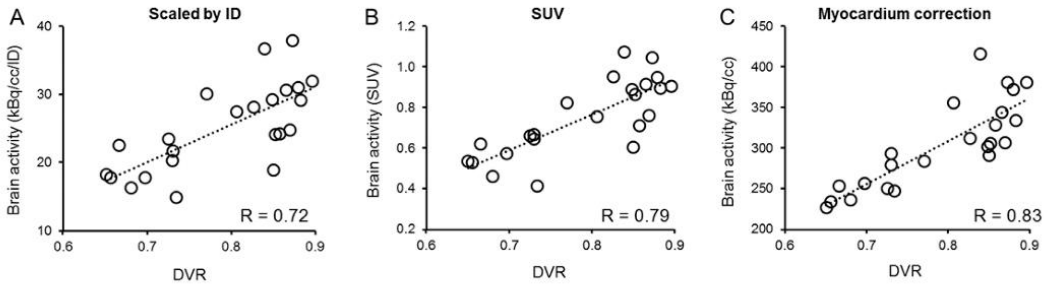

Fig. 3. Correlation analysis of different normalization methods with full dynamic imaging in an amyloid mouse model (PS2APP). Plots show the correlation of brain-independent 60–90 min PET quantification of the cortex by (**A**) ID%, (**B**) SUV, (**C**) myocardium correction, with 0–90 min distribution volume ratios (DVR), deriving from Logan analysis with white matter reference.

methods indicated highly diverging variance ($L = 69.85$; $p < 0.001$) to follow-up. Variance was significantly lower by the myocardium correction method (CV: 6.5 ± 2.0%) when compared to ID (CV: 14.5 ± 2.5%; $p < 0.001$) and SUV (CV: 14.5 ± 1.8%; $p < 0.001$). The normalization to white matter (Brendel et al., 2016) gave significantly lower variance than the present brain-independent approaches (CV: 3.3 ± 0.6%; all: $p < 0.001$). Fig. 5 illustrates the test-retest variance of all different normalization methods graphically.

Visual interpretation of individual longitudinal TSPO kinetics in control mice over 20 weeks indicated far higher stability when using the myocardium correction method when compared to ID and SUV, as illustrated in Fig. 6. When using the mean slope of each method over time, significantly lower RMSD were observed for the myocardium correction method (7.7%) when compared to ID (13.5%; $p < 0.005$) and SUV (13.5%; $p < 0.005$). The intracerebral reference scaling yielded lower intra-individual deviations from the mean slope (RMSD: 2.8%).

Blocking experiments and TSPO expression analyses

Results of pre-blocking of TSPO by treatment with non-radioactive GE180 indicated a higher specific binding in the myocardium (80% of total tracer binding) when compared to that in brain (36% of total tracer binding), (see Fig. 1A in (Deussing et al., 2017)). There was a correlation between specific TSPO binding in myocardium and brain, whereas unspecific binding was not correlated (see Fig. 1B in (Deussing et al., 2017)). The specific TSPO activity in the myocardium exceeded that of the whole brain by 17-fold. Regional analyses revealed the highest specific binding in regions with abundant ependymal glia cells, e.g. adjacent to the fourth ventricle, whereas specific binding in the cortex was low (see Fig. 2 in (Deussing et al., 2017)). qPCR gave comparable results showing far higher TSPO gene expression levels (11-fold) in the myocardium when compared to the brain (see Fig. 3 in (Deussing et al., 2017)).

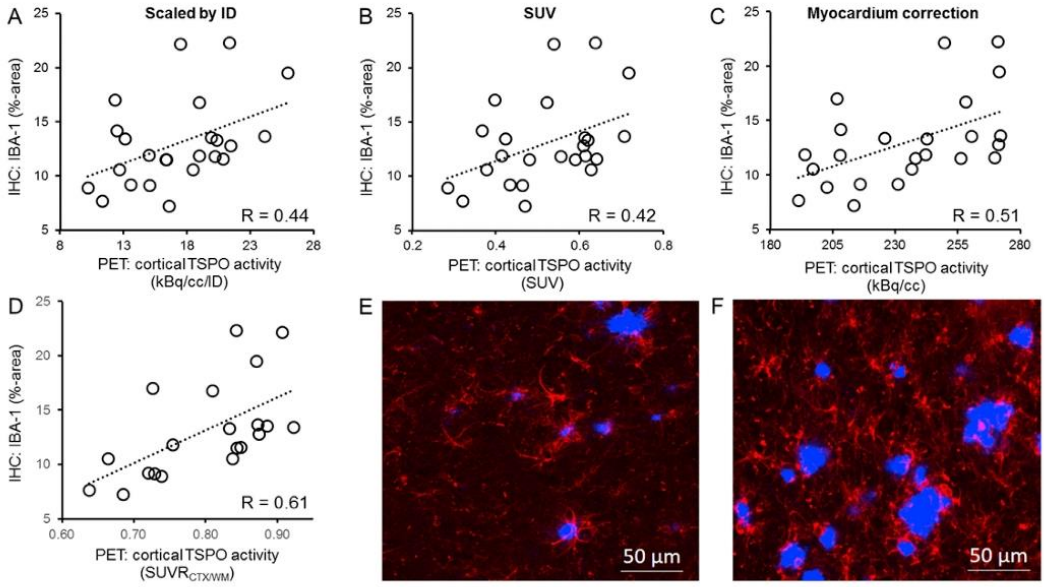

Fig. 4. Correlation analysis of different normalization methods with TSPO immunohistochemistry in an amyloid mouse model (PS2APP). Plots show the correlation of cortical PET quantification by (**A**) ID%, (B) SUV, (**C**) myocardium correction, and (**D**) SUVR with activated microglia as assessed by IBA-1 staining (%-area). Stainings illustrate an exemplary mouse (**E**) with low IBA-1 reactivity (red) and low amyloidosis (blue) as well as an exemplary mouse (**F**) with high IBA-1 reactivity (red) and high amyloidosis (blue).

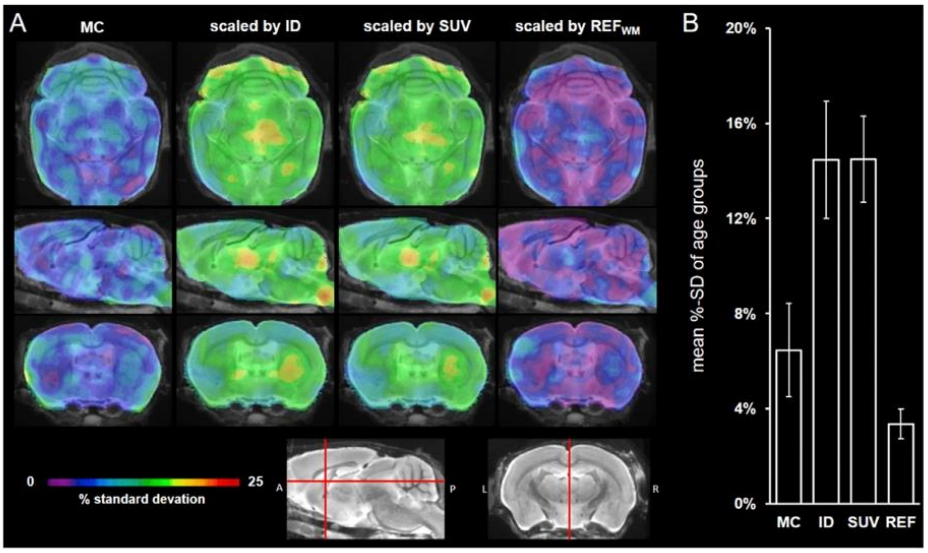

Fig. 5. Test-retest variance of different [^{18}F] GE180 normalization methods in groups of PS2APP mice. (**A**) Standard deviation maps of uptake in coronal and axial views indicate the lower %-SD exemplified for the baseline group for normalized including a myocardium correction or by intra-cerebral reference region, compared to results with scaling by ID or SUV. (**B**) Bar graphs represent mean %-SD of the four age groups subdivided for the different normalization methods. MC = myocardium correction; ID = scaling by the injected dose; SUV = standardized uptake value; REF = intracerebral reference region.

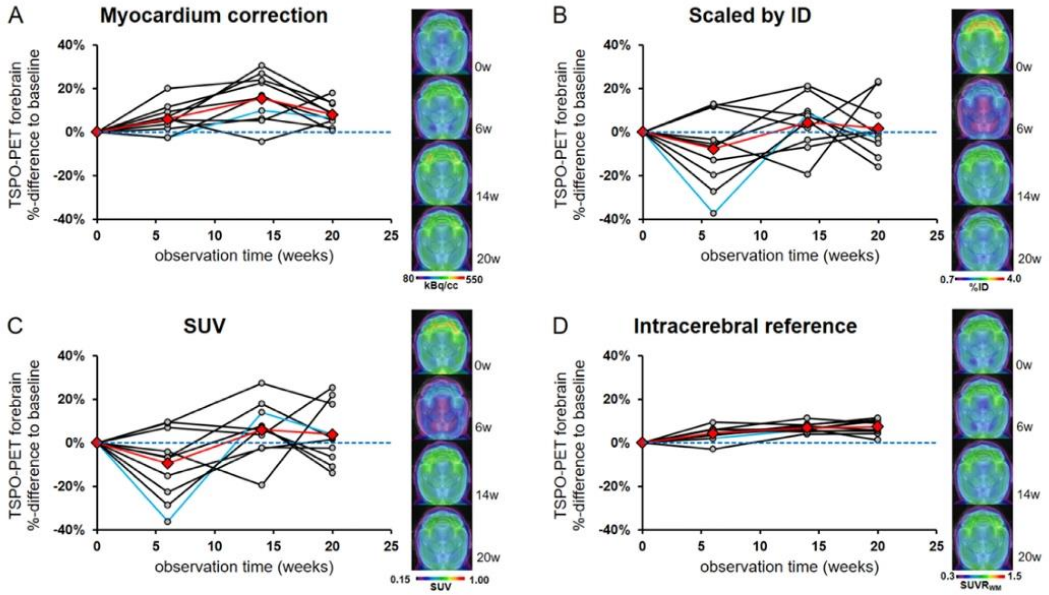

Fig. 6. Longitudinal progression of [^{18}F] GE180 PET in a murine AD disease model by use of different normalization methods: Serial observations of increasing TSPO uptake in brain of the PS2APP animals over 20 weeks indicates higher stability and less %-variance from the mean slope when using the myocardium correction method (**A**) compared to ID (**B**) and SUV (**C**). Intracerebral reference (**D**) gave the lowest intra-individual deviations. Note the axial slices of a representative mouse (blue lines) to the right of the plots, which visually convey an implausible longitudinal kinetic of the [^{18}F]GE180 PET signal when ID or SUV normalization was used (**B, C**). Black lines represent individual mice, and red lines represents the group mean (N = 10 PS2APP mice; 8–13 months of age).

Discussion

This is the first preclinical investigation comparing different normalization methods for late phase brain TSPO PET-imaging using the novel third generation ligand [^{18}F]GE180. Relative to gamma counter measurements *ex vivo*, we saw significant and independent impacts of ID, body weight and myocardial uptake on the cerebral tracer uptake in groups of control mice expected to have similar and homogeneous TSPO binding in brain. Regression analysis in a large dataset revealed far superior explanation of the variance in cerebral [^{18}F]GE180 uptake when myocardial uptake was additionally considered for normalization, as compared to ordinary ID and SUV normalizations. Thus, the strikingly observed coupling between cerebral and myocardial TSPO expression under physiological conditions stabilized the quantification of tracer uptake in the brain. The myocardium correction method was successfully validated by scan-rescan data and histologically verified datasets deriving from animals with pathologically elevated TSPO expression. Application to a longitudinal dataset of these transgenic AD mice showed a reduced number of outliers in sequential imaging, aiming to monitor disease-related elevation of TSPO expression, and decreased variance of the uptake through use of the proposed myocardium correction method.

The question arises why myocardial [^{18}F]GE180 uptake serves so aptly for normalization of the individual brain uptake. To date, there is a single report showing a possible relationship between TSPO binding sites (also measured with [^{18}F]GE180) in heart and brain in a mouse model of myocardial infarction (Hupe et al., 2016). We suppose that the TSPO expression in brain and heart might be under common regulation, depending upon the physiological state of the animal. This would potentially minimize confounders differentially affecting TSPO expression between tissue types. The observations of high variances when scaling cerebral uptake to the ID or SUV (Fig. 2) indeed suggest that diverse intra-individual factors may destabilize these normalizations between individual mice, but also between longitudinal scans of the same animal (Fig. 6 B C). Elaborating this concept further, TSPO levels in different tissues can be upregulated by acute stress or down-regulated by chronic stress (Morin et al., 2016). It seems obvious that individual mice may have differing vulnerability to stress from handling and anesthesia induction. However, for the present it remains a matter of conjecture that stress levels can contribute to the variability of [^{18}F]GE180 PET signals normalized by SUV calculation. We suppose that coupled regulation of TSPO in heart and brain, irrespective of altered regulation of TSPO in other tissues, likely account for strong stabilization of cerebral TSPO uptake by myocardium normalization. Importantly, the coupling was absent for the additional pathophysiological increase of the TSPO signal seen in the AD disease model, which is known to have increased cerebral TSPO binding (sections 3.3 and 3.4). Thus, our scaling method only stabilizes the estimation of physiological background uptake, and thus enables the sensitive detection pathological alterations with a lower variance. This conclusion was also strengthened by results of blocking experiments, which revealed inter-relation of the specific physiological binding densities in brain and myocardium of WT mice (Deussing et al., 2017).

The observed scan-rescan variability with the newly-introduced myocardium correction method was gratifyingly low (2.6%), which substantiates its superiority to conventional ID or SUV normalizations. Regression analysis in a large dataset of control mice (assumed to have similar TSPO binding in brain) also showed that variance in myocardial uptake was the major driver for accommodating the variance ($R^2 = 0.94$). Thus, our method proved to be very robust, although with the caveat that we have not measured arterial input functions, and assume that our immunological marker is a surrogate for the true TSPO expression in brain. Robust preclinical imaging of late phase [^{18}F]GE180 uptake with brief PET recordings will likely decrease the number of drop-outs and increase the cost-efficiency for large-scale studies with, for example, intervention arms.

The rationale for the PS2APP AD mouse model in the longitudinal validation arm of this study was based on the known correlation of the [^{18}F]GE180 PET signal with microglia measurements with IBA-1 immunohistochemistry in vitro (Brendel et al., 2016). This relationship as well allowed us to test for agreement between cortical [^{18}F]GE180 uptake values and %-area of IBA-1 in the same cortical region. Here we found higher agreement for the myocardium correction method than for other approaches, excepting the intracerebral (white matter) reference approach. Thus, the immunohistochemically-assessed surrogate of neuroinflammatory disease was well captured by the proposed method for [^{18}F]GE180 PET analysis. Furthermore, we found that with this normalization the progress of neuropathology tended to be nearly linear across the present age group of AD mice, a trait which facilitated the testing of individual longitudinal data (relative to baseline) against the mean slope of the group, as an indicator of stability. Our data clearly revealed superior performance of the myocardium correction method compared to ID and SUV scaling. Outliers with implausible decreases in brain uptake occurred by ID and SUV normalization (Fig. 6), which would substantially hamper the reliability of such analysis methods for longitudinal observations of individual mice. Scaling to our previously-evaluated intracerebral pseudo-reference region was feasible and valid in the PS2APP model, as the developing amyloid pathology has a negligible effect on TSPO expression in white matter regions of cerebellum and brainstem. Such approaches are likewise feasible when disease pathology is restricted to one hemisphere, as in a focal cerebral ischemia model (Tiwari et al., 2015). We find the highest longitudinal stability by the pseudo-reference white matter scaling, but with the caveat that global effects of treatment or disease model on TSPO expression in brain cannot be excluded a priori. In such scenarios, the pseudo-reference region approach would induce bias masking the real microglial changes in the cerebral grey matter.

Relative to rodent studies, TSPO imaging in humans suffers from low brain permeability, and the consequently low signal-to-noise ratio hampers quantification (Vivash and O'Brien, 2016). Although signal-to-noise ratios have improved with development of third generation TSPO ligands, the optimal quantification method remains an issue (Vivash and O'Brien, 2016). In a recent human PET study with kinetic modelling of [^{18}F]GE180 uptake relative to the metabolite corrected arterial input, the authors settled upon dynamic imaging over 90 min and a reversible two-tissue compartment model as the optimal method for this ligand in humans (Fan et al., 2016; Feeney et al., 2016). While this seems beyond dispute, it remains the case that such a demanding experimental protocol can hardly be transferable to routine clinical (or for that matter preclinical) imaging. Thus, there remains an urgent need for robust and facile simplified approaches to TSPO quantitation. We can only speculate that our preclinical myocardium correction method may be translatable to the case of human imaging. However, a single pilot study has shown promising results with scaling to a single 5-min myocardial scan after completion of the [^{18}F]GE180 head scan (unpublished observations). Naturally, it must be considered that cardiac disease may perturb myocardial tracer uptake, thus limiting the applicability of this approach in clinic. However, many patients with conditions presenting a target for TSPO imaging, such as multiple sclerosis or glioblastoma, will undergo clinical imaging at ages were cardiac diseases are rare. Thus, the proposed method may find translational employment in human PET studies.

Limitations

Body weight did not exhibit a significant independent influence on [^{18}F]GE180 brain uptake to PET in the regression analysis of the extensive dataset of WT mice. This presumably indicates the leveling effect of rather homogenous body weights and dosages in that group. Nonetheless, body weight contributed a significant explanation of variance to the gamma counter analysis, a difference presumably related to the greater variation of body weight in that experiment, which occurred by design. We included older animals in that group, aiming to obtain higher variance in body weight. Thus, favor including body weight as a minor factor

influencing the myocardium scaling method, especially if the study group includes mice as heavy as 40 g.

Skeletal muscle tracer activity proved difficult to measure accurately by PET, which propagated to excessively high test-retest variability. Hybrid PET/MR or PET/CT imaging would probably facilitate a more accurate VOI definition, perhaps supporting more convenient scaling of brain uptake to skeletal muscle. The variability could as well be decreased by expending more effort in repeated assessments (e.g. the mean of 10 replications). The use of skeletal muscle for PET normalization in studies investigating pathological alterations of TSPO activity in the myocardium might be particularly interesting.

Conclusion

Scaling to myocardial uptake has great potential to facilitate stabilization of late phase cerebral TSPO imaging by [^{18}F]GE180 in mice. In cases when intracerebral pseudo-reference regions are not suitable, myocardial scaling presents a workable approach for convenient analysis of rodent brain [^{18}F]GE180 uptake, being clearly superior to ID or SUV scaling. Translation of this approach to human scanning, requiring only a brief second recording over the thorax, may prove useful for TSPO PET data analysis in a practicable clinical setting, where economy is of great importance.

Conflict of interest statement

MD reports no disclosures; TB reports no disclosures; LV reports no disclosures; CM reports no disclosures; CF reports no disclosures; KB is an employee of F. Hoffmann-La Roche; AT reports no disclosures; MU reports no disclosures; NA reports no disclosures; SL reports no disclosures; BU reports no disclosures; AZ reports no disclosures; PB received consultant fees from GE and Piramal Imaging, and honoraria from Siemens; JH reports no disclosures; AR received consultant fees from Piramal Imaging and GE; MB reports no disclosures.

Author contributions

MD carried out the PET experiments, performed the data analysis, contributed to statistical analysis and drafted the manuscript; TB carried out the histological experiments, and performed the histological data analysis; LV performed statistical programming and PET analysis; CM carried out qPCR analysis and interpretation; CF carried out the PET experiments, and performed PET data analysis; AT transferred knowledge for the method and contributed intellectual content to the data analysis; MU worked on the translational aspect and provided intellectual content; NA worked on the translational aspect and provided intellectual content; SL carried out the radiosynthesis and performed radiochemical analysis; BU contributed to PET experiments and supervised animal care; AZ participated in the design of the study and helped to draft the manuscript; KB participated in the design of the study and helped to draft the manuscript; PB participated in the design of the study and helped to draft the manuscript; JH conceived of the study, and drafted the manuscript; AR conceived of the study, and participated in its design and coordination, contributed to interpretation of the data and drafted the manuscript; MB participated in the design of the study, contributed to global data analysis, performed the statistical analysis, and drafted the manuscript.

Funding

The study was financially supported by the SyNergy Cluster (Core 2 project).

Acknowledgement

This paper originated from the doctoral thesis of Maximilian Deussing. We thank Karin Bormann-Giglmaier and Rosel Oos for excellent technical assistance. We note manuscript editing by Inglewood Biomedical Editing. GE180 cassettes were received from GE. We acknowledge textural revisions by Inglewood Biomedical Editing.

References

Airas, L., Rissanen, E., Rinne, J.O., 2015. Imaging neuroinflammation in multiple sclerosis using TSPO-PET. Clin. Transl. Imaging 3, 461–473.
Biesmans, S., Acton, P.D., Cotto, C., Langlois, X., Ver Donck, L., Bouwknecht, J.A., Aelvoet, S.A., Hellings, N., Meert, T.F., Nuydens, R., 2015. Effect of stress and peripheral immune activation on astrocyte activation in transgenic bioluminescent Gfap-luc mice. Glia 63, 1126–1137.
Brendel, M., Probst, F., Jaworska, A., Overhoff, F., Korzhova, V., Albert, N.L., Beck, R., Lindner, S., Gildehaus, F.J., Baumann, K., Bartenstein, P., Kleinberger, G., Haass, C., Herms, J., Rominger, A., 2016. Glial activation and glucose metabolism in a transgenic amyloid mouse model: a triple-tracer PET study. J. Nucl. Med. 57, 954–960.
Buck, J.R., McKinley, E.T., Fu, A., Abel, T.W., Thompson, R.C., Chambless, L., Watchmaker, J.M., Harty, J.P., Cooper, M.K., Manning, H.C., 2015. Preclinical TSPO ligand PET to visualize human glioma xenotransplants: a preliminary study. PLoS One 10, e0141659.
Chen, M.K., Guilarte, T.R., 2008. Translocator protein 18 kDa (TSPO): molecular sensor of brain injury and repair. Pharmacol. Ther. 118, 1–17.
Deussing, M., Blume, T., Vomacka, L., Mahler, C., Focke, C., Todica, A., Unterrainer, M., Albert, N.L., Lindner, S., Von Ungern-Sternberg, B., Baumann, K., Zwergal, A., Bartenstein, P., Herms, J., Rominger, A., Brendel, M., 2017. Specificity of [18F] GE180 Uptake and TSPO Expression in Rodent Brain and Myocardium Data in Brief. D-17-00993, submitted for publication.
Dorr, A., Sled, J.G., Kabani, N., 2007. Three-dimensional cerebral vasculature of the CBA mouse brain: a magnetic resonance imaging and micro computed tomography study. Neuroimage 35, 1409–1423.
Fan, Z., Calsolaro, V., Atkinson, R.A., Femminella, G.D., Waldman, A., Buckley, C., Trigg, W., Brooks, D.J., Hinz, R., Edison, P., 2016. Flutriciclamide (18F-GE180) PET: first-in-human PET study of novel third-generation in vivo marker of human translocator protein. J. Nucl. Med. 57, 1753–1759.
Feeney, C., Scott, G., Raffel, J., Roberts, S., Coello, C., Jolly, A., Searle, G., Goldstone, A.P., Brooks, D.J., Nicholas, R.S., Trigg, W., Gunn, R.N., Sharp, D.J., 2016. Kinetic analysis of the translocator protein positron emission tomography ligand [18F]GE-180 in the human brain. Eur. J. Nucl. Med. Mol. Imaging 43, 2201–2210.
Gargiulo, S., Anzilotti, S., Coda, A.R., Gramanzini, M., Greco, A., Panico, M., Vinciguerra, A., Zannetti, A., Vicidomini, C., Dolle, F., Pignataro, G., Quarantelli, M., Annunziato, L., Brunetti, A., Salvatore, M., Pappata, S., 2016. Imaging of brain TSPO expression in a mouse model of amyotrophic lateral sclerosis with (18)F-DPA-714 and micro-PET/CT. Eur. J. Nucl. Med. Mol. Imaging 43, 1348–1359.
Gerhard, A., 2016. TSPO imaging in parkinsonian disorders. Clin. Transl. Imaging 4, 183–190.
Gross, L., Paintmayer, L., Lehner, S., Brandl, L., Brenner, C., Grabmaier, U., Huber, B., Bartenstein, P., Theiss, H.D., Franz, W.M., Massberg, S., Todica, A., Brunner, S., 2016. FDG-PET reveals improved cardiac regeneration and attenuated adverse remodelling following Sitagliptin + G-CSF therapy after acute myocardial infarction. Eur. Heart J. Cardiovasc Imaging 17, 136–145.
Hupe, H.C., Thackeray, J., Postema, J., Wang, Y., Ross, T.L., Wollert, K., Bankstahl, J., Bengel, F., 2016. Myocardial infarction is associated with neuroinflammation-a systemic analysis using TSPO-targeted molecular imaging. J. Nucl. Med. 57, 404.
Israel, I., Ohsiek, A., Al-Momani, E., Albert-Weissenberger, C., Stetter, C., Mencl, S., Buck, A.K., Kleinschnitz, C., Samnick, S., Siren, A.L., 2016. Combined [(18)F]DPA-714 micro-positron emission tomography and autoradiography imaging of microglia activation after closed head injury in mice. J. Neuroinflammation 13, 140.
James, M.L., Belichenko, N.P., Nguyen, T.V., Andrews, L.E., Ding, Z., Liu, H., Bodapati, D., Arksey, N., Shen, B., Cheng, Z., Wyss-Coray, T., Gambhir, S.S., Longo, F.M., Chin, F.T., 2015. PET imaging of translocator protein (18 kDa) in a mouse model of Alzheimer's disease using N-(2,5-dimethoxybenzyl)-2-18F-fluoro-N-(2-phenoxyphenyl)acetamide. J. Nucl. Med. 56, 311–316.
Liu, B., Le, K.X., Park, M.A., Wang, S., Belanger, A.P., Dubey, S., Frost, J.L., Holton, P., Reiser, V., Jones, P.A., Trigg, W., Di Carli, M.F., Lemere, C.A., 2015. Vivo detection of age- and disease-related increases in neuroinflammation by 18F-GE180 TSPO MicroPET imaging in wild-type and Alzheimer's transgenic mice. J. Neurosci. 35, 15716–15730.
Lyoo, C.H., Ikawa, M., Liow, J.S., Zoghbi, S.S., Morse, C.L., Pike, V.W., Fujita, M., Innis, R.B., Kreisl, W.C., 2015. Cerebellum can serve as a pseudo-reference region in alzheimer disease to detect neuroinflammation measured with PET radioligand binding to translocator protein. J. Nucl. Med. 56, 701–706.
Mirzaei, N., Tang, S.P., Ashworth, S., Coello, C., Plisson, C., Passchier, J., Selvaraj, V., Tyacke, R.J., Nutt, D.J., Sastre, M., 2016. In vivo imaging of microglial activation by positron emission tomography with [(11)C]PBR28 in the 5XFAD model of Alzheimer's disease. Glia 64, 993–1006.
Morin, D., Musman, J., Pons, S., Berdeaux, A., Ghaleb, B., 2016. Mitochondrial translocator protein (TSPO): from physiology to cardioprotection. Biochem. Pharmacol. 105, 1–13.
Overhoff, F., Brendel, M., Jaworska, A., Korzhova, V., Delker, A., Probst, F., Focke, C., Gildehaus, F.J., Carlsen, J., Baumann, K., Haass, C., Bartenstein, P., Herms, J., Rominger, A., 2016. Automated spatial brain normalization and hindbrain white

matter reference tissue give improved [(18)F]-Florbetaben PET quantitation in Alzheimer's model mice. Front. Neurosci. 10, 45.
Ozmen, L., Albientz, A., Czech, C., Jacobsen, H., 2009. Expression of transgenic APP mRNA is the key determinant for beta-amyloid deposition in PS2APP transgenic mice. Neurodegener. Dis. 6, 29–36.
Pihlaja, R., Takkinen, J., Eskola, O., Vasara, J., Lopez-Picon, F.R., Haaparanta-Solin, M., Rinne, J.O., 2015. Monoacylglycerol lipase inhibitor JZL184 reduces neuroinflammatory response in APdE9 mice and in adult mouse glial cells. J. Neuroinflammation 12, 81.
Richards, J.G., Higgins, G.A., Ouagazzal, A.M., Ozmen, L., Kew, J.N., Bohrmann, B., Malherbe, P., Brockhaus, M., Loetscher, H., Czech, C., Huber, G., Bluethmann, H., Jacobsen, H., Kemp, J.A., 2003. PS2APP transgenic mice, coexpressing hPS2mut and hAPPswe, show age-related cognitive deficits associated with discrete brain amyloid deposition and inflammation. J. Neurosci. 23, 8989–9003.
Tang, D., Nickels, M.L., Tantawy, M.N., Buck, J.R., Manning, H.C., 2014. Preclinical imaging evaluation of novel TSPO-PET ligand 2-(5,7-Diethyl-2-(4-(2-[(18)F] fluoroethoxy)phenyl)pyrazolo[1,5-a]pyrimidin-3-yl)- N,N-diethylacetamide ([(18)F] VUIIS1008) in glioma. Mol. Imaging Biol. 16, 813–820.
Tiwari, A.K., Ji, B., Yui, J., Fujinaga, M., Yamasaki, T., Xie, L., Luo, R., Shimoda, Y., Kumata, K., Zhang, Y., Hatori, A., Maeda, J., Higuchi, M., Wang, F., Zhang, M.R., 2015. [18F]FEBMP: positron emission tomography imaging of TSPO in a model of neuroinflammation in rats, and in vitro autoradiograms of the human brain. Theranostics 5, 961–969.
Turkheimer, F.E., Rizzo, G., Bloomfield, P.S., Howes, O., Zanotti-Fregonara, P., Bertoldo, A., Veronese, M., 2015. The methodology of TSPO imaging with positron emission tomography. Biochem. Soc. Trans. 43, 586–592.
Vivash, L., O'Brien, T.J., 2016. Imaging microglial activation with TSPO PET: lighting up neurologic diseases? J. Nucl. Med. 57, 165–168.
Wickstrom, T., Clarke, A., Gausemel, I., Horn, E., Jorgensen, K., Khan, I., Mantzilas, D., Rajanayagam, T., in 't Veld, D.J., Trigg, W., 2014. The development of an automated and GMP compliant FASTlab Synthesis of [(18) F]GE-180; a radiotracer for imaging translocator protein (TSPO). J. Label. Comp. Radiopharm. 57, 42–48.
Zheng, J., Winkeler, A., Peyronneau, M.A., Dolle, F., Boisgard, R., 2016. Evaluation of PET imaging performance of the TSPO radioligand [18F]DPA-714 in mouse and rat models of cancer and inflammation. Mol. Imaging Biol. 18, 127–134.

Data in Brief 19 (2018) 331–336

Contents lists available at ScienceDirect

Data in Brief

journal homepage: www.elsevier.com/locate/dib

Data Article

Data on specificity of [^{18}F]GE180 uptake for TSPO expression in rodent brain and myocardium

Maximilian Deussing [a], Tanja Blume [a,b], Lena Vomacka [a], Christoph Mahler [c,d], Carola Focke [a], Andrei Todica [a], Marcus Unterrainer [a], Nathalie L. Albert [a], Simon Lindner [a], Barbara von Ungern-Sternberg [a], Karlheinz Baumann [e], Andreas Zwergal [f], Peter Bartenstein [a,g], Jochen Herms [b,g,h], Axel Rominger [a,g], Matthias Brendel [a,*]

[a] Dept. of Nuclear Medicine, Ludwig-Maximilians-Universität München, Munich, Germany
[b] Center for Neuropathology and Prion Research, Ludwig-Maximilians-Universität München, Munich, Germany
[c] Inst. of Clinical Neuroimmunology, Ludwig-Maximilians-Universität München, Munich, Germany
[d] Biomedical Center (BMC), Ludwig-Maximilians-Universität München, Munich, Germany
[e] Roche Pharma Research and Early Development, Neuroscience Discovery, Roche Innovation Center Basel, F. Hoffmann-La Roche Ltd, Basel, Switzerland
[f] Dept. of Neurology, Ludwig-Maximilians-Universität München, Munich, Germany
[g] Munich Cluster for Systems Neurology (SyNergy), Munich, Germany
[h] Department of Translational Brain Research, DZNE - German Center for Neurodegenerative Diseases, Munich, Germany

ARTICLE INFO

Article history:
Received 5 October 2017
Received in revised form
19 January 2018
Accepted 30 April 2018
Available online 5 May 2018

ABSTRACT

Data in this article show radioligand uptake (to gamma counter and positron-emission-tomography) as well as polymerase chain reaction analyses of 18 kDa translocator protein (TSPO) quantification. We confirmed specificity of [^{18}F]GE180 binding of rodent brain and myocardium by blocking experiments with prior application of non-radioactive GE180, using dynamic in vivo positron-emission-tomography and ex vivo gamma counter measurements.

DOI of original article: https://doi.org/10.1016/j.neuroimage.2017.10.006
* Corresponding author.
E-mail address: matthias.brendel@med.uni-muenchen.de (M. Brendel).

https://doi.org/10.1016/j.dib.2018.04.133

Expression of TSPO was compared between rodent brain and myocardium by quantitative polymerase chain reaction.

Specifications Table

Subject area	*Nuclear Medicine*
More specific subject area	*Preclinical PET imaging of neuroinflammation*
Type of data	*PET images, blocking plots, correlation plots*
How data was acquired	*[^{18}F]GE180 TSPO PET, gamma counter, TSPO qPCR*
Data format	*Quantification of PET and tissue samples, Listmode, NIFTI*
Experimental factors	*C57Bl6 mice, cold GE180, [^{18}F]GE180, Analysis of TSPO expression*
Experimental features	*TSPO PET, TSPO qPCR*
Data source location	*Department of Nuclear Medicine, Munich, Germany*
Data accessibility	*The data is provided within this article*

Value of the data

- Blocking by pretreatment with non-radioactive GE180 for quantification of specific [^{18}F]GE180 TSPO binding in rodent brain and myocardium to positron-emission-tomography.
- Regional analysis for characterization of [^{18}F]GE180 binding specificity in different areas of the rodent brain.
- Data provide information about the physiological relationship between specific 18 kDa translocator protein (TSPO) tracer signal in normal rodent brain and myocardium.
- Quantitative polymerase chain reaction gives additional information about the relative magnitudes of TSPO expression in brain and myocardium.

1. Data

We observed that the myocardium presents a potential extra-cerebral reference region for [^{18}F]GE180 TSPO positron-emission-tomography quantitation [1]. The following data provide additional information about the association and specificity of brain and myocardium TSPO tracer binding, as obtained by blocking experiments (Fig. 1, Fig. 2). Furthermore, we performed quantitative polymerase chain reaction for assessment of TSPO gene expression in brain and myocardium, independent of tracer-based measurements (Fig. 3).

2. Experimental design, materials and methods

2.1. Radiochemistry

Radiosynthesis of [^{18}F]GE180 was performed as previously described [3], with slight modifications [4], in a procedure yielding radiochemical purity $>$ 98%, and specific activity of 1400 $\pm$ 500 GBq/μmol at end of synthesis. For blocking, non-radioactive GE180 was used at a mass concentration ratio of 1000:1 compared to the radiolabeled ligand.

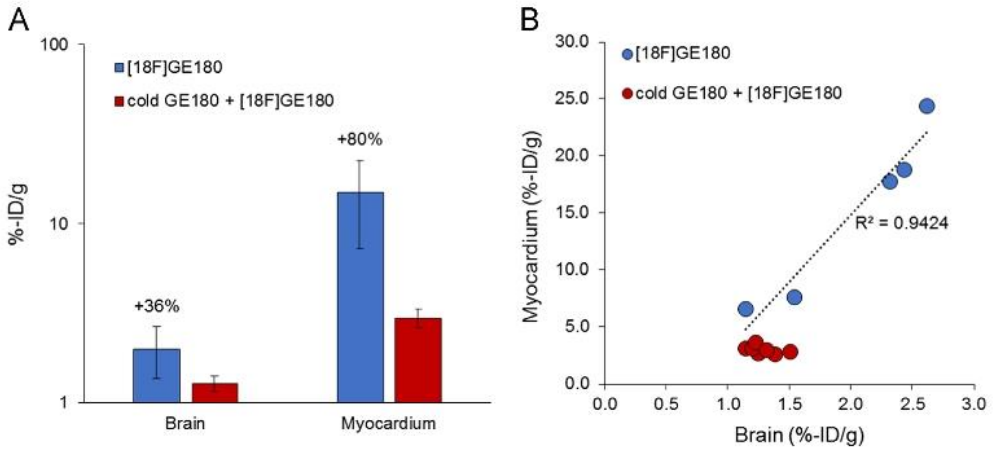

Fig. 1. Gamma counter measurements of tracer uptake in brain and myocardium ex vivo. (A) Bar graphs (logarithmic scale) show %-injected dose-(ID)/g at 107 min after injection of [^{18}F]GE180 with (red) and without (blue) prior blocking with excess non-radioactive GE180 (1000:1). Specific binding was estimated to be 36% in the brain and 80% in the myocardium. Absolute specific binding was 17-fold higher in the myocardium when compared to the brain. (B) Correlation between %-ID/g of brain and myocardium in single mice indicate a relationship between specific TSPO tracer binding in the two tissues, whereas nonspecific binding did not correlate ($R^2 < 0.2$). Data derive from $N = 5$ unblocked and $N = 7$ blocked C57Bl/6 mice at seven months of age. Error bars indicate standard deviations. Single data points are available in the supplement.

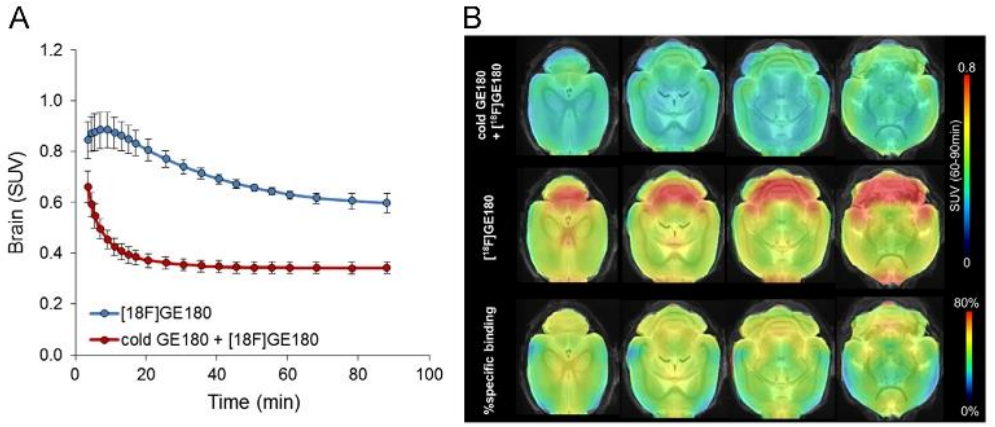

Fig. 2. Dynamic and regional in vivo positron-emission-tomography (PET) measurements of the brain. (A) Mean dynamic brain PET standardized uptake value (SUV) plots for groups of unblocked (blue) and blocked (red) mice during 90 min after injection of [^{18}F]GE180. Error bars indicate standard deviations. (B) Regional analysis shows axial slices of 60–90 min [^{18}F]GE180 PET SUV projected upon a magnetic resonance imaging template [2]. Upper row illustrates mice with prior blocking by a large mass dose of GE180 (1000:1), whereas the middle row shows unblocked mice. Voxel-wise percentage of specific binding in the rodent brain is depicted in the bottom row. Highest specific binding was observed in regions with high abundance of ependymal glia cells, e.g. adjacent to the fourth ventricle, whereas specific binding in the cortex was low. Data derive from $N = 3$ unblocked and $N = 5$ blocked C57Bl/6 mice at seven months of age. Error bars indicate standard deviations. Single data points are available in the supplement.

2.2. Gamma counter analysis

We performed blocking experiments with excess non-radioactive tracer for quantification of specific [^{18}F]GE180 binding components in the rodent brain and myocardium. A total of twelve female C57Bl6 mice were analyzed at the age of seven months. Isoflurane anesthesia (1.5% in 2–4 l/min O_2)

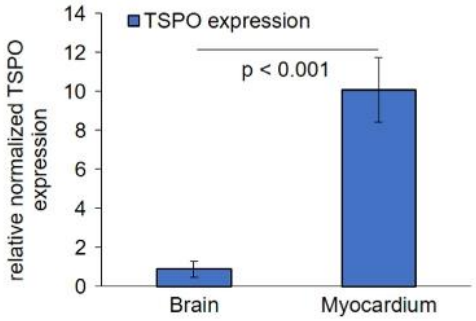

Fig. 3. Quantitative polymerase chain reaction assessment of TSPO gene expression in brain and myocardium. Bar graphs show relative normalized (actin-beta and glyceraldehyde 3-phosphate dehydrogenase) TSPO expression as assessed by the quantitative polymerase chain reaction. TSPO expression was 11-fold higher in the myocardium compared to that in brain. Data derive from $N = 6$ C57Bl/6 mice at seven months of age. Error bars indicate standard deviations. Single data points are available in the supplement.

was maintained during the experimental procedure, and mice were finally killed by cervical decapitation at 107 min post injection, while in a state of deep narcosis. Five mice received an injection of 14.7 $\pm$ 2.2 MBq [^{18}F]GE180 into the tail vein (150 µl saline) Seven mice received an injection of excess non-radioactive GE180 (1000:1) prior to injection of 14.5 $\pm$ 2.1 MBq [^{18}F]GE180 (in 150 µl saline) to a tail vein. Brain and myocardium tissues were quickly removed, and radioactivity concentration was measured in a gamma counter (Cobra Quantum 5002, Packard) with decay-correction to time of tracer injection [5].

2.3. Positron-emission-tomography acquisition and analysis

A subset of mice ($N = 5$ with blocking and $N = 3$ without blocking) was placed in the tomograph (Siemens Inveon DPET) immediately after injection of [^{18}F]GE180, whereupon we began a 90 min dynamic emission recording as described previously [6]. A 15 min transmission scan was then obtained using a rotating [^{57}Co] point source. The image reconstruction procedure consisted of three-dimensional ordered subset expectation maximization with four iterations and twelve subsets followed by a maximum a posteriori algorithm with 32 iterations. Framing was 3 $\times$ 60 s, 6 $\times$ 180 s, 9 $\times$ 300 s, 3 $\times$ 600 s. Scatter and attenuation correction were performed and a decay correction for [^{18}F] was applied. With a zoom factor of 1.0 and a 128 $\times$ 128 $\times$ 159 matrix, a final voxel dimension of 0.78 $\times$ 0.78 $\times$ 0.80 mm was obtained.

Summations of the dynamic emission datasets were manually co-registered to a magnetic resonance imaging mouse atlas [2] by a rigid-body transformation using the PMOD fusion tool (V3.5, PMOD Technologies Ltd.), after blinding the reader to the mouse status (blocked/unblocked). In the second step, a reader-independent automatic re-registration to tracer-specific templates was performed, as reported previously [7]. Initial manual positron-emission-tomography to magnetic resonance imaging atlas fusion images were normalized by non-linear brain normalization to the template using the PMOD brain normalization tool (equal modality; smoothing by 0.6 mm; nonlinear warping; 16 iterations; frequency cutoff 3; regularization 1.0; no thresholding). The concatenation of both transformations was then applied to positron-emission-tomography frames in the native space, to obtain optimal resampling with a minimum of interpolation. The whole brain [^{18}F]GE180 concentration (standardized uptake value; SUV) was measured in a volume-of-interest defined by the magnetic resonance imaging template. The volume-of-interest, comprising 525 mm^3, included the entire cerebrum, cerebellum, brainstem and olfactory bulb. The 60–90 min image frames were used to calculate voxel-wise percentages of specific [^{18}F]GE180 binding throughout the rodent brain.

3. Quantitative TSPO polymerase chain reaction

3.1. RNA isolation and reverse transcription

Brain and heart tissue from adult mice was immediately frozen to − 80 °C in liquid nitrogen after resection. Tissue was lysed with QIAzol Lysis Reagent (Quiagen) and homogenized. The InviTrap® Spin Universal RNA Mini Kit (Stratec) was used to isolate RNA and to separate it from contaminating DNA. RNA concentration was measured with NanoDrop™ 2000 Spectrophotometer (Thermo Fisher Scientific, Waltham, MA, USA). Extracted RNA was assessed based on spectral data and purity ratios (A260/A280). Reverse transcription from 50 µL of 50 ng/µL RNA was performed by incubating with 4 µL 25x dNTPs, 10 µL 10x random primers, 5 µL MultiScribe™ Reverse Transcriptase 50 U/µL, 21 µL Nuclease-free H_2O for 10 min at 25 °C, then 120 min at 37 °C. The transcription was terminated by incubating at 85 °C for 5 min.

3.2. Real-time polymerase chain reaction

TSPO mRNA expression was measured using a CFX connect optics module RT-System (BioRad, Hercules, CA, USA). cDNA template 9 µl was added to 20 × TaqMan® Gene Expression Assay Mm00437828_m1 1 µl and 2x TaqMan® Gene Expression Master Mix 10 µl. Thermal cycling conditions were 2 min at 50 °C and 10 min at 95 °C, followed by 40 cycles at 98 °C for 15 s and at 60 °C for 1 min. To test specificity of the polymerase chain reaction product a melt curve analysis was performed. TSPO expression was normalized to the housekeeping genes Actin-beta and glyceraldehyde 3-phosphate dehydrogenase expression was used for comparative quantification.

Acknowledgements

This paper originated from the doctoral thesis of Maximilian Deussing. We thank Karin Bormann-Giglmaier, Rosel Oos, and Lena Schödel for excellent technical assistance. We note manuscript editing by Inglewood Biomedical Editing. GE made available the GE-180 cassettes through an early access model.

Transparency document. Supplementary material

Transparency document associated with this article can be found in the online version at https://doi.org/10.1016/j.dib.2018.04.133.

Appendix A. Supplementary material

Supplementary data associated with this article can be found in the online version at https://doi.org/10.1016/j.dib.2018.04.133.

References

[1] M. Deussing, T. Blume, L. Vomacka, C. Mahler, C. Focke, A. Todica, M. Unterrainer, N.L. Albert, S. Lindner, B. von Ungern-Sternberg, K. Baumann, A. Zwergal, P. Bartenstein, J. Herms, A. Rominger, M. Brendel, Coupling between physiological TSPO expression in brain and myocardium allows stabilization of late-phase cerebral [18F]GE180 PET quantification., Neuroimage 15 (165) (2018) 83–91. http://dx.doi.org/10.1016/j.neuroimage.2017.10.006, Epub 2017 Oct 5..

[2] A. Dorr, J.G. Sled, N. Kabani, Three-dimensional cerebral vasculature of the CBA mouse brain: a magnetic resonance imaging and micro computed tomography study, NeuroImage 35 (4) (2007) 1409–1423.

[3] T. Wickstrom, et al., The development of an automated and GMP compliant FASTlab synthesis of [(18) F]GE-180; a radiotracer for imaging translocator protein (TSPO), J. Label. Compd. Radiopharm. 57 (1) (2014) 42–48.

[4] M. Brendel, et al., Glial activation and glucose metabolism in a transgenic amyloid mouse model: a triple tracer PET study, J. Nucl. Med. (2016).
[5] M. Brendel, et al., Impact of partial volume effect correction on cerebral beta-amyloid imaging in APP-Swe mice using [(18) F]-florbetaben PET, NeuroImage 84 (2014) 843–853.
[6] M. Brendel, et al., Glial activation and glucose metabolism in a transgenic amyloid mouse model: a triple-tracer PET study, J. Nucl. Med. 57 (6) (2016) 954–960.
[7] F. Overhoff, et al., Automated spatial brain normalization and hindbrain white matter reference tissue give improved [(18) F]-florbetaben PET quantitation in alzheimer's model mice, Front. Neurosci. 10 (2016) 45.

frontiers in Aging Neuroscience

ORIGINAL RESEARCH
published: 07 June 2018
doi: 10.3389/fnagi.2018.00174

Comparison of ^{18}F-T807 and ^{18}F-THK5117 PET in a Mouse Model of Tau Pathology

Matthias Brendel[1†], Behrooz H. Yousefi[2,3†], Tanja Blume[4], Michael Herz[2], Carola Focke[1], Maximilian Deussing[1], Finn Peters[4], Simon Lindner[1], Barbara von Ungern-Sternberg[1], Alexander Drzezga[5], Peter Bartenstein[1,6], Christian Haass[4,6,7], Nobuyuki Okamura[8], Jochen Herms[4,6], Igor Yakushev[2,3‡] and Axel Rominger[1,6‡]*

[1] Department of Nuclear Medicine, Ludwig-Maximilians-University of Munich, Munich, Germany, [2] Department of Nuclear Medicine, Technical University of Munich, Munich, Germany, [3] Neuroimaging Center, Technische Universität München, Munich, Germany, [4] German Center for Neurodegenerative Diseases (DZNE), Munich, Germany, [5] Department of Nuclear Medicine, University of Cologne, Cologne, Germany, [6] Munich Cluster for Systems Neurology (SyNergy), Munich, Germany, [7] Biomedical Center, Ludwig-Maximilians-University of Munich, Munich, Germany, [8] Division of Pharmacology, Faculty of Medicine, Tohoku Medical and Pharmaceutical University, Sendai, Japan

OPEN ACCESS

Edited by:
Atsushi Takeda, Sendai Nishitaga National Hospital, Japan

Reviewed by:
Adriaan Anthonius Lammertsma, VU University Medical Center, Netherlands
Cristina Lois, Harvard Medical School, United States

***Correspondence:**
Axel Rominger
axel.rominger@med.uni-muenchen.de

†These authors have contributed equally to this work as first authors.

‡These authors have contributed equally to this work as last authors.

Received: 07 November 2017
Accepted: 22 May 2018
Published: 07 June 2018

Citation:
Brendel M, Yousefi BH, Blume T, Herz M, Focke C, Deussing M, Peters F, Lindner S, von Ungern-Sternberg B, Drzezga A, Bartenstein P, Haass C, Okamura N, Herms J, Yakushev I and Rominger A (2018) Comparison of ^{18}F-T807 and ^{18}F-THK5117 PET in a Mouse Model of Tau Pathology. Front. Aging Neurosci. 10:174. doi: 10.3389/fnagi.2018.00174

Positron-emission-tomography (PET) imaging of tau pathology has facilitated development of anti-tau therapies. While members of the arylquinoline and pyridoindole families have been the most frequently used tau radioligands so far, analyses of their comparative performance *in vivo* are scantly documented. Here, we conducted a head-to-head PET comparison of the arylquinoline ^{18}FT807 and the pyridoindole ^{18}FTHK5117 PET in a mouse model of tau pathology. PET recordings were obtained in groups of (N = 5–7) P301S and wild-type (WT) mice at 6 and 9 months of age. Volume-of-interest based analysis (standard-uptake-value ratio, SUVR) was used to calculate effect sizes (Cohen's d) for each tracer and age. Statistical parametric mapping (SPM) was used to assess regional similarity (dice coefficient) of tracer binding alterations for the two tracers. Immunohistochemistry staining of neurofibrillary tangles was performed for validation *ex vivo*. Significantly elevated ^{18}F-T807 binding in the brainstem of P301S mice was already evident at 6 months (+14%, $p < 0.01$, $d = 1.64$), and increased further at 9 months (+23%, $p < 0.001$, $d = 2.70$). ^{18}F-THK5117 indicated weaker increases and effect sizes at 6 months (+5%, $p < 0.05$, $d = 1.07$) and 9 months (+10%, $p < 0.001$, $d = 1.49$). Regional similarity of binding of the two tracers was high (71%) at 9 months. ^{18}F-T807 was more sensitive than ^{18}F-THK5117 to tau pathology in this model, although both tracers present certain obstacles, which need to be considered in the design of longitudinal preclinical tau imaging studies.

Keywords: tau, small animal PET, transgenic mice, ^{18}F-T807, ^{18}F-THK5117

INTRODUCTION

Neurofibrillary tangles constitute one of the most characteristic neuropathological findings in Alzheimer's disease (AD), which is the most frequent form of dementia, and likewise occur in certain non-AD forms of dementia known as tauopathies (Duyckaerts et al., 2009). Whereas AD is characterized by paired helical filaments containing equal amounts of 3R and 4R isoforms, non-AD tauopathies present with other tau ultrastructures and isoforms. For example, the pathology in

progressive supranuclear palsy and corticobasal degeneration consists of 4R tau aggregating into straight filaments (Murray et al., 2014). The recent development of ^{18}F-fluorinated radioligands for positron-emission-tomography (PET) studies of tau aggregates intensely accelerated research in the field of tau imaging in AD and non-AD tauopathies (Villemagne and Okamura, 2016). Members of the arylquinoline and pyridoindole structural families have been the most frequently used tau radioligands to date. Although tau PET has been hindered due to off-target binding of ligands to neuromelanin (Hansen et al., 2016) and MAO-B (Ng et al., 2017), both tracer classes can differentiate AD and non-AD tauopathy patients from healthy controls.

Small animal PET (μPET) has emerged as a useful tool for translational research involving *in vivo* imaging of β-amyloid and neuroinflammation markers in rodent models of neurodegenerative diseases (Zimmer et al., 2014; Brendel et al., 2015; Liu et al., 2015). However, there have been relatively few tau-PET studies in wild-type (WT) and transgenic mice (Maruyama et al., 2013; Okamura et al., 2013), due in part to concerns about the sensitivity of tau ligands for species-dependent isoforms and intracellular compartmentation of tau aggregates. We previously characterized the performance of μPET with the arylquinoline ^{18}F-THK5117 in two transgenic mouse models of tau pathology (Brendel et al., 2016); this tracer showed elevated brain uptake in both types of model mice relative to WT mice, and brain uptake patterns correlated with autoradiography and immunohistochemistry findings of tau deposition. Nonetheless, the sensitivity of ^{18}F-THK5117 was rather low, with a detection threshold of 10% tau/area, and quantitation was degraded by spillover from extracerebral structures compounded by rapid washout from brain.

In light of the previous findings, further research is needed to improve preclinical imaging of tau pathology in mouse models. Thus, the aim of the current μPET study was to compare representative members of the two major classes of tau radioligands with regard to their ability to track longitudinally the expression of tau pathology in the brain of P301S transgenic mice.

MATERIALS AND METHODS

Radiochemistry

Radiosynthesis of the pyridoindole ^{18}F-T807 was performed as previously described (Gao et al., 2015), with modifications for a fully automated preparation on Neptis perform module[1] as specified in the Supplementary Methods. A radiochemical yield of >20% was achieved, with chemical and radiochemical (HPLC) purities of >98%. The ^{18}F-T807 was directly used for μPET with a specific activity of >216 GBq/μmol at the end of synthesis.

Radiosynthesis of ^{18}F-THK5117 was performed as previously described (Tago et al., 2014), with slight modifications as specified in the Supplementary Methods. The procedure yielded a radiochemical purity >98% and specific activity of 202 ± 56 GBq/μmol at the end of synthesis.

[1]http://www.neptis-vsa.com/

Animals and Study Design

All experiments were carried out in compliance with the German national guidelines for animal protection (TierSchG, Germany) and approval of the local animal care committee (Regierung von Oberbayern), with supervision by a veterinarian. Animals were housed in a temperature- and humidity-controlled environment with a 12-h light–dark cycle, with free access to food (Ssniff, Soest, Germany) and water.

Tau-P301S (P301S) transgenic (TG) mice were investigated in this study together with age-matched WT controls. P301S mice express human P301S mutant 4R/0N tau (Thy1-hTau.P301S) in CBA.C57BL/6 background (Allen et al., 2002). This model is characterized by predominant tau hyperphosphorylation in the brainstem, where tau filaments appear mostly as half-twisted ribbons. Larger paired helical tau filaments reminiscent of those seen in human AD are observed less frequently. The behavioral phenotype manifests as learning deficits from 2 to 3 months of age, and onset of motor impairment at 4 months, leading to early death before 12 months of age. Eight P301S mice and eight age-matched C57Bl/6 littermates serving as controls were included in the study. Imaging with dual tracers was performed at baseline (at 6 months of age) and at follow-up (at 9 months of age). Maximum time span between paired measurements was 10 days.

Tau PET

Data Acquisition and Analyses

For details of data acquisition and reconstruction see Supplementary Methods. In brief, summed 5–65 min dynamic emission frames for each tracer (^{18}F-T807 and ^{18}F-THK5117) were co-registered to an MRI mouse brain atlas (Dorr et al., 2007) after frame-wise correction for motion using the PMOD fusion tool (V3.5, PMOD Technologies Ltd.). The reader was blind to the type of mouse. A second experienced reader ensured accurate alignment of the fusion image and corrected if necessary. Volumes-of interest (VOI) were defined on the MRI mouse atlas (**Figure 1**).

Due to progressively increasing bone labeling with ^{18}F-T807 scan duration, we modified our previously published brainstem VOI (Brendel et al., 2016) by reducing its width and increasing its length, so as to reduce signal spill-in from extra-cerebral structures near the ovoid VOI (11 mm^3). Bone uptake was obtained from a bilateral VOI in the petrous bone (9 mm^3) and uptake in the bilarteral Harderian glands was also measured (40 mm^3). A whole brain VOI was applied to measure the radiotracer uptake in the entire brain (525 mm^3). The cerebellum, with exclusion of voxels of the cerebellar peduncle (volume 56 mm^3), which was the optimal reference VOI identified for ^{18}F-THK5117, (Brendel et al., 2016), proved to be vulnerable to spill-in from the extensive bone uptake occurung in the ^{18}F-T807 scans. Therefore we used the bilateral striata together with the septum (volume 38 mm^3) as the reference tissue VOI, which was unaffected by cranial spill-in from ^{18}F-T807, and is not reported to contain tau deposition in P301S mice (Allen et al., 2002). To enable direct comparisons of both tracers using the same reference region, we performed additional analyses with modified striatal and cerebellar reference regions, which are

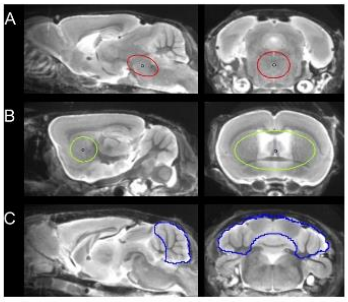

FIGURE 1 | Definition of VOIs projected on the mouse brain MRI atlas (Dorr et al., 2007) in sagittal and coronal slices: **(A)** Oval-shaped brainstem VOI including central parts of the pons and the midbrain (middle row; 11 mm^3; red line). **(B)** Spherical striatal reference VOI (top row; 38 mm^3; green line). **(C)** Crescent-shaped cerebellar reference VOI (top row; 56 mm^3; blue line).

presented in the Supplementary Material. Time-activity-curves of brainstem, striatum, cerebellum, Harderian glands, and petrous bone were extracted from the dynamic emission sequences. Brainstem and reference VOIs were employed for calculation of the mean brainstem-to-striatum ratio for ^{18}F-T807 (40–60 min, $SUVR_{BST/STR}$) and the brainstem-to-cerebellum ^{18}F-THK5117 (30–60 min, $SUVR_{BST/CBL}$), where SUVR is the standardized uptake value ratio. A reader-independent coregistration was established after validation of the optimal time window by stability analysis of ratio TACs in the emission sequence for each tracer. Further details are provided in Supplementary Methods.

Statistical Parametric Mapping (SPM)

For whole-brain voxel-wise comparisons of the two tau tracers, SPM was performed using SPM5 routines (Wellcome Department of Cognitive Neurology, London, United Kingdom) implemented in MATLAB (version 7.1) (Rominger et al., 2013). SUVR images were scaled by the tracer-specific reference region before statistical analysis.

Immunohistochemistry

After completion of the final μPET scans, mice were killed by cervical dislocation, and the brains rapidly removed. After fixation by immersion overnight in 4% paraformaldehyde at 4°C, brains were post-fixed in phosphate buffered saline. Two representative 50 μm thick slices per animal were cut in the sagittal plane using a vibratome (VT 1000 S, Leica, Wetzlar, Germany). Free-floating sections were permeabilized with 2% Triton X-100 overnight and blocked with I-Block™ Protein-Based Blocking Reagent (Thermo Fischer Scientific). We obtained immunohistochemical labeling of microtubule-associated protein tau (MAPT) using PA5-27287 primary antibody (Invitrogen, dilution 1:400) – recognizing amino acids 1 – 286 of human Tau and the A-21244 secondary antibody (Invitrogen, 1:500). The unbound dye was removed by three washing steps with PBS, and the slices were then mounted on microscope slides with fluorescent mounting medium (Dako, Germany). Images were acquired with a LSM 780 confocal microscope (Zeiss) equipped with a 40×/1.4 oil immersion objective. The excitation wavelength was 633 nm and emission was detected from 650 to 758 nm. For each brain slice 3-dimensional 16 bit data stacks of 10240 pixels × 9216 pixels × 67 pixels were acquired from the brainstem (area matching the VOI of PET) at a lateral resolution of 0.35 μm/pixel and an axial resolution of 1.0 μm/pixel. Whole brain overview images were obtained by two-dimensional acquisition.

To quantify tau volume load, we employed custom-written Matlab software. Local background subtraction was used to diminish intensity variations among different stacks. Subsequently, MAPT was identified by applying the 80th percentile as minimal intensity threshold. Noise was excluded by applying a connected component analysis excluding patches of contiguous voxels smaller than 1 μm. Within this tau 3D mask contiguous patches with a minimum diameter of 3 μm in all spatial directions were considered as tau-positive somata. These analyses were performed by an operator who was blind to the μPET results.

Statistics

Group comparisons of VOI-based PET results between TG and WT mice (baseline and follow-up) were assessed by an unpaired Student's *t*-test using IBM SPSS Statistics (version 23.0; SPSS, Chicago, IL, United States). Longitudinal data were compared between baseline and follow-up by a paired Student's *t*-test. A threshold of $p < 0.05$ was considered to be significant for rejection of the null hypothesis.

RESULTS

Overview

One P301S and one WT mouse died before the first PET scan. Two P301S mice had to be euthanized after the follow-up ^{18}F-T807 scan due to poor health and did not receive the second ^{18}F-THK5117 scan. Resulting final animal numbers and PET SUVR results by group are presented in **Table 1**.

Comparison of Tracer Characteristics

Head-to-head comparison of the TACs indicated a faster tracer washout of ^{18}F-THK5117 from whole brain when compared to ^{18}F-T807. Relative to the mean peak activity, 57% remained at 10 min and 11% remained at 60 min after ^{18}F-THK5117 injection, while 72% remained at 10 min and 26% at 60 min after ^{18}F-T807 injection (both contrasts $p < 0.001$; **Figure 2A**). Radioactivity uptake in the petrous bone relative to the whole brain uptake was 42% higher for ^{18}F-T807 than ^{18}F-THK5117 ($p < 0.001$) at 10 min post injection (p.i.), and +164% higher at 60 min p.i. ($p < 0.001$) (**Figure 2B**). ^{18}F-THK5117 uptake in the Harderian glands relative to the whole brain significantly exceeded that for ^{18}F-T807 after 15 min p.i. (+15%, $p < 0.05$), with a widening gap between the two tracers until 60 min p.i. (+32%, $p < 0.001$) (**Figure 2C**). A previously reported frontal

cortex hotspot (Brendel et al., 2016) was evident in 31% of ^{18}F-THK5117 SUVR images, but was absent in all ^{18}F-T807 scans.

Dynamic Tau Imaging

TAC ratios ($SUVR_{BST/STR}$) for ^{18}F-T807 stabilized after 30 min p.i. in baseline and follow-up scans, with the 40–60 min p.i. interval period giving the best discrimination between P301S and WT mice at 6 and 9 months of age (**Figures 3A,B**). TAC ratios ($SUVR_{BST/CBL}$) of ^{18}F-THK5117 also stabilized after 30 min p.i. for baseline and follow-up time scans, but the 30–60 min period p.i. gave the best discrimination between P301S and WT mice (**Figures 3C,D**).

VOI and SPM Analyses of Static SUVR Images

^{18}F-T807 indicated significantly higher uptake in the brainstem VOI of P301S mice when compared to WT mice at baseline (+14%, $p < 0.01$) and follow-up PET scanning (+23%, $p < 0.001$). Brainstem uptake of ^{18}F-THK5117 was slightly elevated at baseline (+5%, $p < 0.05$) in the same contrast, and increased further at follow-up (+10%, $p < 0.05$). Effect sizes were distinctly higher for ^{18}F-T807 brainstem uptake when compared to ^{18}F-THK5117 at both scanning ages (**Figure 4A**). Utilization of the same reference regions resulted in a loss of the significant results for ^{18}F-T807 when the modified cerebellum was used, and for ^{18}F-THK5117 when the modified striatum was used (see Supplementary Results). The modified cerebellar reference region appeared to be generally less affected by bone uptake for ^{18}F-T807, but the substantial bone uptake in some animals distinctly increased the variance and made group results unreliable. Even a modified striatal VOI degraded the otherwise significant results for ^{18}F-THK5117, most likely due to hot spot noted above. SPM congruently showed higher *T*-scores for baseline and follow-up contrasts of ^{18}F-T807 in comparison to ^{18}F-THK5117 (**Figures 4B,C**). A comparison of T-score maps of both tau ligands (P301S vs. WT; 9 months) indicated a high dice similarity of 71%.

TABLE 1 | Demographics and result overview.

PET session	Age (months)	SUVR P301S	SUVR WT	Effect size (*d*)
BL ^{18}F-T807	6	1.11 ± 0.07** (*N* = 7)	0.97 ± 0.09 (*N* = 7)	1.64
FU ^{18}F-T807	9	1.18 ± 0.04*** (*N* = 7)	0.95 ± 0.07 (*N* = 7)	2.70
BL ^{18}F-THK5117	6	1.11 ± 0.04* (*N* = 7)	1.06 ± 0.05 (*N* = 7)	1.07
FU ^{18}F-THK5117	9	1.16 ± 0.05*** (*N* = 5)	1.06 ± 0.09 (*N* = 7)	1.49

*BL, baseline; FU, follow-up. P301S versus WT: *p < 0.05; **p < 0.01; ***p < 0.001; d, Cohen's d.*

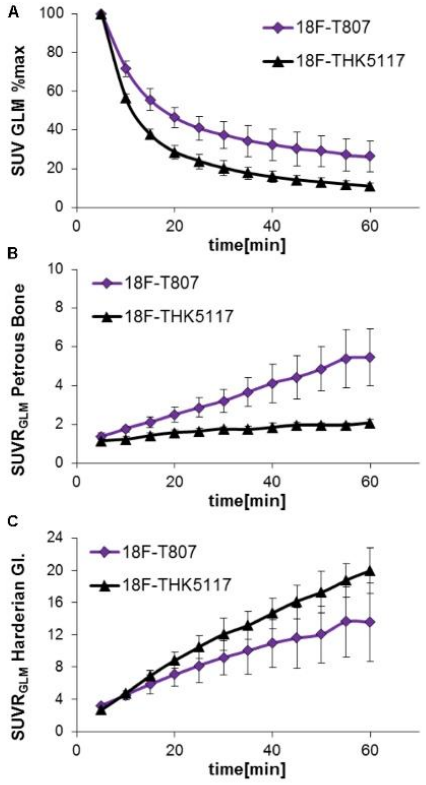

FIGURE 2 | Comparison of ^{18}F-T807 and ^{18}F-THK5117 wash-out from brain **(A)** and uptake in adjacent extracerebral structures (**B**: Petrous bone; **C**: Harderian glands).

Longitudinal Imaging of Tau Pathology in P301S Mice

Longitudinal increases in SUVR between baseline and follow-up scanning in P301S mice were 5.9 ± 4.5% for ^{18}F-T807 ($p < 0.05$) and 4.7 ± 4.4% for ^{18}F-THK5117 [p = not significant (n.s.)]. SPM indicated comparable longitudinal changes in the brainstem of P301S mice by both tracers. (**Figures 5C,D**). WT mice did not show any longitudinal changes in SUVR for either tracer.

Immunohistochemical Validation

P301S mice revealed tau-positive staining predominantly in the brainstem, and penetrating into the cerebellar peduncles, with lesser amounts in the forebrain, and complete absence in the cerebellar hemispheres, as previously demonstrated (Brendel et al., 2016). Similarly, the striatum did not indicate any tau deposition to immunohistochemistry. The tau burden was

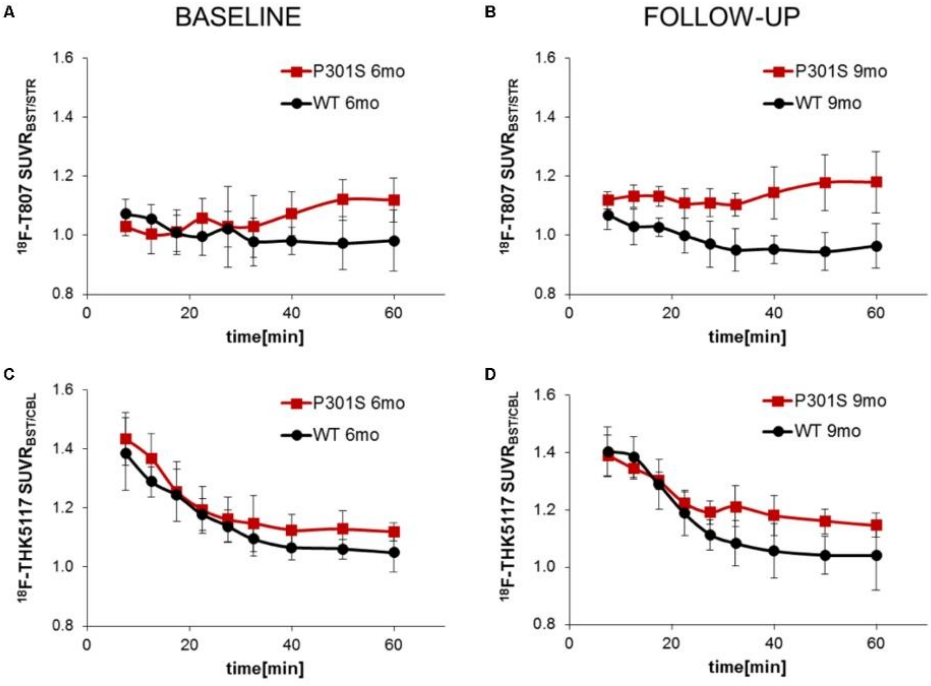

FIGURE 3 | Curves of ratios over time derived from dynamic PET imaging of ^{18}F-T807 **(A,B)** and ^{18}F-THK5117 **(C,D)**. Red lines/squares show transgenic P301S mice and black lines/circles indicate WT mice. Each point is the mean of 5–7 measurements, with error bars indicating SD.

15.4 ± 1.5% per volume in the brainstem by the new 3-dimensional approach. %-tau positively correlated with SUVR of ^{18}F-T807 (R = 0.68, p = 0.21) and SUVR of ^{18}F-THK5117 (R = 0.42, p = 0.48), although these associations did not reach significance (**Figure 6**).

DISCUSSION

This is to our knowledge the first longitudinal small animal PET study of tau distribution in a transgenic mouse model of tau pathology, comprising an *in vivo* comparison of representatives of the two currently most frequently used tau PET tracers. Quantitation of the pyridoindole ligand ^{18}F-T807 and the arylquinoline ligand ^{18}F-THK5117 present specific obstacles for preclinical PET imaging, arising from the substantial uptake in bone and Harderian glands, resulting in signal spill-in, compounded by especially fast washout of brain signal from ^{18}F-THK5117. In addition, we again observed the inexplicable accumulation of ^{18}F-THK5117 at the frontal pole of some mice, irrespective of the genotype. Despite these issues, the current data provide compelling evidence that longitudinal preclinical PET imaging of tau pathology in P301S mice is feasible with both radioligands. We found moderately superior sensitivity of ^{18}F-T807 for the contrast of P301S versus age-matched WT mice, compared to ^{18}F-THK5117. Voxel-wise analysis of the age-dependent increases in SUVR in P301S mice indicated high regional similarity for the two ligands, suggesting that they are both sensitive to tau accumulation in the brainstem.

Head to Head Comparison of ^{18}F-T807 and ^{18}F-THK5117

A strength of this study lies in the head-to-head dual tau tracer assessment in the same animals examined within a span of only a few days. By this approach, we were able to directly compare ^{18}F-T807 and ^{18}F-THK5117 labeling of tau pathology in the brainstem of P301S mice at two different ages. Higher effect sizes were observed with ^{18}F-T807 for baseline and follow-up comparisons of P301S versus WT groups. Thus, considering results of the baseline scans, the detection threshold of tau burden (%/area) in the brainstem of P301S mice is evidently lower for ^{18}F-T807 than for ^{18}F-THK5117. This is in accord with results of a recent study showing higher sensitivity for ^{18}F-AV-1451 in a head-to-head comparison ^{18}F-THK5351 by PET imaging of AD patients *in vivo* (Jang et al., 2017). As

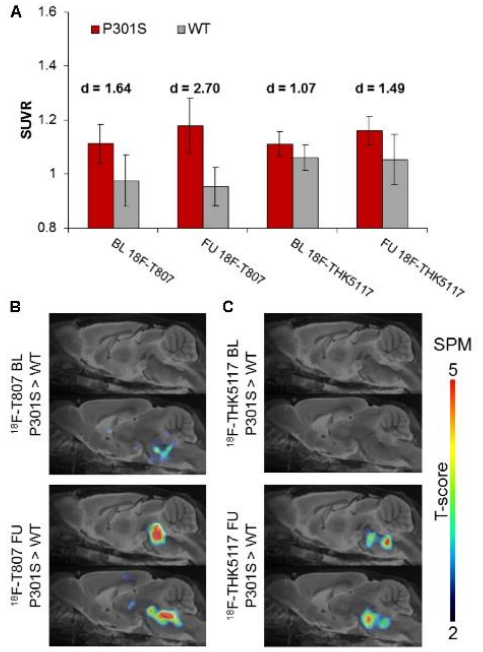

FIGURE 4 | (A) Bar graphs show group mean SUVRs of P301S (red) and WT (gray) mice for baseline and follow-up PET measurements of ^{18}F-T807 and ^{18}F-THK5117. Error bars indicate SD, effect sizes are given by Cohen's *d*. Sagittal slices (median and 0.6 mm paramedian) show voxel-wise statistical parametric mapping (SPM) between transgenic P301S and WT mice at baseline (BL) and follow-up (FU) for ^{18}F-T807 **(B)** and ^{18}F-THK5117 **(C)**. SPM-maps are depicted upon a MRI mouse atlas and extracerebral voxels are masked. The *t*-score threshold of 2 complies a significance threshold of 0.01 uncorrected.

histological tau burden is already present at the age of 6 months in these mice (Brendel et al., 2016), it seems that both ligands are practically insensitive to early tau deposition in the rodent brain. A limitation of our comparison lies in the impossibility of using exactly the same reference region for both tracers. While reasons for this difficulty are discussed below, we are convinced that using the optimal reference tissue for either tracer is a valid approach. Both reference tissues were lacking in tau pathology to immunohistochemical analyses, which substantiates their suitability, despite the lack of a single region optimal for both tracers. In general, the signal of both radioligands was only moderately increased (versus WT) at the follow-up PET scan at 9 months of age, despite the very heavy tau burden in the brainstem of P301S mice at this age (14–18%). The lower histological tau concentrations in the frontal cortex were not detected by either PET ligand irrespective of the TG mouse age. In this regard, present results are consistent with our previous ^{18}F-THK5117 investigation in the same TG mouse model (Brendel et al., 2016), although we note that percentages of the newly developed 3-dimensional approach fell distinctly below the earlier 2-dimensional immunohistological assessment. This is surely related to overlay effects arrising from a 2-dimensional acquisition, were several cell layers are summed in the calculation (illustrated in **Figures 6B–D**).

There is still some controversy about the specificity of pyridoindole and arylquinoline ligands for non-AD tau, with conflicting findings reported *in vivo* and *in vitro* (Chiotis et al., 2016; Ishiki et al., 2016; Smith et al., 2016). Aged P301S mice contain 4R tau, mainly occurring in a half-twisted ribbon conformation typical of human frontotemporal dementia, but they also express paired-helical filaments similar to those occurring in AD (Allen et al., 2002). Although both radioligand classes showed binding to 4R non-AD tau in brain of patients with corticobasal degeneration or progressive supranuclear palsy *in vivo* (Josephs et al., 2016; Hammes et al., 2017; Smith et al., 2017), and likewise to *post mortem* examination (Josephs et al., 2016; Kikuchi et al., 2016), other studies did not find significant binding in 4R-tauopathies, e.g., using ^{18}F-T807 (Coakeley et al., 2016; Marquie et al., 2017). The ultrastructure of tau as expressed in P301S mice might not be perfectly suited for high affinity binding by ^{18}F-T807 and ^{18}F-THK5117. This issue will only be circumvented if sensitive and specific ligands for the 4R form of tau are developed. For the present, translational comparisions between tracer binding to tau in mice and humans should be interpreted with caution as tau ultrastructures in mouse models only partially match the human pathology.

We have also evaluated the arylquinoline ^{18}F-THK5351 in mouse models of tau pathology and WT mice. However, ^{18}F-THK5351 proved to have such rapid kinetics in mouse brain that specific tau signal in brain was overwhelmed by spill-in from extra-cerebral regions (see Supplementary Results). Thus, we elected to use the previsously evaluated arylquinoline^{18}F-THK5117 for the current study.

Challenges of Preclinical Tau PET

Bone uptake is more pronounced for ^{18}F-T807 than to ^{18}F-THK5117 (**Figure 2**), but extracerebral binding must be taken into consideration when planning the target and reference region of preclinical tau PET studies with either of these ligands. In general, bone labeling is indicative of hepatic defluorination of the tracer, which is often more pronounced in rodents than in humans or non-human primates. Present results suggest that tracking of mouse cortical tau pathology may be favored with ^{18}F-THK5117, due to the less contribution of signal spill-in than from ^{18}F-T807. On the other hand, imaging of tau in the frontal pole of the cortex is problematic for ^{18}F-THK5117 due to spill-over from the Harderian glands, and the still inexplicable hot-spot signal in about one third of mice with C57Bl/6 background, irrespective of their transgenic status. Mice of other backgrounds do not seem to be affected by the latter phenomenon (Brendel et al., 2016). The current brainstem target region (in the modified version) did not indicate clear advantages or disadvantages for one or the other of the ligands, although we chose in the present study to alter its shape so as to better avoid spill-over from the petrosal bone, which is pronounced in the case of ^{18}F-T807 μPET.

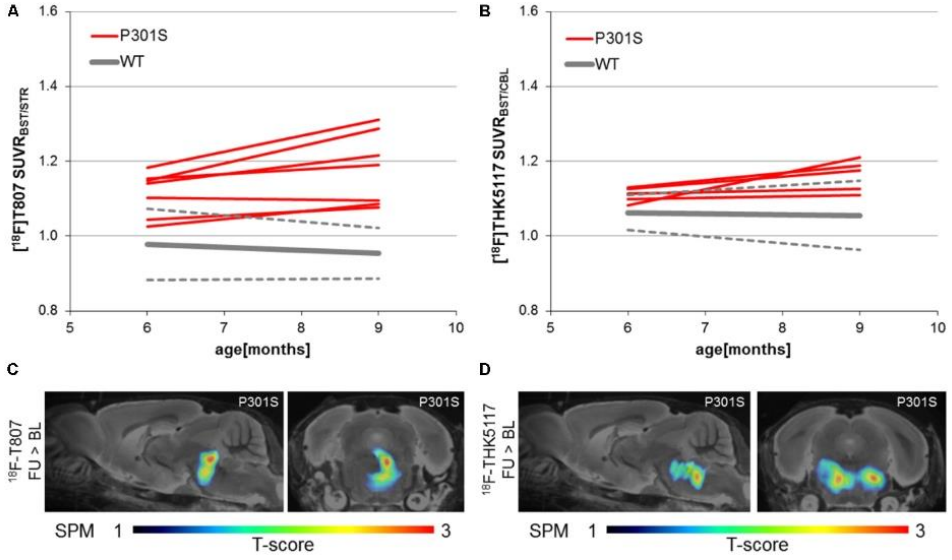

FIGURE 5 | Longitudinal findings of SUVR for **(A)** ^{18}F-T807 and **(B)** ^{18}F-THK5117 in individual WT and TG mice. Red lines represent SUVR of individual P301S mice at baseline and follow-up scanning. WT mice are presented in gray by group mean (solid) ± SD (dotted). Sagittal (0.6 mm paramedian) and coronal (pons/midbrain junction) slices show voxel-wise results of longitudinal statistical parametric mapping (SPM) showing regions with significantly increased tau ligand binding in transgenic P301S mice (**C**: ^{18}F-T807; **D**: ^{18}F-THK5117). SPM-maps are projected upon a MRI mouse atlas and extracerebral voxels are masked. The *t*-score threshold of 1 complies a significance threshold of 0.05 uncorrected.

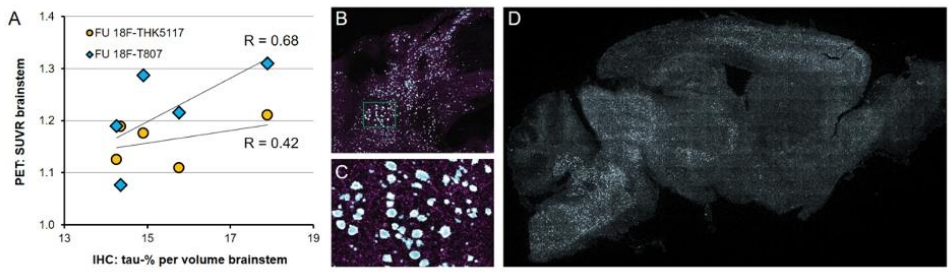

FIGURE 6 | (A) PET-Immunohistochemistry correlation of ^{18}F-T807 (blue diamonds) and ^{18}F-THK5117 (yellow circles) SUVR with %tau/area to PA5-27287 antibody staining. **(B)** 3-dimensional brainstem acquisition of PA5-27287 staining and **(C)** zoomed image indicating automatically detected tau positive cell somata. **(D)** 2-dimensional whole brain overview shows tau-positive cells predominantly in the brainstem, and lower amounts in the neocortex. Data derive from *N* = 5 P301S mice.

Another difficulty presented by tau PET with the arylquinoline ^{18}F-THK5351 and also the pyridoindole ^{18}F-T807 is off-target binding to monoamine oxidases (MAO) A or B (Vermeiren et al., 2015; Ng et al., 2017). A recent study has also indicated off-target binding of ^{18}F-THK5117 to MAO-B in brain (Lemoine et al., 2017), which might have been predicted from structural motifs. However, the contribution of MAO to the ^{18}F-THK5117 binding signal in mouse brain remains to be established. Additional *in vivo* blocking experiments by MAO inhibitors were not possible in the present cohort due to the high rate of drop-outs expected for aged TG exposed to additional scanning sessions. Thus, we cannot presently exclude a contribution of MAO binding to the present findings with ^{18}F-T807 and ^{18}F-THK5117 PET, although we note that the immunohistochemical findings support our attribution of the PET results mainly to tau deposition. Most relevantly, MAO can be elevated as part

of inflammatory responses in the course of neurodegenerative diseases (Carter et al., 2012). If parts of the tracer signal in our tau model indeed belongs to MAO binding, it will be necessary to separate the binding components by pharmacological blocking studies, or in double TG mice with knockout of MAO A or B. Due to the configuration of our animal holder, we are unable to obtain blood samples during the recording. This introduces some variance due to individual differences in tracer metabolism, although our use of SUVR values should largely compensate for such factors.

Longitudinal Imaging

Present data give a first demonstration of the value of longitudinal μPET imaging in tau transgenic models. The phenotype of mouse models of neurodegenerative diseases is well-known to show considerable heterogeneity, as seen in the present study from the different baseline SUVR results of P301S mice for both tau tracers in **Figure 5**. By recording the kinetics of tau deposition in individual animals it should in future studies be feasible to minimize possible biasing effects of differing pathological trajectories depending on baseline differences. This scenario is reminiscent of our earlier preclinical findings with amyloid-PET, whereby individual responses to an anti-amyloid treatment proved to be dependent on the amyloidosis at baseline (Brendel et al., 2015). Thus, PET imaging of P301S mice can be translationally used to monitor anti-tau drugs during preclinical evaluation and this data will potentially lead to a better understanding of tau-PET monitoring in humans. As a limitation we note that longitudinal increases of MAO could as well lead to a elevated PET signal due to off-target binding, however, recent data in AD suggests different time courses for astrocytosis and tau protein deposition (Scholl et al., 2015).

CONCLUSION

Longitudinal μPET imaging of tau pathology is feasible in a preclinical setting using P301S mice. Analysis of brainstem uptake showed ^{18}F-T807 to be moderately superior to ^{18}F-THK5117 regarding sensitivity for preclinical tau imaging. The two tracers, which represent distinct structural classes, both suffer from particular shortcomings in the present mouse model, which must be considered in the design of longitudinal studies of tau deposition.

AUTHOR CONTRIBUTIONS

MB and BY organized and executed the research project, executed the statistical analysis, and wrote the first draft of manuscript. TB, MH, CF, MD, FP, SL, and BvU-S executed the research project and reviewed and critiqued the manuscript. AD, CH, and JH reviewed and critiqued the statistical analysis. AD, CH, JH, PB, and NO reviewed and critiqued the manuscript. IY and AR conceived and organized the research project, designed, reviewed, and critiqued the statistical analysis, and reviewed and critiqued the manuscript.

FUNDING

This study was financially supported by the SyNergy Cluster, the European Union's Seventh Framework Program FP7/2013-2017/ under MINDView grant agreement no. (603002) and the Deutsche Forschungsgemeinschaft (RO 5194/1-1 and BR 4580/1-1).

ACKNOWLEDGMENTS

We thank Karin Bormann-Giglmaier, Rosel Oos, Marina Schenk, and Reinhold Klitsch for the excellent technical assistance. We also acknowledge *Inglewood Biomedical Editing* for the professional editing of the manuscript.

SUPPLEMENTARY MATERIAL

The Supplementary Material for this article can be found online at: https://www.frontiersin.org/articles/10.3389/fnagi.2018.00174/full#supplementary-material

REFERENCES

Allen, B., Ingram, E., Takao, M., Smith, M. J., Jakes, R., Virdee, K., et al. (2002). Abundant tau filaments and nonapoptotic neurodegeneration in transgenic mice expressing human P301S tau protein. *J. Neurosci.* 22, 9340–9351. doi: 10.1523/JNEUROSCI.22-21-09340.2002

Brendel, M., Jaworska, A., Herms, J., Trambauer, J., Rotzer, C., Gildehaus, F. J., et al. (2015). Amyloid-PET predicts inhibition of de novo plaque formation upon chronic gamma-secretase modulator treatment. *Mol. Psychiatry* 20, 1179–1187. doi: 10.1038/mp.2015.74

Brendel, M., Jaworska, A., Probst, F., Overhoff, F., Korzhova, V., Lindner, S., et al. (2016). Small-animal PET imaging of tau pathology with 18F-THK5117 in 2 transgenic mouse models. *J. Nucl. Med.* 57, 792–798. doi: 10.2967/jnumed.115.163493

Carter, S. F., Scholl, M., Almkvist, O., Wall, A., Engler, H., Langstrom, B., et al. (2012). Evidence for astrocytosis in prodromal Alzheimer disease provided by 11C-deuterium-L-deprenyl: a multitracer PET paradigm combining 11C-Pittsburgh compound B and 18F-FDG. *J. Nucl. Med.* 53, 37–46. doi: 10.2967/jnumed.110.087031

Chiotis, K., Saint-Aubert, L., Savitcheva, I., Jelic, V., Andersen, P., Jonasson, M., et al. (2016). Imaging in-vivo tau pathology in Alzheimer's disease with THK5317 PET in a multimodal paradigm. *Eur. J. Nucl. Med. Mol. Imaging* 43, 1686–1699. doi: 10.1007/s00259-016-3363-z

Coakeley, S., Cho, S. S., Koshimori, Y., Rusjan, P., Harris, M., Ghadery, C., et al. (2016). Positron emission tomography imaging of tau pathology in progressive supranuclear palsy. *J. Cereb. Blood Flow Metab.* 37, 3150–3160. doi: 10.1177/0271678X16683695

Dorr, A., Sled, J. G., and Kabani, N. (2007). Three-dimensional cerebral vasculature of the CBA mouse brain: a magnetic resonance imaging and micro computed tomography study. *Neuroimage* 35, 1409–1423. doi: 10.1016/j.neuroimage.2006.12.040

Duyckaerts, C., Delatour, B., and Potier, M. C. (2009). Classification and basic pathology of Alzheimer disease. *Acta Neuropathol.* 118, 5–36. doi: 10.1007/s00401-009-0532-1

Gao, M., Wang, M., and Zheng, Q. H. (2015). Fully automated synthesis of [(18)F]T807, a PET tau tracer for Alzheimer's disease. *Bioorg. Med. Chem. Lett.* 25, 2953–2957. doi: 10.1016/j.bmcl.2015.05.035

Hammes, J., Bischof, G. N., Giehl, K., Faber, J., Drzezga, A., Klockgether, T., et al. (2017). Elevated in vivo [18F]-AV-1451 uptake in a patient with progressive supranuclear palsy. *Mov. Disord.* 32, 170–171. doi: 10.1002/mds.26727

Hansen, A. K., Knudsen, K., Lillethorup, T. P., Landau, A. M., Parbo, P., Fedorova, T., et al. (2016). In vivo imaging of neuromelanin in Parkinson's disease using 18F-AV-1451 PET. *Brain* 139(Pt 7), 2039–2049. doi: 10.1093/brain/aww098

Ishiki, A., Harada, R., Okamura, N., Tomita, N., Rowe, C. C., Villemagne, V. L., et al. (2016). Tau imaging with [^{18}F]THK-5351 in progressive supranuclear palsy. *Eur. J. Neurol.* 24, 130–136. doi: 10.1111/ene.13164

Jang, Y. K., Lyoo, C. H., Park, S., Oh, S. J., Cho, H., Oh, M., et al. (2017). Head to head comparison of [^{18}F] AV-1451 and [^{18}F] THK5351 for tau imaging in Alzheimer's disease and frontotemporal dementia. *Eur. J. Nucl. Med. Mol. Imaging* 45, 432–442. doi: 10.1007/s00259-017-3876-0

Josephs, K. A., Whitwell, J. L., Tacik, P., Duffy, J. R., Senjem, M. L., Tosakulwong, N., et al. (2016). [18F]AV-1451 tau-PET uptake does correlate with quantitatively measured 4R-tau burden in autopsy-confirmed corticobasal degeneration. *Acta Neuropathol.* 132, 931–933. doi: 10.1007/s00401-016-1618-1

Kikuchi, A., Okamura, N., Hasegawa, T., Harada, R., Watanuki, S., Funaki, Y., et al. (2016). In vivo visualization of tau deposits in corticobasal syndrome by 18F-THK5351 PET. *Neurology* 87, 2309–2316. doi: 10.1212/WNL.0000000000003375

Lemoine, L., Gillberg, P. G., Svedberg, M., Stepanov, V., Jia, Z., Huang, J., et al. (2017). Comparative binding properties of the tau PET tracers THK5117, THK5351, PBB3, and T807 in postmortem Alzheimer brains. *Alzheimers Res. Ther.* 9:96. doi: 10.1186/s13195-017-0325-z

Liu, B., Le, K. X., Park, M. A., Wang, S., Belanger, A. P., Dubey, S., et al. (2015). In vivo detection of age- and disease-related increases in neuroinflammation by 18F-GE180 TSPO MicroPET imaging in wild-type and Alzheimer's transgenic mice. *J. Neurosci.* 35, 15716–15730. doi: 10.1523/JNEUROSCI.0996-15.2015

Marquie, M., Normandin, M. D., Meltzer, A. C., Siao Tick Chong, M., Andrea, N. V., Anton-Fernandez, A., et al. (2017). Pathological correlations of [F-18]-AV-1451 imaging in non-Alzheimer tauopathies. *Ann. Neurol.* 81, 117–128. doi: 10.1002/ana.24844

Maruyama, M., Shimada, H., Suhara, T., Shinotoh, H., Ji, B., Maeda, J., et al. (2013). Imaging of tau pathology in a tauopathy mouse model and in Alzheimer patients compared to normal controls. *Neuron* 79, 1094–1108. doi: 10.1016/j.neuron.2013.07.037

Murray, M. E., Kouri, N., Lin, W. L., Jack, C. R. Jr., Dickson, D. W., and Vemuri, P. (2014). Clinicopathologic assessment and imaging of tauopathies in neurodegenerative dementias. *Alzheimers Res. Ther.* 6:1. doi: 10.1186/alzrt231

Ng, K. P., Pascoal, T. A., Mathotaarachchi, S., Therriault, J., Kang, M. S., Shin, M., et al. (2017). Monoamine oxidase B inhibitor, selegiline, reduces 18F-THK5351 uptake in the human brain. *Alzheimers Res. Ther.* 9:25. doi: 10.1186/s13195-017-0253-y

Okamura, N., Furumoto, S., Harada, R., Tago, T., Yoshikawa, T., Fodero-Tavoletti, M., et al. (2013). Novel 18F-labeled arylquinoline derivatives for noninvasive imaging of tau pathology in Alzheimer disease. *J. Nucl. Med.* 54, 1420–1427. doi: 10.2967/jnumed.112.117341

Rominger, A., Brendel, M., Burgold, S., Keppler, K., Baumann, K., Xiong, G., et al. (2013). Longitudinal assessment of cerebral beta-amyloid deposition in mice overexpressing Swedish mutant beta-amyloid precursor protein using 18F-florbetaben PET. *J. Nucl. Med.* 54, 1127–1134. doi: 10.2967/jnumed.112.114660

Scholl, M., Carter, S. F., Westman, E., Rodriguez-Vieitez, E., Almkvist, O., Thordardottir, S., et al. (2015). Early astrocytosis in autosomal dominant Alzheimer's disease measured in vivo by multi-tracer positron emission tomography. *Sci. Rep.* 5:16404. doi: 10.1038/srep16404

Smith, R., Schain, M., Nilsson, C., Strandberg, O., Olsson, T., Hagerstrom, D., et al. (2017). Increased basal ganglia binding of 18 F-AV-1451 in patients with progressive supranuclear palsy. *Mov. Disord.* 32, 108–114. doi: 10.1002/mds.26813

Smith, R., Scholl, M., Honer, M., Nilsson, C. F., Englund, E., and Hansson, O. (2016). Tau neuropathology correlates with FDG-PET, but not AV-1451-PET, in progressive supranuclear palsy. *Acta Neuropathol.* 133, 149–151. doi: 10.1007/s00401-016-1650-1

Tago, T., Furumoto, S., Okamura, N., Harada, R., Ishikawa, Y., Arai, H., et al. (2014). Synthesis and preliminary evaluation of 2-arylhydroxyquinoline derivatives for tau imaging. *J. Labelled Comp. Radiopharm.* 57, 18–24. doi: 10.1002/jlcr.3133

Vermeiren, C., Mercier, J., Viot, D., Mairet-Coello, G., Hannestad, J., Courade, J.-P., et al. (2015). T807, a reported selective tau tracer, binds with nanomolar affinity to monoamine oxidase a. *Alzheimers Dement. J. Alzheimers Assoc.* 11:283. doi: 10.1016/j.jalz.2015.07.381

Villemagne, V. L., and Okamura, N. (2016). Tau imaging in the study of ageing, Alzheimer's disease, and other neurodegenerative conditions. *Curr. Opin. Neurobiol.* 36, 43–51. doi: 10.1016/j.conb.2015.09.002

Zimmer, E. R., Parent, M. J., Cuello, A. C., Gauthier, S., and Rosa-Neto, P. (2014). MicroPET imaging and transgenic models: a blueprint for Alzheimer's disease clinical research. *Trends Neurosci.* 37, 629–641. doi: 10.1016/j.tins.2014.07.002

Conflict of Interest Statement: The authors declare that the research was conducted in the absence of any commercial or financial relationships that could be construed as a potential conflict of interest.

5. Literaturverzeichnis

Adlard, P. A., Tran, B. A., Finkelstein, D. I., Desmond, P. M., Johnston, L. A., Bush, A. I., & Egan, G. F. (2014). A review of beta-amyloid neuroimaging in Alzheimer's disease. *Front Neurosci, 8*, 327. doi:10.3389/fnins.2014.00327

Airas, L., Rissanen, E., & Rinne, J. O. (2015). Imaging neuroinflammation in multiple sclerosis using TSPO-PET. *Clinical and Translational Imaging, 3*(6), 461-473. doi:10.1007/s40336-015-0147-6

Allen, B., Ingram, E., Takao, M., Smith, M. J., Jakes, R., Virdee, K., . . . Goedert, M. (2002). Abundant tau filaments and nonapoptotic neurodegeneration in transgenic mice expressing human P301S tau protein. *J Neurosci, 22*(21), 9340-9351.

Ballatore, C., Lee, V. M., & Trojanowski, J. Q. (2007). Tau-mediated neurodegeneration in Alzheimer's disease and related disorders. *Nat Rev Neurosci, 8*(9), 663-672. doi:10.1038/nrn2194

Barthel, H., Gertz, H. J., Dresel, S., Peters, O., Bartenstein, P., Buerger, K., . . . Sabri, O. (2011). Cerebral amyloid-beta PET with florbetaben ((18)F) in patients with Alzheimer's disease and healthy controls: a multicentre phase 2 diagnostic study. *Lancet Neurol, 10*(5), 424-435. doi:S1474-4422(11)70077-1 [pii] 10.1016/S1474-4422(11)70077-1

Bickel, H. (2000). [Dementia syndrome and Alzheimer disease: an assessment of morbidity and annual incidence in Germany]. *Gesundheitswesen, 62*(4), 211-218. doi:10.1055/s-2000-10858

Biesmans, S., Acton, P. D., Cotto, C., Langlois, X., Ver Donck, L., Bouwknecht, J. A., . . . Nuydens, R. (2015). Effect of stress and peripheral immune activation on astrocyte activation in transgenic bioluminescent Gfap-luc mice. *Glia, 63*(7), 1126-1137. doi:10.1002/glia.22804

Brackhan, M., Bascunana, P., Ross, T. L., Bengel, F. M., Bankstahl, J. P., & Bankstahl, M. (2018). [(18) F]GE180 positron emission tomographic imaging indicates a potential double-hit insult in the intrahippocampal kainate mouse model of temporal lobe epilepsy. *Epilepsia, 59*(3), 617-626. doi:10.1111/epi.14009

Brendel, M., Jaworska, A., Griessinger, E., Rotzer, C., Burgold, S., Gildehaus, F. J., . . . Rominger, A. (2015). Cross-sectional comparison of small animal [18F]-florbetaben amyloid-PET between transgenic AD mouse models. *PLoS One, 10*(2), e0116678. doi:10.1371/journal.pone.0116678

Brendel, M., Jaworska, A., Probst, F., Overhoff, F., Korzhova, V., Lindner, S., . . . Rominger, A. (2016). Small-Animal PET Imaging of Tau Pathology with 18F-THK5117 in 2 Transgenic Mouse Models. *J Nucl Med, 57*(5), 792-798. doi:10.2967/jnumed.115.163493

Brendel, M., Probst, F., Jaworska, A., Overhoff, F., Korzhova, V., Albert, N. L., . . . Rominger, A. (2016). Glial Activation and Glucose Metabolism in a Transgenic Amyloid Mouse Model: A Triple-Tracer PET Study. *J Nucl Med, 57*(6), 954-960. doi:10.2967/jnumed.115.167858

Brookmeyer, R., Johnson, E., Ziegler-Graham, K., & Arrighi, H. M. (2007). Forecasting the global burden of Alzheimer's disease. *Alzheimers Dement, 3*(3), 186-191. doi:10.1016/j.jalz.2007.04.381

Brown, R. C., & Papadopoulos, V. (2001). Role of the peripheral-type benzodiazepine receptor in adrenal and brain steroidogenesis. *Int Rev Neurobiol, 46*, 117-143.

Buch, K., Riemenschneider, M., Bartenstein, P., Willoch, F., Müller, U., Schmolke, M., . . . Kurz, A. (1998). Tau-ProteinEin potentieller biologischer Indikator zur Früherkennung der Alzheimer-Krankheit. *Der Nervenarzt, 69*(5), 379-385. doi:10.1007/s001150050286

Buck, J. R., McKinley, E. T., Fu, A., Abel, T. W., Thompson, R. C., Chambless, L., . . . Manning, H. C. (2015). Preclinical TSPO Ligand PET to Visualize Human Glioma Xenotransplants: A Preliminary Study. *PLOS ONE, 10*(10), e0141659. doi:10.1371/journal.pone.0141659

Chaney, A., Williams, S. R., & Boutin, H. (2018). In vivo molecular imaging of neuroinflammation in Alzheimer's disease. *J Neurochem*. doi:10.1111/jnc.14615

Cohen, A. D., & Klunk, W. E. (2014). Early detection of Alzheimer's disease using PiB and FDG PET. *Neurobiol Dis*. doi:10.1016/j.nbd.2014.05.001

Dickens, A. M., Vainio, S., Marjamaki, P., Johansson, J., Lehtiniemi, P., Rokka, J., . . . Airas, L. (2014). Detection of microglial activation in an acute model of neuroinflammation using PET and radiotracers 11C-(R)-PK11195 and 18F-GE-180. *J Nucl Med, 55*(3), 466-472. doi:10.2967/jnumed.113.125625

Dorr, A., Sled, J. G., & Kabani, N. (2007). Three-dimensional cerebral vasculature of the CBA mouse brain: a magnetic resonance imaging and micro computed tomography study. *Neuroimage, 35*(4), 1409-1423. doi:10.1016/j.neuroimage.2006.12.040

Drummond, E., & Wisniewski, T. (2017). Alzheimer's disease: experimental models and reality. *Acta Neuropathol, 133*(2), 155-175. doi:10.1007/s00401-016-1662-x

Dupont, A. C., Largeau, B., Santiago Ribeiro, M. J., Guilloteau, D., Tronel, C., & Arlicot, N. (2017). Translocator Protein-18 kDa (TSPO) Positron Emission Tomography (PET) Imaging and Its Clinical Impact in Neurodegenerative Diseases. *Int J Mol Sci, 18*(4). doi:10.3390/ijms18040785

Focke, C., Blume, T., Zott, B., Shi, Y., Deussing, M., Peters, F., . . . Brendel, M. (2018). Early and longitudinal microglial activation but not amyloid accumulation predict cognitive outcome in PS2APP mice. *J Nucl Med*. doi:10.2967/jnumed.118.217703

Fox, N. C., Warrington, E. K., Freeborough, P. A., Hartikainen, P., Kennedy, A. M., Stevens, J. M., & Rossor, M. N. (1996). Presymptomatic hippocampal atrophy in Alzheimer's disease. A longitudinal MRI study. *Brain, 119 (Pt 6)*, 2001-2007.

Gargiulo, S., Anzilotti, S., Coda, A. R. D., Gramanzini, M., Greco, A., Panico, M., . . . Pappatà, S. (2016). Imaging of brain TSPO expression in a mouse model of amyotrophic lateral sclerosis with 18F-DPA-714 and micro-PET/CT. *European Journal of Nuclear Medicine and Molecular Imaging, 43*(7), 1348-1359. doi:10.1007/s00259-016-3311-y

Gross, L., Paintmayer, L., Lehner, S., Brandl, L., Brenner, C., Grabmaier, U., . . . Brunner, S. (2016). FDG-PET reveals improved cardiac regeneration and attenuated adverse remodelling following Sitagliptin + G-CSF therapy after acute myocardial infarction. *Eur Heart J Cardiovasc Imaging, 17*(2), 136-145. doi:10.1093/ehjci/jev237

Hardy, J., & Selkoe, D. J. (2002). The amyloid hypothesis of Alzheimer's disease: progress and problems on the road to therapeutics. *Science, 297*(5580), 353-356. doi:10.1126/science.1072994

Heneka, M. T., Carson, M. J., El Khoury, J., Landreth, G. E., Brosseron, F., Feinstein, D. L., . . . Kummer, M. P. (2015). Neuroinflammation in Alzheimer's disease. *Lancet Neurol, 14*(4), 388-405. doi:10.1016/s1474-4422(15)70016-5

Hommet, C., Mondon, K., Camus, V., Ribeiro, M. J., Beaufils, E., Arlicot, N., . . . Chalon, S. (2014). Neuroinflammation and beta amyloid deposition in Alzheimer's disease: in vivo quantification with molecular imaging. *Dement Geriatr Cogn Disord, 37*(1-2), 1-18. doi:10.1159/000354363

Israel, I., Ohsiek, A., Al-Momani, E., Albert-Weissenberger, C., Stetter, C., Mencl, S., . . . Sirén, A.-L. (2016). Combined [18F]DPA-714 micro-positron emission tomography and autoradiography imaging of microglia activation after closed head injury in mice. *J Neuroinflammation, 13*(1), 140. doi:10.1186/s12974-016-0604-9

Jack, C. R., Jr., Bennett, D. A., Blennow, K., Carrillo, M. C., Dunn, B., Haeberlein, S. B., . . . Sperling, R. (2018). NIA-AA Research Framework: Toward a biological definition of Alzheimer's disease. *Alzheimers Dement, 14*(4), 535-562. doi:10.1016/j.jalz.2018.02.018

James, M. L., Belichenko, N. P., Nguyen, T. V., Andrews, L. E., Ding, Z., Liu, H., . . . Chin, F. T. (2015). PET imaging of translocator protein (18 kDa) in a mouse model of Alzheimer's disease using N-(2,5-dimethoxybenzyl)-2-18F-fluoro-N-(2-phenoxyphenyl)acetamide. *J Nucl Med, 56*(2), 311-316. doi:10.2967/jnumed.114.141648

Jonasson, M., Wall, A., Chiotis, K., Leuzy, A., Eriksson, J., Antoni, G., . . . Lubberink, M. (2019). Optimal timing of tau pathology imaging and automatic extraction of a reference region using dynamic [(18)F]THK5317 PET. *Neuroimage Clin, 22*, 101681. doi:10.1016/j.nicl.2019.101681

LaFerla, F. M. (2010). Pathways linking Abeta and tau pathologies. *Biochem Soc Trans, 38*(4), 993-995. doi:10.1042/BST0380993

Latta, C. H., Brothers, H. M., & Wilcock, D. M. (2014). Neuroinflammation in Alzheimer's disease; A source of heterogeneity and target for personalized therapy. *Neuroscience*. doi:10.1016/j.neuroscience.2014.09.061

Lyoo, C. H., Ikawa, M., Liow, J. S., Zoghbi, S. S., Morse, C. L., Pike, V. W., . . . Kreisl, W. C. (2015). Cerebellum Can Serve As a Pseudo-Reference Region in Alzheimer Disease to Detect Neuroinflammation Measured with PET Radioligand Binding to Translocator Protein. *J Nucl Med, 56*(5), 701-706. doi:10.2967/jnumed.114.146027

Maruyama, M., Shimada, H., Suhara, T., Shinotoh, H., Ji, B., Maeda, J., . . . Higuchi, M. (2013). Imaging of tau pathology in a tauopathy mouse model and in Alzheimer patients compared to normal controls. *Neuron, 79*(6), 1094-1108. doi:10.1016/j.neuron.2013.07.037

Mirzaei, N., Tang, S. P., Ashworth, S., Coello, C., Plisson, C., Passchier, J., . . . Sastre, M. (2016). In vivo imaging of microglial activation by positron emission tomography with [(11)C]PBR28 in the 5XFAD model of Alzheimer's disease. *Glia, 64*(6), 993-1006. doi:10.1002/glia.22978

Monson, N. L., Ireland, S. J., Ligocki, A. J., Chen, D., Rounds, W. H., Li, M., . . . Zhang, R. (2014). Elevated CNS inflammation in patients with preclinical Alzheimer's disease. *J Cereb Blood Flow Metab, 34*(1), 30-33. doi:10.1038/jcbfm.2013.183

Nack, A., Brendel, M., Nedelcu, J., Daerr, M., Nyamoya, S., Beyer, C., . . . Kipp, M. (2019). Expression of Translocator Protein and [18F]-GE180 Ligand Uptake in Multiple Sclerosis Animal Models. *Cells, 8*(2). doi:10.3390/cells8020094

Ng, K., Massarweh, G., Soucy, J., Gravel, P., Pascoal, T., Mathotaarachchi, S., . . . Rosa-Neto, P. (2017). Selegiline reduces brain [18F]THK5351 binding. *HAI 2017 Conference Abstract 187*.

Okamura, N., Furumoto, S., Fodero-Tavoletti, M. T., Mulligan, R. S., Harada, R., Yates, P., . . . Villemagne, V. L. (2014). Non-invasive assessment of Alzheimer's disease neurofibrillary pathology using 18F-THK5105 PET. *Brain, 137*(Pt 6), 1762-1771. doi:10.1093/brain/awu064

Okamura, N., Furumoto, S., Harada, R., Tago, T., Yoshikawa, T., Fodero-Tavoletti, M., . . . Kudo, Y. (2013). Novel 18F-labeled arylquinoline derivatives for noninvasive imaging of tau pathology in Alzheimer disease. *J Nucl Med, 54*(8), 1420-1427. doi:10.2967/jnumed.112.117341

Ossenkoppele, R., Schonhaut, D. R., Scholl, M., Lockhart, S. N., Ayakta, N., Baker, S. L., . . . Rabinovici, G. D. (2016). Tau PET patterns mirror clinical and neuroanatomical variability in Alzheimer's disease. *Brain, 139*(Pt 5), 1551-1567. doi:10.1093/brain/aww027

Ozmen, L., Albientz, A., Czech, C., & Jacobsen, H. (2009). Expression of transgenic APP mRNA is the key determinant for beta-amyloid deposition in PS2APP transgenic mice. *Neurodegener Dis, 6*(1-2), 29-36. doi:10.1159/000170884

Parhizkar, S., Arzberger, T., Brendel, M., Kleinberger, G., Deussing, M., Focke, C., . . . Haass, C. (2019). Loss of TREM2 function increases amyloid seeding but reduces plaque-associated ApoE. *Nat Neurosci, 22*(2), 191-204. doi:10.1038/s41593-018-0296-9

Pihlaja, R., Takkinen, J., Eskola, O., Vasara, J., Lopez-Picon, F. R., Haaparanta-Solin, M., & Rinne, J. O. (2015). Monoacylglycerol lipase inhibitor JZL184 reduces neuroinflammatory response in APdE9 mice and in adult mouse glial cells. *J Neuroinflammation, 12*, 81. doi:10.1186/s12974-015-0305-9

Reitz, C., & Mayeux, R. (2014). Alzheimer disease: epidemiology, diagnostic criteria, risk factors and biomarkers. *Biochem Pharmacol, 88*(4), 640-651. doi:10.1016/j.bcp.2013.12.024

Rice, L., & Bisdas, S. (2017). The diagnostic value of FDG and amyloid PET in Alzheimer's disease-A systematic review. *Eur J Radiol, 94*, 16-24. doi:10.1016/j.ejrad.2017.07.014

Richards, J. G., Higgins, G. A., Ouagazzal, A. M., Ozmen, L., Kew, J. N., Bohrmann, B., . . . Kemp, J. A. (2003). PS2APP transgenic mice, coexpressing hPS2mut and hAPPswe, show age-related cognitive deficits associated with discrete brain amyloid deposition and inflammation. *J Neurosci, 23*(26), 8989-9003.

Rominger, A., Brendel, M., Burgold, S., Keppler, K., Baumann, K., Xiong, G., . . . Bartenstein, P. (2013). Longitudinal Assessment of Cerebral beta-Amyloid Deposition in Mice Overexpressing Swedish Mutant beta-Amyloid Precursor Protein Using 18F-Florbetaben PET. *J Nucl Med*. doi:10.2967/jnumed.112.114660

Scheichenberger, S., & Scharb, B. (2018). *Spezielle validierende Pflege* (Vol. 4): Springer-Verlag Berlin Heidelberg.

Selkoe, D. J. (1999). Translating cell biology into therapeutic advances in Alzheimer's disease. *Nature, 399*(6738 Suppl), A23-31.

Selkoe, D. J. (2002). Alzheimer's disease is a synaptic failure. *Science, 298*(5594), 789-791. doi:10.1126/science.1074069

Smith, R., Schain, M., Nilsson, C., Strandberg, O., Olsson, T., Hagerstrom, D., . . . Hansson, O. (2016). Increased basal ganglia binding of 18 F-AV-1451 in patients with progressive supranuclear palsy. Personalized medicine in

Alzheimer's disease and depression. *Contemp Clin Trials, 36*(2), 616-623. doi:10.1016/j.cct.2013.06.012
Stefaniak, J., & O'Brien, J. (2016). Imaging of neuroinflammation in dementia: a review. *J Neurol Neurosurg Psychiatry, 87*(1), 21-28. doi:10.1136/jnnp-2015-311336
Sütterlin, S., Hoßmann, I., & Klingholz, R. (2001). *Demenz-Report: wie sich die Regionen in Deutschland, Österreich und der Schweiz auf die Alterung der Gesellschaft vorbereiten können*.
Tang, D., Nickels, M. L., Tantawy, M. N., Buck, J. R., & Manning, H. C. (2014). Preclinical imaging evaluation of novel TSPO-PET ligand 2-(5,7-Diethyl-2-(4-(2-[(18)F]fluoroethoxy)phenyl)pyrazolo[1,5-a]pyrimidin-3-yl)- N,N-diethylacetamide ([(18)F]VUIIS1008) in glioma. *Mol Imaging Biol, 16*(6), 813-820. doi:10.1007/s11307-014-0743-2
Teipel, S. J., Buchert, R., Thome, J., Hampel, H., & Pahnke, J. (2011). Development of Alzheimer-disease neuroimaging-biomarkers using mouse models with amyloid-precursor protein-transgene expression. *Prog Neurobiol, 95*(4), 547-556. doi:10.1016/j.pneurobio.2011.05.004
Terry, R. D., Masliah, E., Salmon, D. P., Butters, N., DeTeresa, R., Hill, R., . . . Katzman, R. (1991). Physical basis of cognitive alterations in Alzheimer's disease: synapse loss is the major correlate of cognitive impairment. *Ann Neurol, 30*(4), 572-580. doi:10.1002/ana.410300410
Villemagne, V. L., & Okamura, N. (2016). Tau imaging in the study of ageing, Alzheimer's disease, and other neurodegenerative conditions. *Curr Opin Neurobiol, 36*, 43-51. doi:10.1016/j.conb.2015.09.002
Visser, E. P., Disselhorst, J. A., Brom, M., Laverman, P., Gotthardt, M., Oyen, W. J., & Boerman, O. C. (2009). Spatial resolution and sensitivity of the Inveon small-animal PET scanner. *J Nucl Med, 50*(1), 139-147. doi:10.2967/jnumed.108.055152
Wickstrom, T., Clarke, A., Gausemel, I., Horn, E., Jorgensen, K., Khan, I., . . . Trigg, W. (2014). The development of an automated and GMP compliant FASTlab Synthesis of [(18) F]GE-180; a radiotracer for imaging translocator protein (TSPO). *J Labelled Comp Radiopharm, 57*(1), 42-48. doi:10.1002/jlcr.3112
Wirths, O., Breyhan, H., Cynis, H., Schilling, S., Demuth, H. U., & Bayer, T. A. (2009). Intraneuronal pyroglutamate-Abeta 3-42 triggers neurodegeneration and lethal neurological deficits in a transgenic mouse model. *Acta Neuropathol, 118*(4), 487-496. doi:10.1007/s00401-009-0557-5
Zheng, J., Winkeler, A., Peyronneau, M. A., Dolle, F., & Boisgard, R. (2016). Evaluation of PET Imaging Performance of the TSPO Radioligand [18F]DPA-714 in Mouse and Rat Models of Cancer and Inflammation. *Mol Imaging Biol, 18*(1), 127-134. doi:10.1007/s11307-015-0877-x
Zimmer, E. R., Leuzy, A., Benedet, A. L., Breitner, J., Gauthier, S., & Rosa-Neto, P. (2014). Tracking neuroinflammation in Alzheimer's disease: the role of positron emission tomography imaging. *J Neuroinflammation, 11*, 120. doi:10.1186/1742-2094-11-120
Zimmer, E. R., Parent, M. J., Cuello, A. C., Gauthier, S., & Rosa-Neto, P. (2014). MicroPET imaging and transgenic models: a blueprint for Alzheimer's disease clinical research. *Trends Neurosci*. doi:10.1016/j.tins.2014.07.002

6. Danksagung

Meinem Doktorvater, Herrn Prof. Dr. med. Axel Rominger und Betreuer Herrn Dr. med. Matthias Brendel von der Klinik und Poliklinik für Nuklearmedizin der Universität München danke ich für die unermüdliche Unterstützung, die exzellente Betreuung und die stete Ansprechbarkeit bei jeder noch so kleinen Fragestellung.

Prof. Dr. med. Peter Bartenstein danke ich für seine Unterstützung und promotionsbegleitenden Ratschläge.

Federico Probst und Felix Overhoff danke ich für die hervorragende Einarbeitung und das Mitwirken bei den ersten Experimenten. Meiner Doktorandenkollegin Carola Focke gilt mein Dank für die kompetente Unterstützung und Zusammenarbeit bei den vielzähligen Projekten sowie für die vielen interessanten, aber auch unterhaltsamen Stunden im Doktorandenraum. Meinen Nachfolgern Florian Eckenweber und Christian Sacher danke ich für die Unterstützung bei den finalen Versuchen.

Darüber hinaus danke ich Karin Bormann-Giglmaier und Rosel Oos für die exzellente methodische und technische Unterstützung und die hervorragende Zusammenarbeit bei der Durchführung der Experimente bis spät in die Nacht sowie an Wochenend- und Feiertagen.

Für die Unterstützung bei allen Lebensfragen und das Ermöglichen des Studiums gilt mein tiefer Dank meinen Eltern und Großeltern.

Ganz besonders möchte ich mich auch bei meiner Freundin Julia bedanken, die mich stets bei allen Angelegenheiten unterstützte und nach einem langen Tag im Labor immer noch ein offenes Ohr sowie eine warme Mahlzeit bereithielt.